UNIVERSITY OF CAPE TOWN

DEPARTMENT OF MECHANICAL ENGINEERING
RONDEBOSCH, CAPE TOWN, SOUTH AFRICA

Development of a Robotic Platform for the Exploration of Hazardous Environments

Prepared by
Eugene Dreyer

Prepared for
Stephen Marais
Robotics and Agents Research Laboratory
August 2012

Executive Summary

Figure 1: The Explorer Robot Platform

This report documents the research, design, manufacturing and testing of an Unmanned Ground Vehicle (UGV) robotic platform. Robotic platforms such as these are typically used as Urban Search and Rescue (USAR) platforms, as in the World Trade Tower collapses in 2001, however this platform was designed to be a general purpose platform with applications beyond search and rescue.

This is the 5th iteration of the platform. It was originally conceived as a platform for transporting mapping equipment into the ore passes of mines. As the project matured it progressed from a solution to this specific problem into a general purpose vehicle for transporting a variety of equipment into a variety of hazardous environments. Through The University of Cape Town (UCT) Robotics and Agents Research Laboratory's involvement with the RoboCup Soccer project, the RoboCup Rescue competition emerged as an ideal test bed and development community for this type of platform. While the competition focuses specifically on USAR robots, the test procedures and equipment in use have many possible applications. Papers detailing the design of participating robots were analysed for useful design features and failings to avoid the many stumbling blocks for development of such a platform. Commercial robotic platforms such as the iRobot® PackBot were also investigated.

The platform was designed using Pro\Engineer design software. Design was done according to a top down methodology, where a central document containing key specifications was maintained and component dimensions were derived from this document. Thus changing any key specification would automatically alter the geometry of affected parts. This was deemed desirable due to the complex and compact nature of the design. The design of the platform (see Figure 2) is dominated by the two wide drive tracks. Each track encloses a sidepod in which the Lithium-Ion drive batteries are housed, while much of the rest of the sidepod was left empty to provide space for future equipment to be added. Each track runs on 2 wide pulleys with the front pulley serving as the drive pulley. Each of the 4 corners of the platform also feature

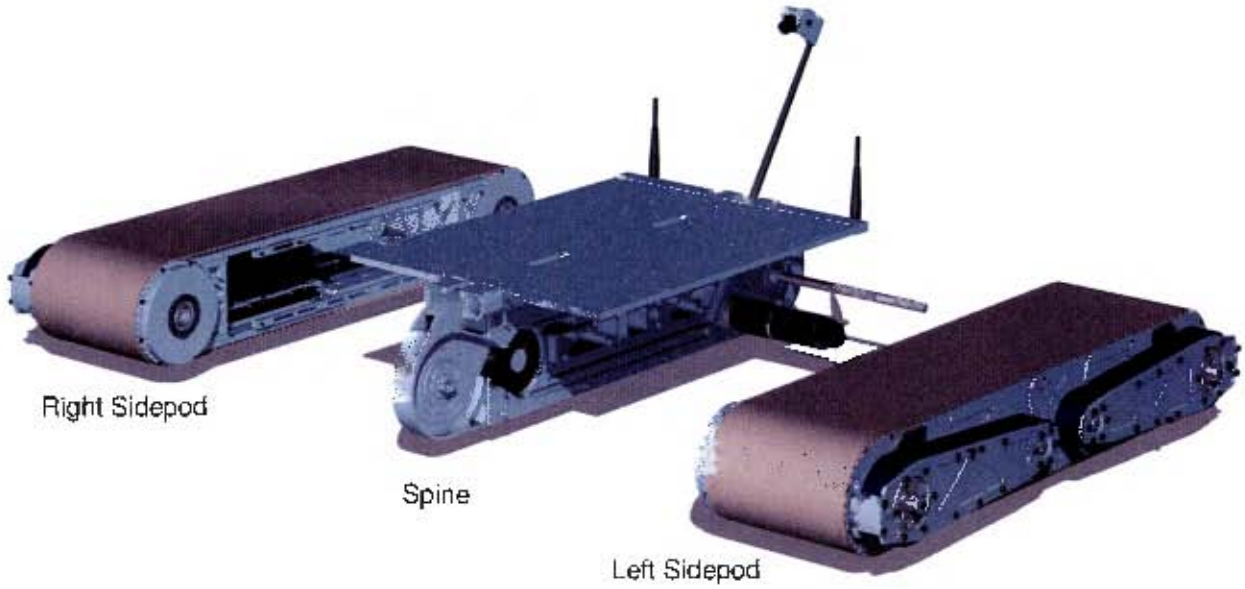

Figure 2: The major sub-systems of the platform.

a flipper arm which provides added flexibility in maneuvering around and over obstacles. The drive motors for the front flippers are located inside the front drive pulleys, while the rear flippers are driven together by a single motor inside the left sidepod. In addition to the flipper motors, the drive motors for the main tracks are also enclosed within the front pulley to make optimum use of the available space on the small platform. The layout of the drive pulleys is shown in Figure 3. The main structural element of the platform is the central spine onto which the sub-assemblies attach. The platform also features an accessory deck designed to allow the mounting of general purpose equipment in light of the multiple use objective for the platform. The design attempts to make use of as few unique parts as possible. For instance, left and right sidepods are made up of identical parts with the exception of the mount for the rear flipper motor in the left sidepod. All 4 pulleys were designed to be identical, with different covers being used on the front and rear. The design also requires only size 2.5 and 3 Allen keys to disassemble, as care was taken to use only fasteners accepting these tool sizes to minimize the requirements for maintenance in the field.

Manufacturing of the components making up the platform took place in the UCT Mechanical Engineering workshop. Where possible parts were machined on a standard mill or lathe. Many of the parts made use of the CNC machining facilities available in the workshop. This allowed for the functions of multiple parts to be combined into a single more complex part. It also allowed for complex patterns for machining away material to reduce the mass of parts where possible. This is particularly evident on the spine of the robot which has locating, fixing and cable routing features integrated into one part. In total the platform required 68 unique parts with a total of 170 machined components.

Tests were run to benchmark the performance of the platform. These measured the power requirements while performing maneuvers at various speeds. Testing of the platform revealed a number of problems particularly with track alignment and torque requirements. A few alterations were made to partially rectify the track alignment issue and gearboxes with higher reductions were placed on the drive motors to compensate for the increased torque requirements. A number of recommendations are made for future development of a platform such as this, the critical ones being a reduction in weight and the development of a system to manage track alignment.

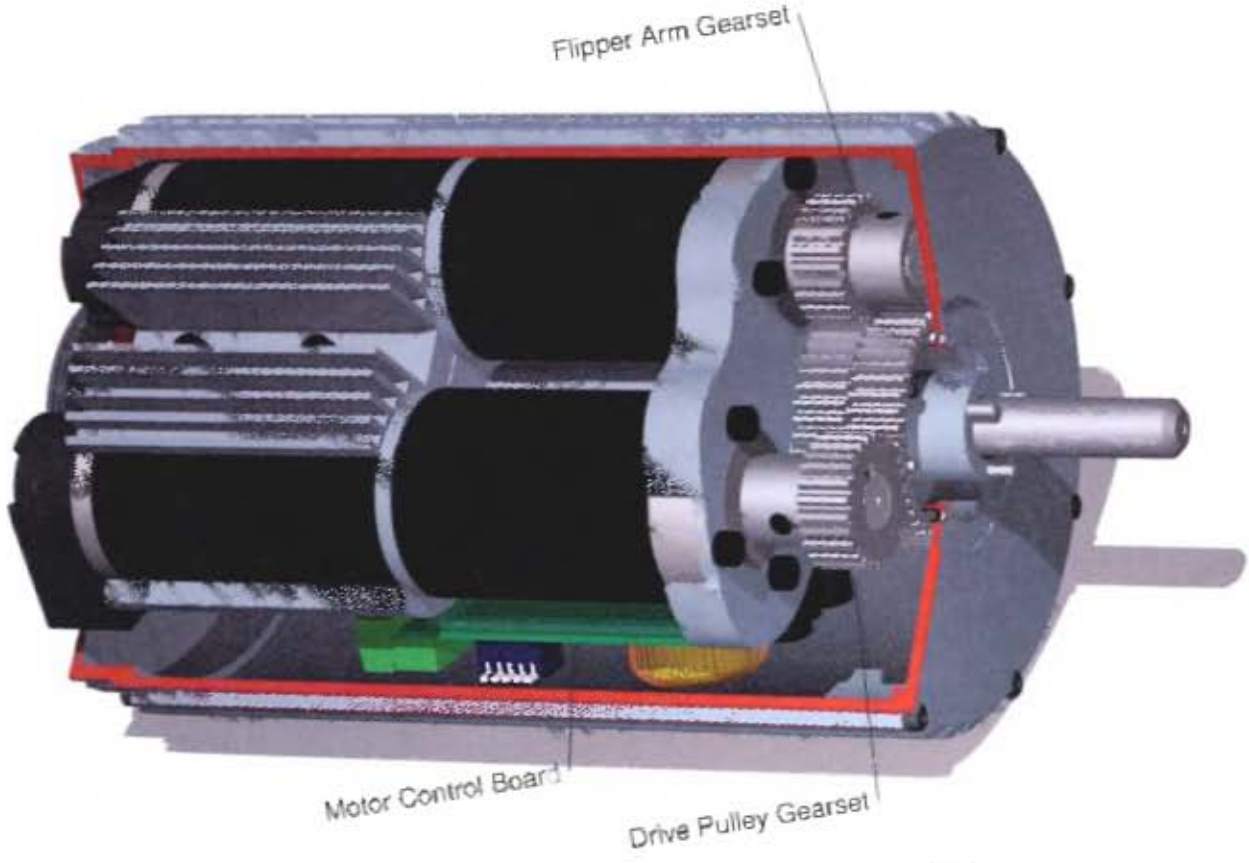

Figure 3: A cutaway view of the front drive pulley.

Declaration

This thesis is submitted in complete fulfilment of a M.Sc.(Eng) (Mechanical Engineering) at the University of Cape Town.

I know the meaning of plagiarism and declare that all of the work in the thesis, save for that which is properly acknowledged, is my own. Each contribution to, and quotation in, this thesis from the work(s) of other people has been attributed, and has been cited and referenced according to the style for IEEE Transactions.

I have not allowed, and will not allow anyone to copy my work with the intention of passing it off as their own.

November 19, 2012

Eugene Dreyer

Acknowledgements

I owe a great deal of gratitude to my supervisor, **Stephen Marais**, for his many years of unwavering support and supervision.

Thanks is also owed to **Glen Newins** and the rest of the workshop staff, for their willingness to suffer the onslaught from the unceasing quantity and complexity brought about by my parts and drawings.

Thanks too is owed to **Tracy Booysen**, Chief Scientific Officer in the Department of Mechanical Engineering, for her technical assistance, cheerfulness and deft hand with a soldering iron.

No small gratitude is owed to my colleagues in the lab, especially **David Lwabona**, for his months of assistance especially after I broke my arm and he took on the dangerous job of becoming my hands by proxy.

A final thanks has to go to my family and friends for their support and sympathetic ears during times of heartbreak and hopelessness.

Contents

List of Figures

List of Tables

Glossary

Glossary

DAC Digital to Analogue Convertor. 67, 68

GUI Graphical User Interface. 84

HDPE High Density Polyethylene. 28

HID Human Interface Device. 75

NIST National Institute of Standards and Technology. 1, 101

TDP Team Description Paper. 12

UCT University of Cape Town. i, ii, ix, 1–3, 7

UGV Unmanned Ground Vehicle. i, 1, 2

USAR Urban Search and Rescue. i, 1, 14

Chapter 1

Introduction

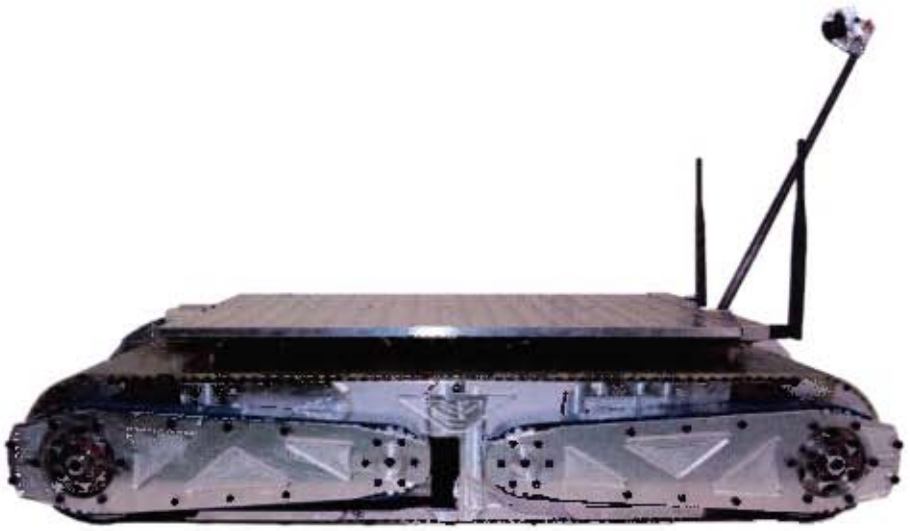

Figure 1.1. The Robotic Platform

A core impetus for technological development has always been to remove humans from jobs which are too dirty, dull and dangerous. Unmanned Ground Vehicles (UGVs) may address one or all of those criteria. Urban Search and Rescue (USAR), environmental assessment and mapping, specifically in hazardous environments meet all three criteria. While the level of danger involved would dissuade most from considering these tasks dull, few would deny that they are tedious, and when the level of danger is coupled with the level of tedium these tasks entail, they become prime candidates for robotic endeavors.

Research into rescue robotics began in earnest in 1995 after the loss of life in the Hanshin-Awajii earthquake in Japan, and the Oklahoma City Bombing in the United States. Technological development in the early 1990's had made it feasible that challenges faced by rescuers in these disasters could be alleviated by robotics. The next push came after the 2001 attacks on the World Trade Towers in New York City. The rescue efforts in the immediate aftermath of the building collapses utilised a number of robots up to the point of failure, and provided the first analysis of rescue robot performance in a real disaster area [1]. The robots used in search and rescue efforts at the World Trade Tower collapse are shown in Figure 1.2. The intersection of research interest, availability of technology and military funding for UGVs ensued with the subsequent wars in Iraq and Afghanistan. A number of commercial vehicles emerged to meet this market. One of the most successful, with real world law-enforcement, search and rescue and military use, is the iRobot® PackBot, shown in Figure 1.3.

The UCT Robotics and Agents Laboratory had historically been involved in various RoboCup Soccer leagues. In 2005 a RoboCup Rescue league was formed to evaluate current search and rescue technologies, and to provide a community around which search and rescue robotics development could cluster. This competition is spearheaded by the National Institute of Standards and Technology (NIST) which has developed a comprehensive set of performance metrics to assess the suitability of a platform for search and rescue operations [4]. These metrics are useful not only for search and rescue, but for general operation, particularly the metrics designed to assess mobility (such as that shown in Figure 1.4).

Figure 1.2: The various robots used in rescue operations at the World Trade Center collapse [2].

Figure 1.3: The iRobot® PackBot shown in one possible configuration [3].

Previous development of a UGV platform has taken place at UCT, the last iteration being that shown in Figure 1.5. The goal of this project is to continue the development of the robotic platform so that it may be useful for the transport of general purpose equipment, while meeting the requirements of the RoboCup Rescue competition.

The following chapters elaborate on the points brought up in this introduction. First is background research into the past and present of comparable robotic platforms, followed by a detailed list of specifications, then a detailed analysis of the design of the platform, and finally the testing and resulting conclusions and recommendations drawn from those tests.

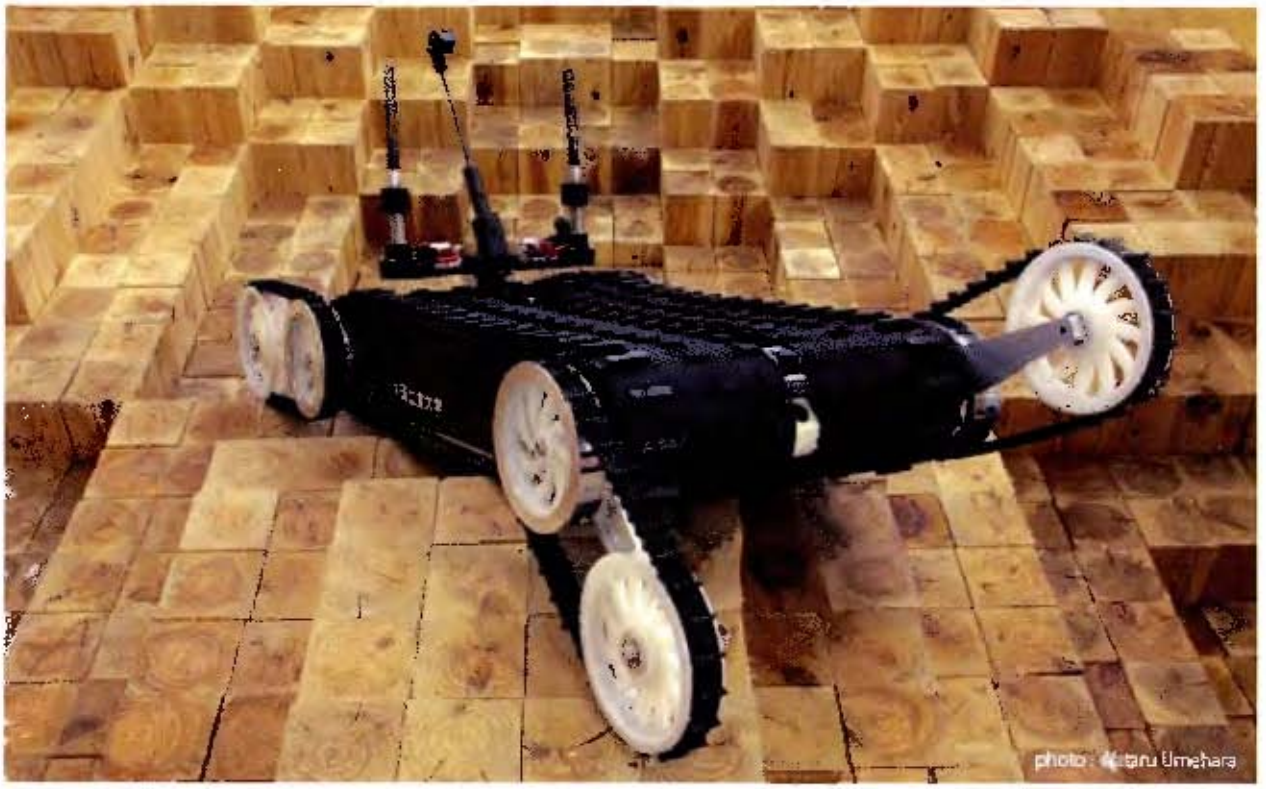

Figure 1.4: The Quince robotic platform moving over a stepfield designed to simulate rubble [5].

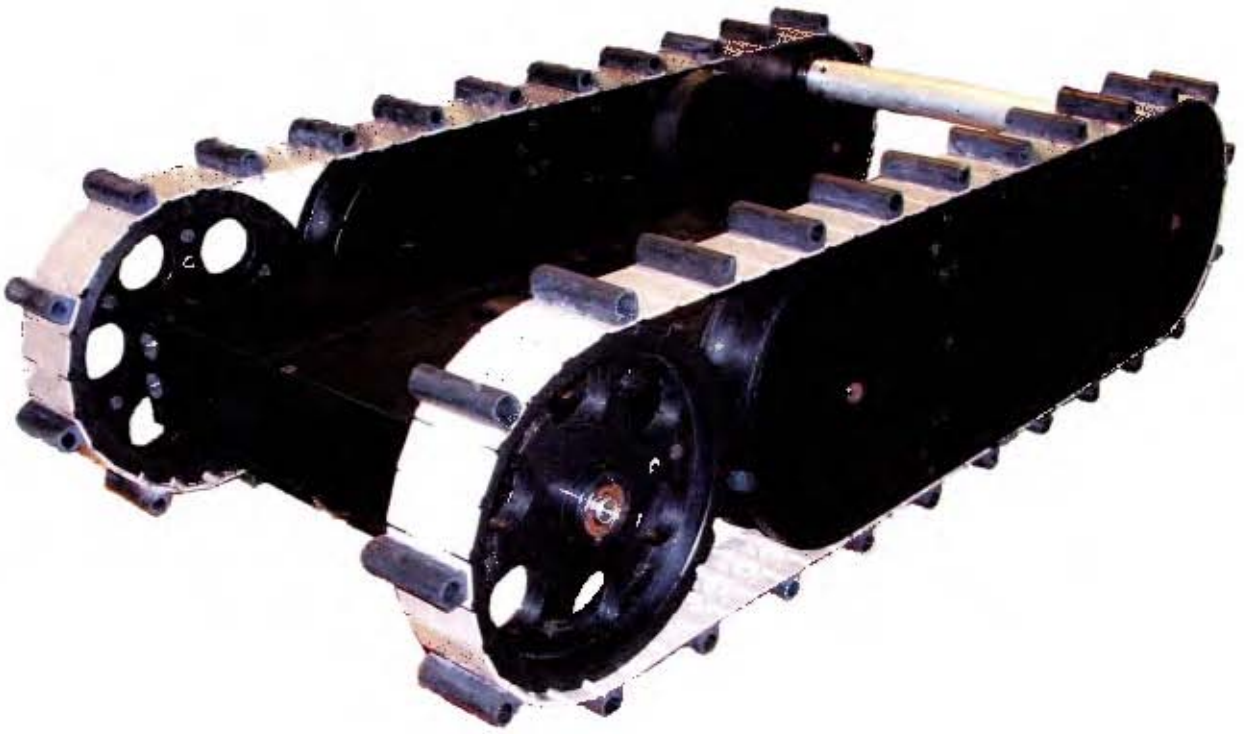

Figure 1.5: The previous generation platform developed in the UCT Robotics and Agents Laboratory.

Chapter 2

Background Research

In order to develop a rescue robot platform it is necessary to understand not only what robots are available today, what they look like and how they function, but also to consider how they have come to be that way. It is also necessary to consider the environment in which this platform will have to operate both today and in the future. This chapter looks at the evolution of modern day rescue robots and considers the environment and obstacles which it may have to traverse.

2.1 History of Rescue Robotics

A rescue robot platform as considered in this report can be defined as an unmanned ground vehicle operated by a human operator from some distance away. As the robot operates in environments designed for humans, the robot should also be physically no larger than a typical person. Additionally the robot is designed so that it can carry some arbitrary payload, with the single exception that the payload should not be a human operator.

For the sake of brevity this history does not attempt to document the innumerable research prototypes that have paved the road of robot development. Instead a focus is placed on commercial and military robots deployed at various times which could be considered a snapshot of the state of the art at that time. It is however worth noting that no robot mentioned in the following history emerged out of nowhere, each is representative of a steady evolution of the control, communication, actuation, power and other subsystems which make up such a robot.

2.1.1 Origins

Perhaps the first suggestion of what might be considered a teleoperated robot was by Nikola Tesla in a patent filing for a remote controlled boat intended for military purposes [6] as shown in Figure 2.1. This idea was never commercialised as described, however beginning in 1930 the Soviet army deployed what were known as Teletanks. These were Soviet T-26 tanks which were outfitted for remote control from a distance of 500-1500m. The tanks were designed to be driven by human teams to a safe distance from an enemy position. The tank crew would then exit the tank and control the Teletank from another tank in the battalion. The Soviet army created two battalions of Teletanks, one was destroyed by German bombing, while difficulties in navigating a cumbersome tank over large distances without visual aids on difficult terrain meant the remaining battalion never saw wide deployment. The Teletanks were a highly classified piece of Soviet technology and all tanks were to be remotely destroyed if in risk of being captured by enemy forces. The teleoperation system made use of a glass valve radio system which used solenoids to trigger pneumatic actuators. Due to the fragility of valves, the control module was separately suspended from the rest of the tank [7]. A destroyed Teletank is shown in Figure 2.2.

The level of technological sophistication of the Teletank is evident when one compares the Soviet systems to those employed by the German forces during World War 2 shown in Figures 2.3 and 2.4. In late 1940, developing on a recovered French prototype, the German Army deployed the Goliath mobile mine which carried 60kg of explosives in a small tracked vehicle using an electric, and later diesel, motor for propulsion. However the Goliath could be stopped by fire from a standard issue M1 Garand rifle, or alternatively by simply cutting the control tether as the Goliath was controlled by an operator through a cable. Approximately 7500 Goliath's were manufactured, it was not generally considered to be a success due mostly to its slow speed (9km/h) and inadequate ground clearance (11cm) [9]. After the fall of Nazi Germany, Allied forces found around 4000 Goliaths unused [10].

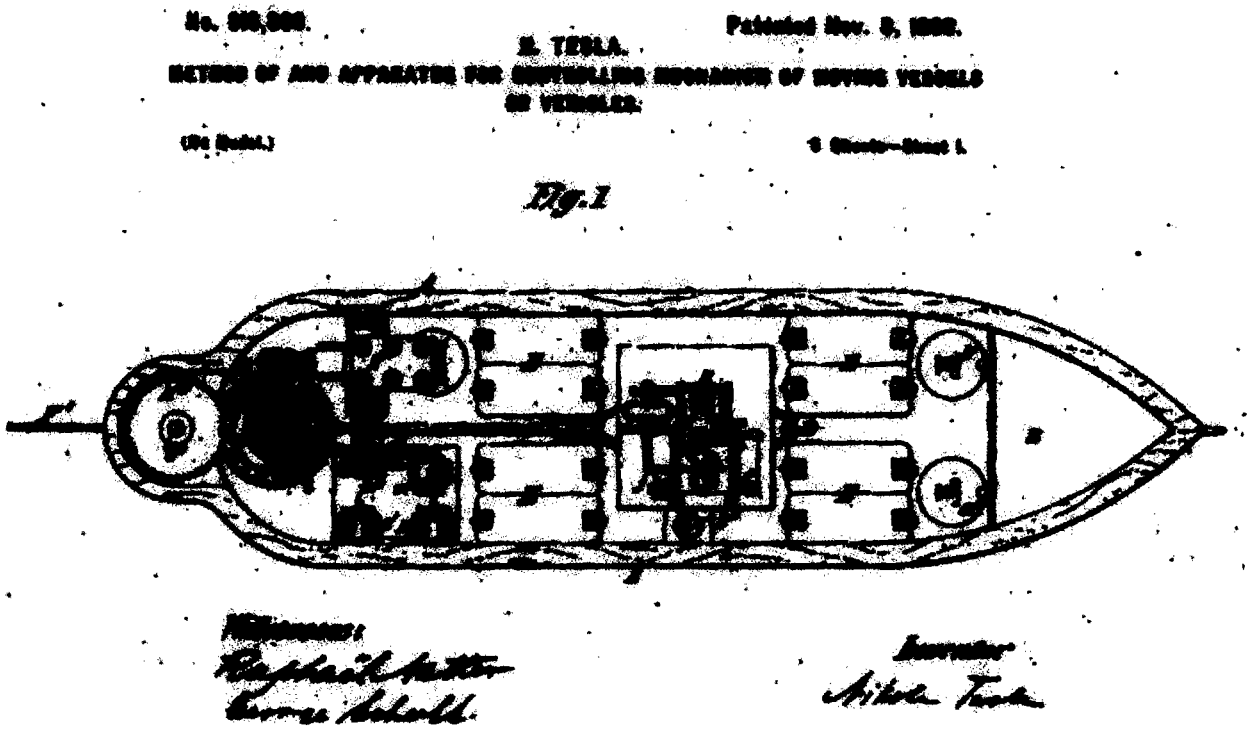

Figure 2.1: A figure from Nikola Tesla's patent for a remote controlled boat [6].

An interesting addition to this section is that of the Japanese Radio Controlled tank of Major Nagayama and the Type 98 Mini Engineer Vehicle "Ya-I Go" shown in Figure 2.5. These vehicles were predecessors of the Teletank and the Goliath tracked mine as the Nagayama tank was first tested in 1929 and the Type 98 Mini Engineer Vehicle in 1934. Despite this head start, both of these vehicles never saw active duty for reasons which are not entirely clear [12].

2.1.2 Transition into Modern Era

One of the first robot platforms recognisable as a modern rescue robot platform is the Wheelbarrow bomb disposal robot. The robot was created to stem the increasing fatalities of British Army bomb disposal experts while trying to destroy car bombs in Northern Ireland during the 1970's. Lieutenant-Colonel Peter Miller devised the robot based on a teleoperated lawn-mower he had designed for his own use. The Wheelbarrow name was given because the first model used a wheelbarrow as the body for the robot seen in Figure 2.6. The robot has continued to be developed for bomb disposal and is currently still in use with the latest iteration known as the Wheelbarrow Revolution shown in Figure 2.7.

2.1.3 Modern Era

The modern age of mobile ground based robotic platforms can be said to have begun in earnest with the advent of war in the Middle East post 9/11. Indeed, during the rescue efforts of the World Trade Tower collapse the state of rescue robotics was such that the robot rescue efforts were undertaken by researchers rather than rescue workers [17]. In late 2002 the first prototype robots were deployed in Iraq. These were iRobot Packbots sent to scout suspected bunkers, a job which previously required a soldier with a rifle. In the subsequent 9 years, iRobot® alone has sold over 4000 Packbots for use in Iraq and Afghanistan [18].

While iRobot is not alone as a supplier of ground robots to the military, its Packbot represents the state of the art for modern unmanned ground robots in active duty. The Packbot platform was designed from the start as a flexible platform which is capable of accommodating a variety of payloads. This flexibility has led the Packbot to be deployed in various guises. It has been deployed as an explosive ordinance disposal robot, a sniper detection robot, an explosives detection robot, a mapping robot, a scouting robot, a hostage negotiation robot and a research platform [3]. A few of its many possible configurations are shown in Figure 2.8.

Figure 2.2: TT-26 - Soviet Teletank based on the T-26 tank. This particular tank was destroyed by enemy fire [8].

Figure 2.3: German WWII Goliath Tracked Mine preserved in a museum [9].

Figure 2.4: German WWII Goliath Tracked Mine and operators on a field exercise [11].

2.2 Previous Prototype Robot

A prototype explorer robot platform was built in 2007 as an undergraduate project in the UCT Robotics Laboratory. The platform was originally conceived as a platform for transporting mapping equipment into mine shafts. It is shown in Figure 2.9. The platform features 2 driven tracks. In place of flipper arms the platform makes use of 3 wheels per track, with the front wheel being adjustable so as to allow the robot to climb objects up to 300mm in height. The geometry of the robot allowed for the track tension to remain approximately constant in its various orientations. The variable track geometry system is shown in Figures 2.10 and 2.11.

Each of the drive tracks and lifting arm is powered by a 65W brushless DC motor. The control system consisted of a Mac Mini receiving commands via WiFi and then transmitting them via serial communications to motor control boards developed in house. Power to the system was supplied by 6 12V Lead-acid batteries.

The platform was found to be underpowered for its mass of 62kg. Additionally the motor controllers were problematic and it was evident that they would require further development to be ready for deployment in the real world. While this prototype was not designed for use in the RoboCup Rescue competition, it does provide insight into the development path the current robot platform should take.

A RoboCup Rescue platform would need to be significantly lighter and smaller than this platform. The

August, 1930 POPULAR SCIENCE MONTHLY

NO MEN IN RADIO OPERATED TANK

In the future, monster implements of war may be controlled from a distance by the mere turning of a radio dial. A Japanese army officer, Major Nagayama, has invented a means of directing by radio the movements of a tank able to travel at a speed of five miles an hour.

Already wireless control of airplanes has been successfully attempted in England, according to reports. A master radio set took the place of the pilot, acting through tiny compressed air motors which worked the plane's controls.

Such a system of radio control as that of the tank or airplane does not imply the transmission of any appreciable quantity of power by radio. In the tank, for example, the radio impulses serve simply to trip a relay that sets in motion the tank's regular gasoline-driven machinery. Other relays, tuned to proper wave lengths, operate the steering controls.

The amount of power required to operate these relays is as little as that which brings the voices of Amos 'n' Andy into your radio receiver. Just as your own set supplies the power to amplify the faint impulses, so the relays in tank and airplane permit gasoline engines to supply the actual motive power. The transmission of real quantities of power without wires remains at present a dream.

Figure 2.5: The Nagayama remote controlled tank [13][14]

Figure 2.6: The wheelbarrow Mkl robot from 1971 [15].

Figure 2.7: The present day Wheelbarrow Revolution robot [16].

major contribution to the final weight of the robot was the batteries and plastic structure. Together these items contributed more than 50% of the mass. It also became evident that skid steering a tracked robot requires a substantial amount of slip on the tracks, and thus tracks with too much grip steeply increased the power requirements of the robot.

2.3 RoboCup Rescue Competition

This project began as a platform for exploring and mapping ore passes in mines, and over time developed into a general purpose robotic platform suitable for carrying an array of sensors into a variety of hazardous environments. It was decided that rather than focusing on the development of a robot strictly for mapping ore passes a robotic platform capable of performing mapping and participating in the RoboCup Rescue competition would be more versatile and provide a larger scope for future development. The RoboCup organisation formed in 1997 with the goal of advancing the state of the art of robotics and artificial intelligence. Through a yearly competition, academic efforts are focused on a set of common goals, allowing for swift and focused development, testing and collaboration. The main focus of RoboCup is on the development of the hardware and software for a team of entirely autonomous soccer playing robots [19].

Figure 2.8: From left to right, top to bottom, PackBots for: First Responders, Armed Forces, Combat Engineers, Sniper Detection, EOD Technicians and the PackBot Explorer [3].

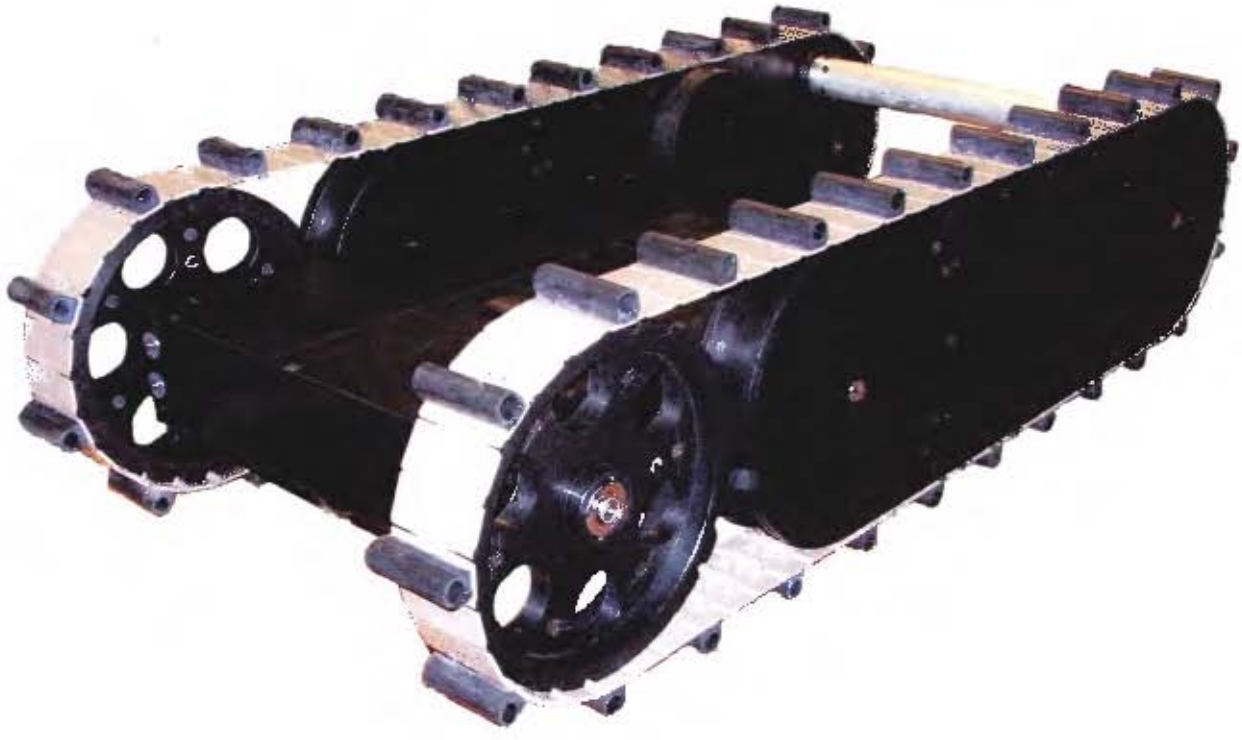

Figure 2.9: Previous prototype explorer robot.

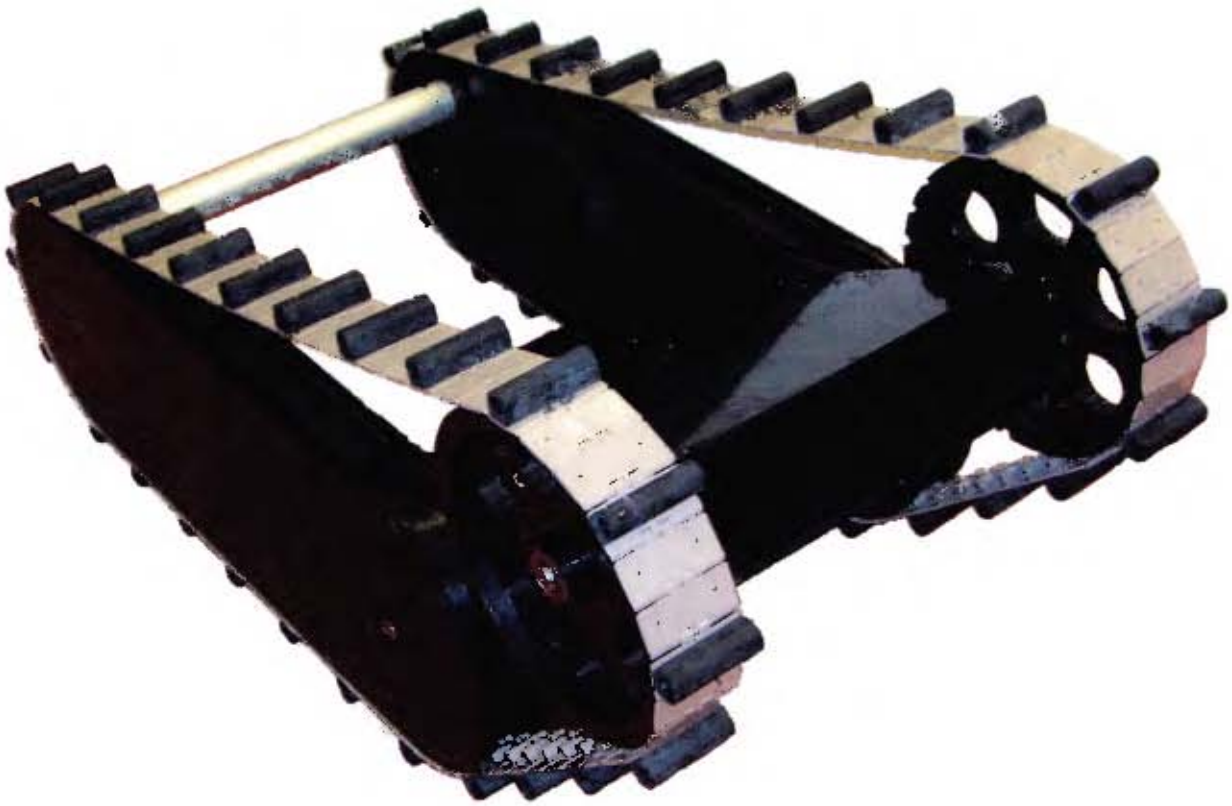

Figure 2.10: Prototype robot showing the function of the variable geometry track.

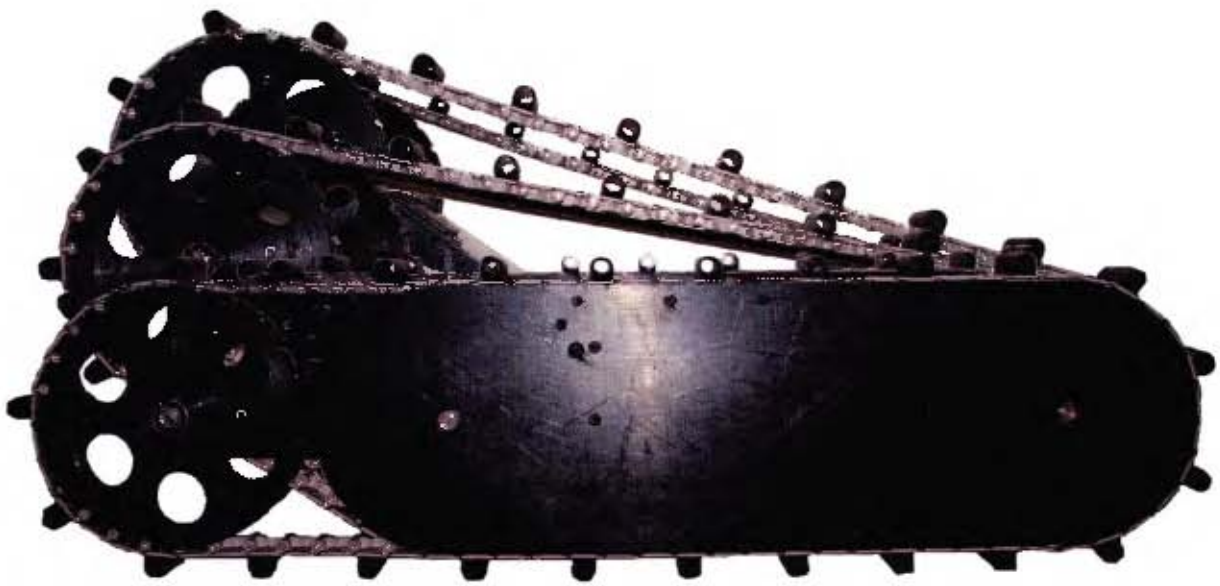

Figure 2.11: Side view of the prototype robot's variable geometry track in various positions.

RoboCup Rescue formed as an offshoot of the core RoboCup soccer challenges. The competition hopes to advance rescue robotics in the same way as soccer robotics, through a focus on a well defined challenge with constant collaboration and evaluation. Thus participation in RoboCup Rescue provides a rich testing ground, source of inspiration and testing metrics for development of this type of robotic platform [20].

Each team is required to submit a Team Description Paper (TDP) which is made publicly available. This TDP provides an overview of each team and their robot. From surveying these TDPs it is possible to determine the components and capabilities of each robot. In addition to learning from the present participants of RoboCup it is also necessary to look forward so that the expense of building a robot is not wasted in making a robot which becomes obsolete with the introduction of new rules. In order to spur development, each year the rules and challenges are incrementally changed and updated in order to make the competition more challenging and improve the capabilities of the participants in a real disaster environment. Fortunately a road-map is provided in the Statement of Requirements for Urban Search and Rescue Robot Performance Standards which is published by the NIST [4].

Further information was gleaned from attending the RoboCup Sympossium in Suzhou, China in 2008. This allowed for live observation of not only the obstacles which would have to be faced, but also the challenges faced by each team during operation.

2.3.1 RoboCup Arena Components

Figure 2.12: A typical RoboCup Rescue arena [21].

Rescue robots are evaluated according to their capabilities in mobility, sensing, mapping and manipulation. Various components in the arena (Shown in Figure 2.12) are thus designed to test the abilities of the robots in those categories. As the objective for this project was the design of a mobility platform, those components which test mobility were considered the most important. Although not a primary focus, keeping the sensing, mapping and manipulation challenges in mind is still important to ensure the robot is suitable for future development.

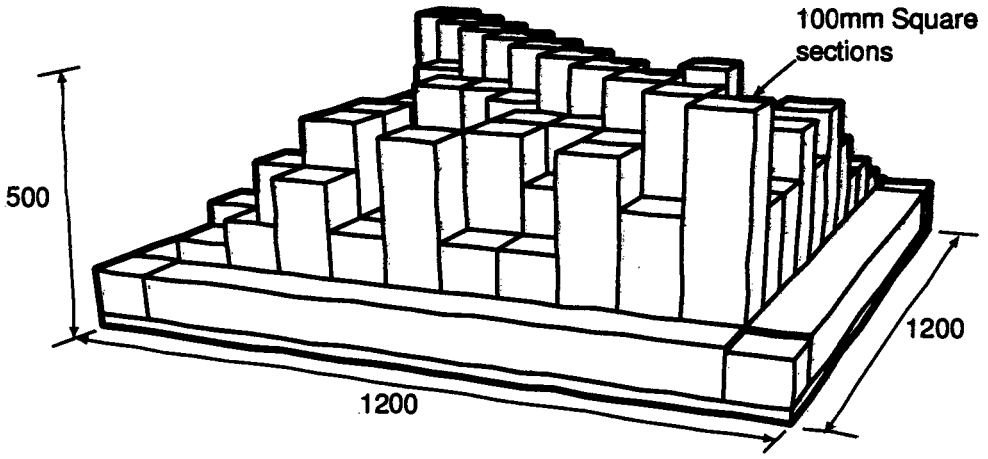

Figure 2.13: A typical stepfield pallet. (All dimensions in mm)

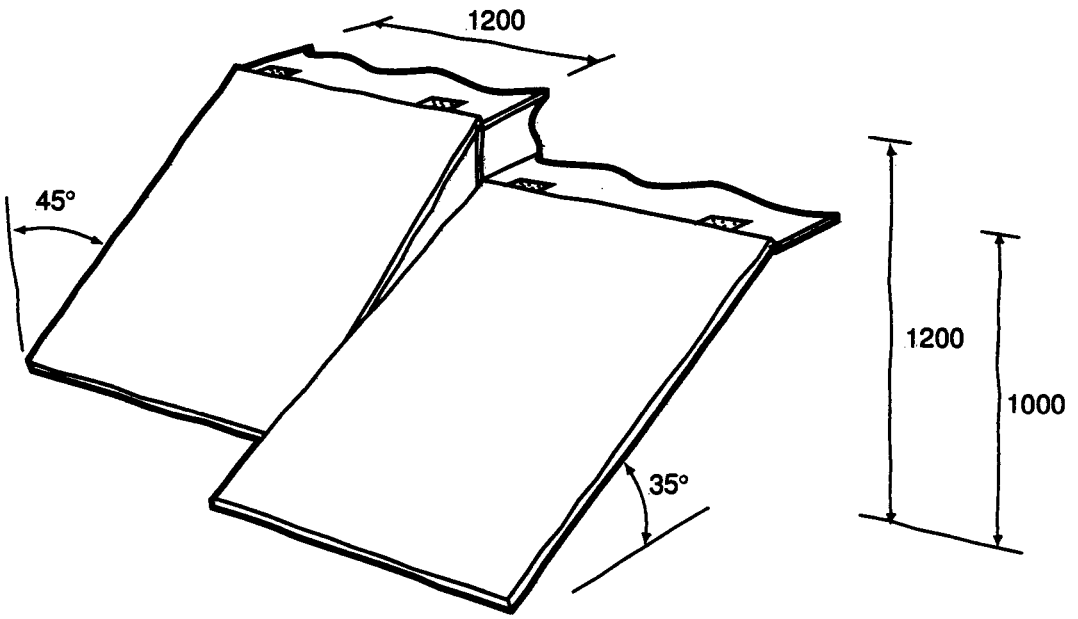

Figure 2.14: The 45°and 35°ramps. Ramps are often covered with carpet tiles or rubber mats to increase traction.(All dimensions in mm)

2.3.1.1 Stepfields

Stepfields are one of the most challenging obstacles for mobility. They are designed to simulate the challenges of crossing rubble but are standardised to ensure that the challenges of a competition can be recreated in the lab. An example of one stepfield configuration is shown in Figure 2.13.

2.3.1.2 Ramps

Two ramps are specified in each arena, one 35°, the other 45°. In Figure 2.14 the general construction is shown. While not a requirement to climb both ramps, the ability to climb both does allow the robot to save time navigating and is thus desirable.

2.3.1.3 Stairs

Stairs are common features across all kinds of buildings and as such a rescue robot has to be able to climb a staircase to be useful in real world situations. Stairs in the RoboCup arena are constructed as depicted in Figure 2.15.

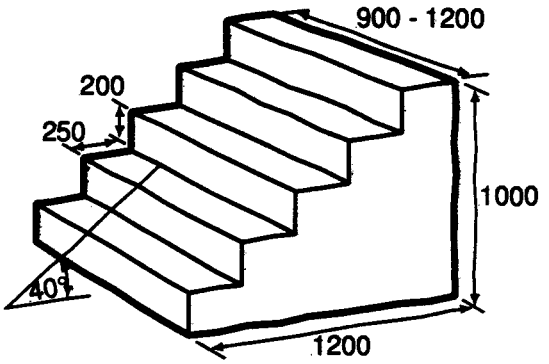

Figure 2.15: The staircase. (All dimensions in mm)

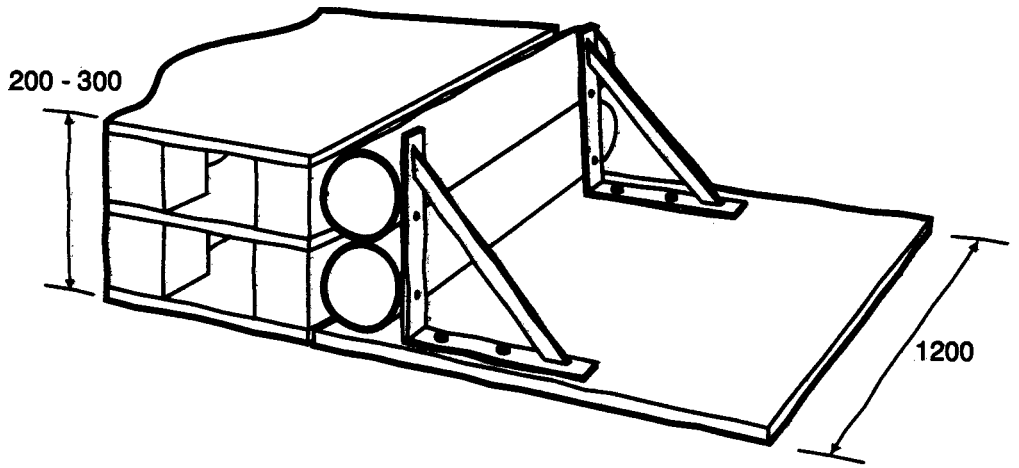

Figure 2.16: The pipe steps. The pipes are allowed to rotate freely, meaning the pipes themselves provide no traction for the robot. Most teams traverse these steps by using flippers to arch over the pipes. The height of the steps can be increased by including additional pipes. The setup shown gives a 200mm step, although future competitions will move to 300mm steps.(All dimensions in mm)

2.3.1.4 Pipes

To test the robot's and operator's ability to traverse a vertical obstacle, a test has been devised which requires the robot to climb a step which is made from 2 PVC pipes which are free to rotate. This layout is shown in Figure 2.16.

2.3.1.5 Victims

Various components which simulate a trapped person in a disaster zone are distributed around the arena. These components are grouped together and test the vision, CO_2, thermal and sound sensing systems. Not all items are present in each victim box. The victim boxes also contain a tumbling E's chart and HAZMAT signs to test the visual acuity of the robot. Finally a realistic doll, manikin or part thereof might be placed in the victim box to test systems which detect human forms or faces. A typical victim box might be constructed as per Figure 2.17.

2.4 Summary

The research produced a number of goals and observations critical to the development of the robotic platform. These are refined into concrete specifications in the next chapter. These specifications can then be used to establish the required performance and operation of a USAR platform. The areas of focus being;

2.4.1 Locomotion

Although a variety of methods of locomotion exist for a robot, every robot in RoboCup Rescue was either tracked, wheeled or some combination of both. While wheels were used in some robots, no wheeled robot was able to complete all of the mobility challenges such as stepfields, stair climbing, ramp climbing and the

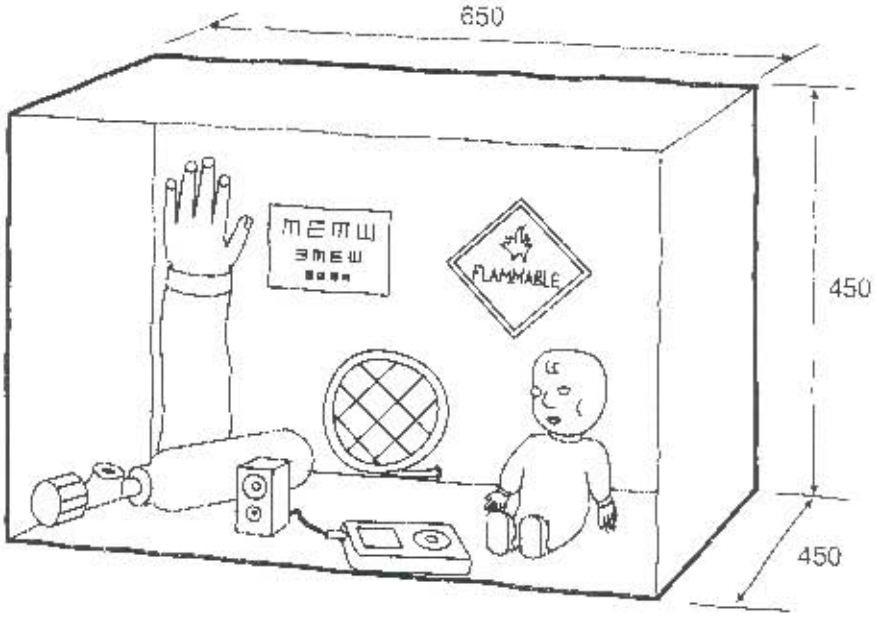

Figure 2.17: An example of a victim box

Figure 2.18: Australian RobotCup team CASualty are an example of a team that has deployed their own sensors on board a commercial robotic platform, in this case the iRobot Negotiator [22].

pipe steps. This observation would seem to indicate that tracks are the most effective drive system for a rescue type robot that can operate in all areas of the RoboCup arena.

2.4.2 Track Design and Construction

Although not catastrophic, the most frequently observed mechanical failure was that of the track elements for tracked robots being torn off the track. Especially in stepfields where it occasionally occurs that the entire drive force of the robot is transferred through one track element.

2.4.3 Motor Selection

A minor observation was the widespread use of Maxon brushless DC motors among RoboCup teams, not only in rescue but also many other fields. Maxon provides an integrated solution for motors, gearboxes and controllers. In the face of problems previously encountered with developing our own brushless motor controller, a Maxon solution, although expensive, held the promise of providing hassle free motor control. Maxon motors had already come to our attention as a world leader in brushless DC motors and are used in a number of demanding applications such as NASA's Mars rover [23].

2.4.4 Beaching

In terms of mobility most tracked robots were particularly susceptible to beaching especially in the stepfields. This typically occurs when a robot drives its chassis onto an obstacle which in turn takes weight off the robot tracks and thus makes removing the robot from the obstacle more difficult. While flippers are useful in this situation, vital time is lost trying to free the robot.

2.4.5 Space Limitations

The first limitation on the size of the robot is the layout of the arena itself. In plan view, the arena is made of a number of squares, each square being 1200mmx1200mm as shown in Figure 2.12. This provides the upper limit for the length of the robot, although in reality, navigating around corners or obstacles would require a smaller robot. The most stringent requirement on the size of the robot is a recently introduced rule for the robot to enter into the arena through a 24inch triangular opening, as commonly created by rescuers into the sides of buildings.

2.4.6 Weight

The weight of the robot ultimately determines how fast the robot can move, how steep a slope it can climb and the stresses put upon the components in the drive-train. Points are also deducted for each person who is required to enter the arena when deploying the robot to incentivize teams to minimize the number of personnel in a potentially dangerous zone. A robot which is reasonably light, less than 25kg, could conceivably be deployed and operated by one person.

2.4.7 Robustness

The major selling point of the PackBot is how robust the platform is. Indeed it is claimed that the PackBot can withstand being thrown out of a low flying helicopter [24]. On the other hand many robots in the RoboCup competition suffer from unreliability. The robots and subsystems are frequently developed on a tight schedule with limited testing. Most robots were constructed in an ad-hoc manner to get the systems working, but little attention is paid to ease of maintenance and repairs to the robot. Much time at RoboCup was seemingly spent taking the robots apart and attempting to troubleshoot subsystems. To attempt to address the issue of reliability teams are increasingly purchasing ready-made platforms to deploy their own equipment on (See Figure 2.18).

2.4.8 Tool Requirements

Many teams required a large amount of tools to be shipped with their robots to RoboCup. Apart from the cost and the logistical difficulties of transporting all of these tools, having to frequently change tools while disassembling a robot wastes valuable time. While it is conceivable that there could be a need to use more than one size of fastener on the robot, consideration to this factor in the design of the robot should make it possible to minimize the requirement for a large number of tools.

2.4.9 Operation

Historically unmanned ground vehicles have faced a major problem in the difficulty of their operation. Certainly before the advent of digital imaging, robots such as the Teletank and the Goliath tracked mine were doomed from the outset as they were almost impossible to operate. Modern commercial robots face the same difficulties. Accomplishing tasks and navigating the robot is hugely difficult and requires a trained operator to simply manoeuvre. RoboCup also highlighted the importance of a skilled operator. A focus on a robot which is easy to operate and requires as little skill as possible is perhaps more important than any other technical feature.

2.4.10 Vision

To emulate real world conditions, the operator of the robot has to rely on the onboard cameras to navigate the arena. Due to the quantity and variety of obstacles in the arena it is hugely advantageous to be able to see the entire robot while navigating. This is typically accomplished through the use of a camera mounted on the end of a stalk overlooking the robot from behind. Another observation is the importance of minimal lag in the control loop. Images or control inputs which lag are detrimental to the operators confidence and speed in placing the robot. It is also necessary to have the capability to look into enclosed spaces, most teams use some kind of pan-tilt camera mechanism on an arm for this. The challenge of maneuvering in the tight confines of the arena also means that forward and rear facing cameras are often helpful for navigation.

2.5 Concluding Remarks

Using the insights and knowledge gained in this Chapter it is now possible to define the performance desired for the platform. The next Chapter lists the desired performance for various systems and the motivation behind those decisions.

Chapter 3

Specifications

From the Background Research in Chapter 2 it is possible to define the problem that this platform is trying to solve. The specifications which follow provide concrete goals against which the platform can eventually be evaluated to determine how well it performs against initial requirements.

3.1 Table of Specifications

#	Description	Value
	Dimensional Specifications	
1	The trackbase of the robot should allow the robot to be in contact with at least 2 steps at all times while climbing a standard staircase.	650mm
2	The cross-section of the platform should be such that it is able to fit through a standard entry triangle used by rescue workers to enter collapsed structures.	24" equilateral triangle
3	The weight of the robot.	< 20kg
	Functional Specifications	
4	The robot should have sufficient power and torque to navigate all RoboCup Rescue arena components.	Yes
5	The maximum speed of the robot on flat ground.	1.4m/s
6	The robot should possess the ability to vary its geometry.	4 Flipper arms
7	The robot should use commercial batteries and chargers.	Yes
8	The technology to communicate with the robot	802.11A Wireless.
9	The platform should allow functional modules to be easily connected by supplying power and inter-module communication infrastructure.	12V, 5V and Ethernet
10	The time delay between a control input and the corresponding action occurring on the robot.	< 30ms
11	Tools required to completely disassemble the platform.	< 3
12	The robot should have a camera mounted on a stalk capable of providing an overview of the entire robot.	Yes
	Drive System Specifications	
13	The portion of the platform not covered by drive track.	< 100mm
14	The construction of the tracks.	Single piece
	Software Specifications	
15	Control software should start ready to function and require no, or minimal user input before control of the robot can begin.	Yes
16	The user software should be as easy to use as possible requiring minimal operator training.	Yes

Table 3.1: Table of Specifications

3.2 Justification of Specifications

1 A shorter trackbase is desirable as it increases the manoeuvrability of the platform. For stability and speed while climbing a staircase, the tracks should be in contact with at least 2 steps at any one time. Using the flippers to temporarily extend the trackbase while climbing stairs was deemed undesirable

due to the amount of time which would be wasted in placing the flippers in the correct positions. The image in Figure 3.1 shows the intended method of climbing stairs.

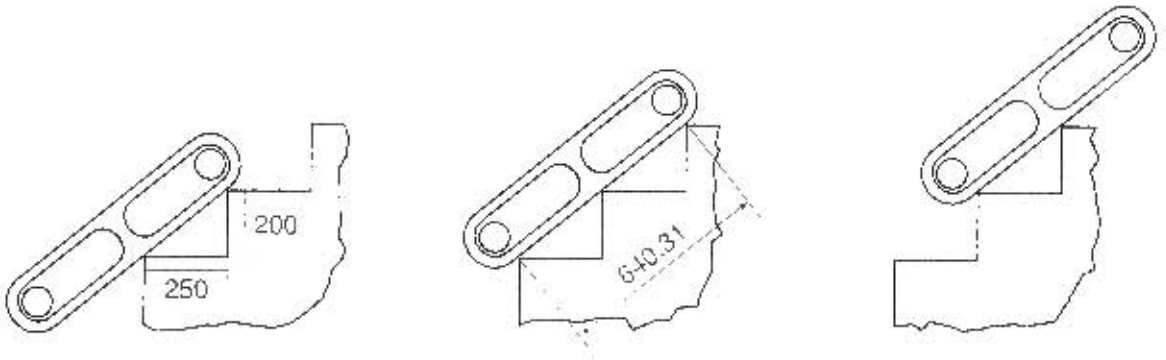

Figure 3.1: The intended method of climbing stairs. Notice that the robot is in contact with at least 2 steps at all times. The dimensions of the stairs are given by the NIST [4]

2 Standard procedure for rescue personnel entering buildings which are no longer accessible through the usual entrances is to cut a 24 inch equilateral triangle into the side of the building [4]. To be useful in rescue environments, the platform should be able to fit through this entry triangle as shown in Figure 3.2.

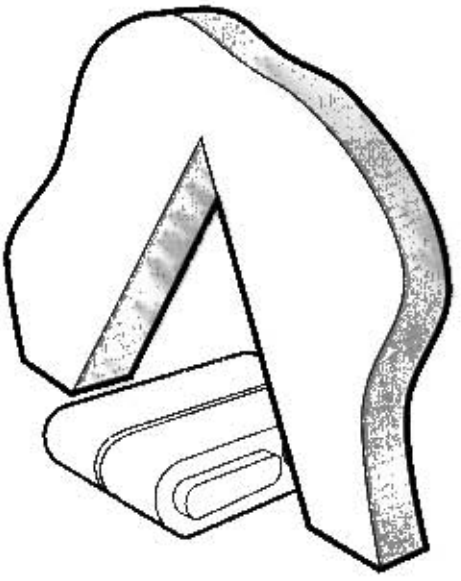

Figure 3.2: The entry triangle a robot must pass through to enter the arena.

3 It is desired that the robot should be portable by one man, as such its weight should be no more than 20kg.

4 The RoboCup Rescue arena has been designed to simulate a real disaster environment. To be useful in a real disaster, the platform should at least be able to navigate the challenges in a RoboCup arena.

5 This robotic platform is envisaged to replace a human rescue worker, as such the robot should not need to travel faster than a human would. Human walking speed is generally accepted to be around 5km/h which is approximately 1.4m/s.

6 Flippers are utilised in many RoboCup and commercial robots. Flippers allow a robot to have a configuration which can be dynamically altered, and also provide a means to right the robot should it topple.

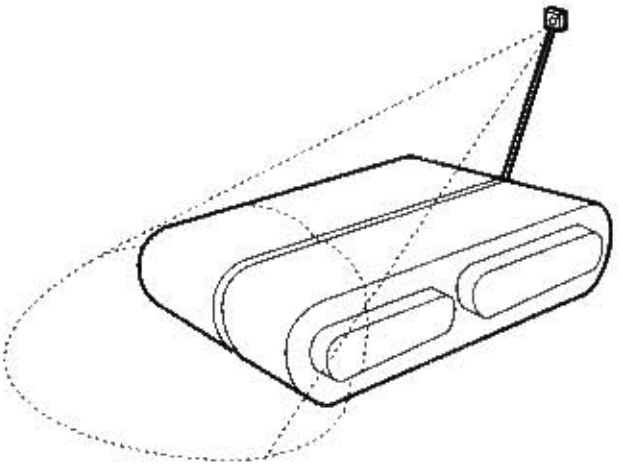

Figure 3.3: An example of a stalk camera and field of view.

7 Using commercial batteries and chargers provides advantages over custom made battery packs in that, providing the batteries are well chosen, spares should be available worldwide, they should be cheaper as they are mass produced and they should be physically and functionally more robust.

8 802.11a Wireless is the designated wireless standard used in the RoboCup Rescue competition. It provides advantages over the more common 802.11g wireless in that it operates at 5GHz rather than 2.4GHz. It thus provides superior signal penetration and conveniently avoids the overcrowded 2.4GHz band.

9 This platform is intended as a research platform onto which a variety of sensors and other equipment can be installed. As it is unknown what these future systems might be, the robot should provide a communications interface and power to any subsystem which may be installed on the platform at some future date.

10 Previous laboratory experience qualitatively indicated that an unresponsive robot was hugely challenging to control. RoboCup experience further reinforced this observations, as lag increased, video feeds from robots became less and less useful. Research indicates that delays become noticeable above 30-40ms [25][26].

11 Using fewer tools reduces the shipping weight and cost of the robot platform, and also allows for the platform to be more easily and quickly assembled and disassembled.

12 Observations of teams at RoboCup indicated that a stalk camera (as shown in Figures 3.3 and 3.4) greatly reduced the difficulty an operator had in controlling a robot.

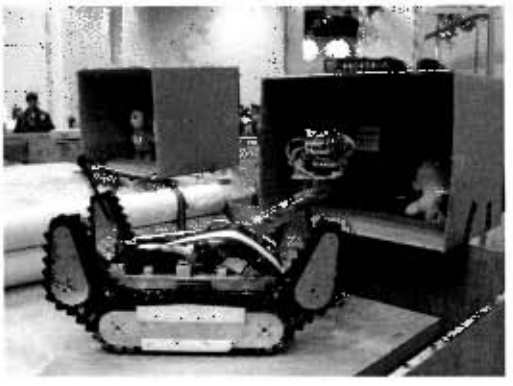

Figure 3.4: A stalk camera on the Resquake RoboCup Rescue robot [27].

13 Flippers are helpful in freeing a robot from a situation in which it is stuck, but it is far easier and faster if the robot would not have gotten stuck in the first place. Making the drive tracks as wide as possible minimizes the likelihood that any part of the robot can become stuck on an object in the environment.

In terms of the RoboCup Rescue arena, the stepfields present the greatest potential for getting stuck. Each stepfield block is 100mm wide [28], thus a gap between tracks of less than 100mm should be sufficient to allow the platform to navigate a stepfield without beaching on a stepfield block as can be seen in Figure 3.5.

Figure 3.5: The Quince robotic platform navigating stepfield. Note the use of tracks with a small gap between them [5].

14 The most commonly observed mechanical failure at RoboCup was that of the track lugs of tracked robots ripping off their tracks. This not only wastes energy and potentially destroys the arena (an offense which may cause points to be deducted from one's score) but also necessitates removing the track and replacing the track element, a potentially avoidable waste of time. By making the tracks and lugs a single piece of material it is hoped that track failures can be entirely avoided. The Pelican Team which uses a custom moulded track as seen in Figure 3.5 provides some evidence as to the effectiveness of this approach.

15 Time taken setting up the robot and control station is time that could be better spent navigating the arena. As such the time required to start up the robot and operator station should be a minimum, especially any start up task which requires waiting for the operator should be performed automatically where possible.

16 As noted in background research, the single most important technical feature is that the robot be easy to use as this ultimately seems to be the deciding factor in the success of a robot.

Figure 3.6: A simple interface used by the Iranian Resquake team. This set-up won the best user interface award at the 2008 RoboCup [27].

3.3 Summary

The specifications describe a tracked robotic platform, with wide drive tracks and 4 flipper arms. The requirement for the platform to fit through a 24" entry triangle results in a cross section similar to that of a human torso, while the length of the platform should be in the region of 650mm. Communication with this platform is to occur via 802.11A wireless, and dedicated sensors on board the platform should consist of at least a camera mounted on a stalk so as to provided an overview of the robot while operating. In addition to this sensor the robot should provide the mechanical, electrical and communication infrastructure for additional sensors and equipment to be fitted.

The next step in development is to determine the layout and size of the robot in more detail, and refine the specifications where possible to allow detailed and final decisions to be made. This process follows in the following chapter, Chapter 4.

Chapter 4

Conceptual Design

Building on the specifications in Chapter 3, a conceptual design which describes the basic operation and lays out what the major components are and how they should be arranged was iteratively developed. The objective of this design stage is to gain the information required for the detailed design to be performed. Once a detailed design is completed the robot can be manufactured using the 3D models generated and the required components can be ordered.

4.1 Concept Development

From the specifications, the starting point for the platform is a pair of drive tracks which each cover about 50% of the width of the robot as shown in Figure 4.1. This arrangement has the advantage that the platform can operate while inverted.

An additional requirement of the specification is that the platform has 4 flipper arms, a layout shown in Figure 4.2.

These arrangements allow for payloads to be contained within the robot itself, however there is the disadvantage that sensors such as cameras or laser scanners which need to be on the outside of the robot and are ideally forward facing cannot be accommodated on the platform. As such the decision was made to narrow the tracks slightly to reveal a central spine on the robot. On this spine an arm can be be fitted which

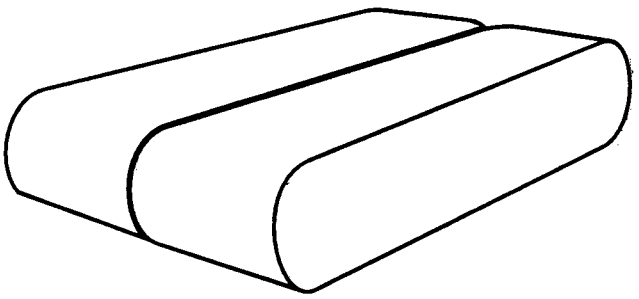

Figure 4.1: A platform concept showing wide tracks.

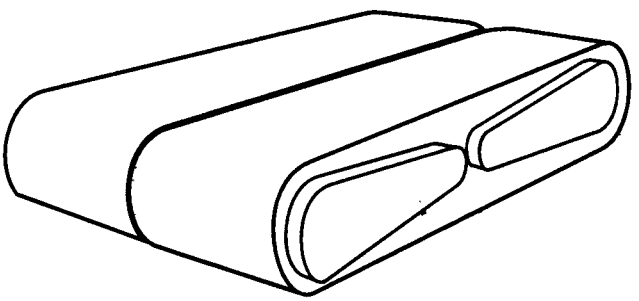

Figure 4.2: A platform concept showing wide tracks with flippers.

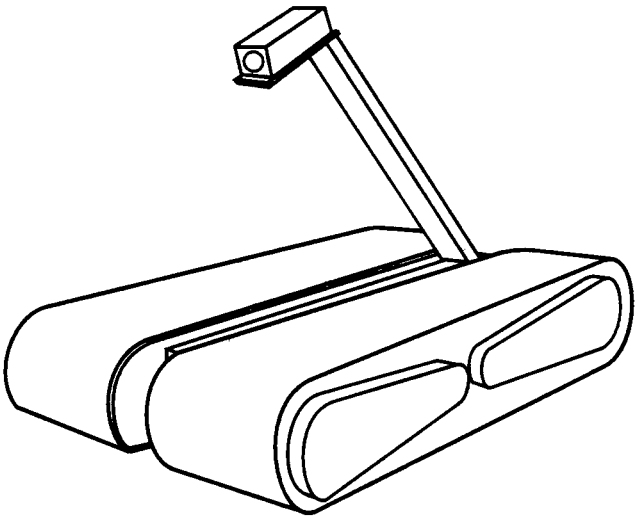

Figure 4.3: A platform concept showing wide tracks with flippers and space to allow a camera on a liftable arm to dock between the tracks.

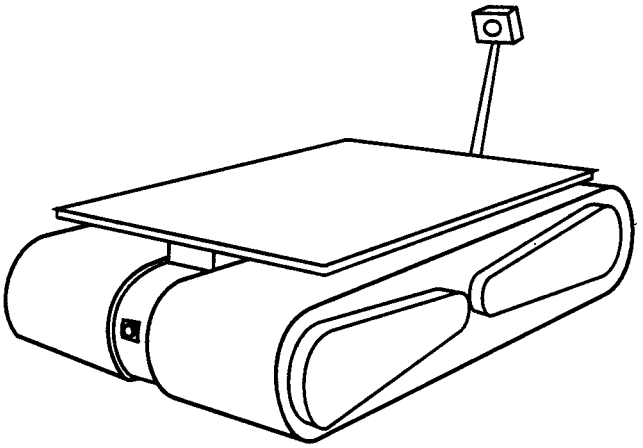

Figure 4.4: A platform concept with wide tracks, flippers, a stalk camera and an accessory deck.

could house a sensor pack at the end of the arm. This arm could be stowed between the tracks to still allow the robot to be inverted and to protect the sensor payload should the robot fall or should debris fall on the robot. This arrangement is shown in Figure 4.3.

This concept, while rugged, provides a very limited amount of space for external payloads to be mounted onto the robot. This layout has the further drawback that only a simple 1 or 2 link arm could feasibly be fitted to the robot. As such the concept in Figure 4.4 was developed. This concept compromises the ability of the robot to operate while inverted, it does however provide a relatively large amount of space for external sensors to be added to the platform at a later date. This compromise was deemed to be acceptable as adding unplanned external accessories to the robot was decided to be preferable to the ability of the robot to operate while upside down. Forward and rear facing cameras as well as a stalk camera are incorporated into the spine for use as navigation aids.

4.2 Battery Pack

The platform which was previously developed as described in Section 2.2 on page 7 made use of lead acid batteries primarily for their low cost, the drawback of this decision was that the batteries alone weighed 15kg, this is unacceptable for a robot that has to be man-portable as the maximum weight for a man portable robot can be considered to be around 25kg. In choosing a battery type for this robot, it had been chosen as a specification that the platform should make use of commercial battery packs. It was thus helpful to consider the various commercial battery technologies available and compare their relative strengths and weaknesses as they relate to this project. The areas in which the batteries were compared is as follows:

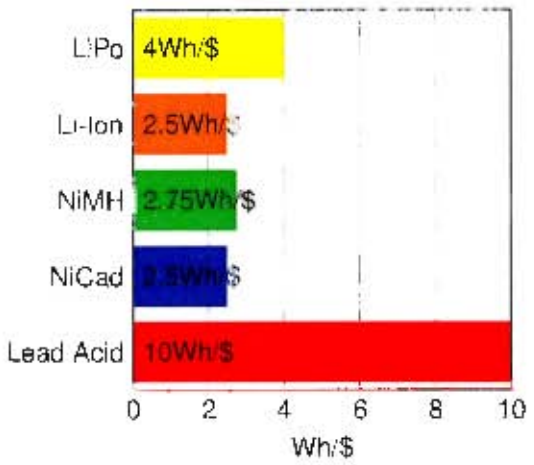

Figure 4.5: The relative cost of various battery technologies.

Low Cost The cost per Wh for each battery type.

Ruggedness An estimated measure of how well the particular battery technology might perform under heavy discharge, shock loads and other adverse conditions which are likely to be encountered on a rescue platform.

Availability An estimate of how difficult it might be to find a replacement battery if necessary, especially in a foreign country.

Low weight A measure of the weight per Wh of energy for each battery technology.

The most prevalent battery technologies at the time of comparison were lead acid, NiMH (Nickel Metal Hydride), NiCad (Nickel Cadmium), Li-Ion (Lithium Ion) and LiPo (Lithium Polymer). Data was gathered on each battery technology which was used to quantify the comparison [29]. The comparison which follows ranks each of the battery technologies relative to each other. All numbers in these comparisons are chosen such that higher numbers indicate an increasingly preferable solution.

4.2.1 Low cost

The price per Wh of each battery type is compared in the bar chart shown in Figure 4.5.

4.2.2 Ruggedness

Lead Acid Probably the most rugged battery for this application, is capable of supplying high surge currents and is not too adversely affected by high discharge rates and shock forces. It can also be very easily charged.

NiCad Is even more rugged than lead acid when considering only discharging, however these batteries are particularly susceptible to changes in temperature and thermal runaway is possible during charging.

NiMH Slightly less rugged than NiCad batteries, but still suitable for use in the platform. They do have the disadvantage of fairly high self discharge, and their capacity degrades fairly quickly with use.

Li-Ion Has low self-discharge, however the capacity of these batteries degrades fairly quickly even when not being used. Lithium Ion batteries are also especially susceptible to overheating, over-discharging and overcharging, any one of which can permanently destroy the cell. Using many of these battery cells in parallel is the usual method for allowing high current draw from this technology.

LiPo These cells while potentially more forgiving than Li-Ion batteries, do have the disadvantage that should their limits be exceed they are particularly susceptible to explosion. While each new crop of Lithium-Polymer batteries which is released improves upon this, their propensity to explode when subjected to shock loads makes their fragility a concern for this platform.

The estimation of the relative ruggedness of each battery is rated in the chart in Figure 4.6.

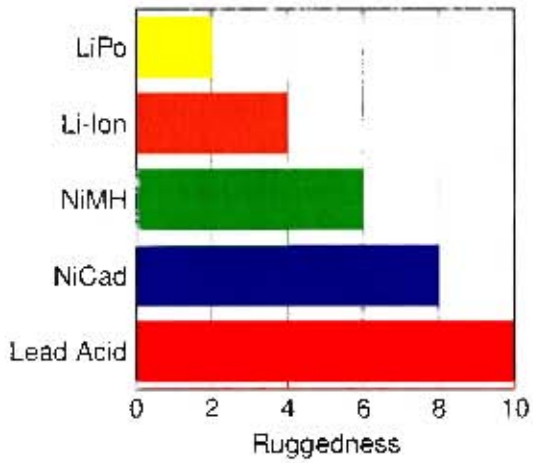

Figure 4.6: Estimation of the ruggedness of suitable cells for each battery technology.

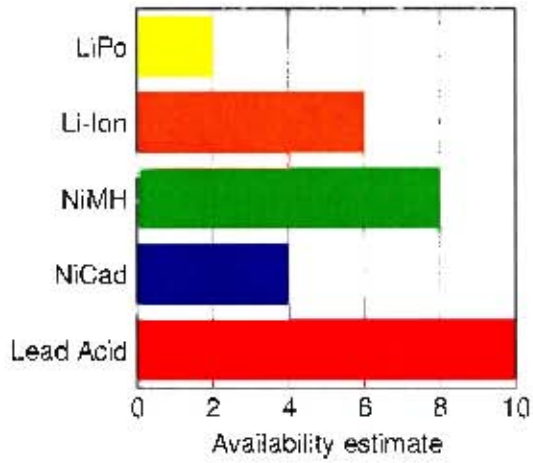

Figure 4.7: Estimation of the availability of suitable cells for each battery technology.

4.2.3 Availability

Lead Acid This type of battery is probably the most widely available battery technology in the world.

NiCad Formerly a relatively popular battery technology, it has largely been replaced by NiMH.

NIMH Was the most popular rechargeable battery technology, has been almost completely replaced by Li-Ion in low power applications, however, still enjoys relative popularity for use in portable tools although this is diminishing as the cost of Li-Ion battery technology decreases.

Li-Ion Due to the almost exclusive use of these batteries in cellular phones this technology can be found in almost every corner of the globe. However, the cells employed in cellular phone batteries would be prohibitively expensive and complicated to adapt for use in high power applications. Suitable lithium ion batteries are thus probably less widely available than suitable NiMH batteries.

LiPo This battery technology has a very specific set of applications and as such is relatively rare.

An estimation of the relative availability is shown in Figure 4.7.

4.2.4 Low Weight

This energy per unit weight for each battery technology [29] is visualised in Figure 4.8.

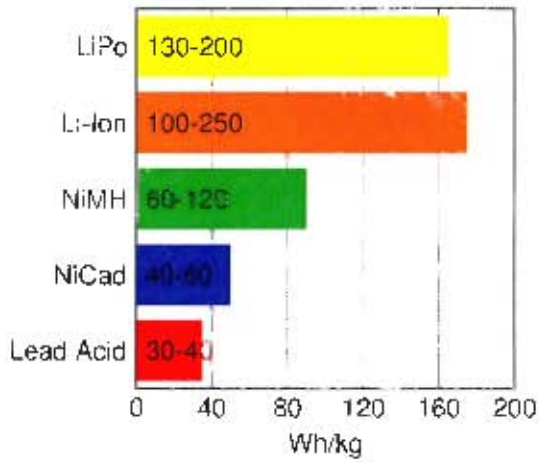

Figure 4.8: Battery technologies compared by the average amount of energy they carry per kg of mass.

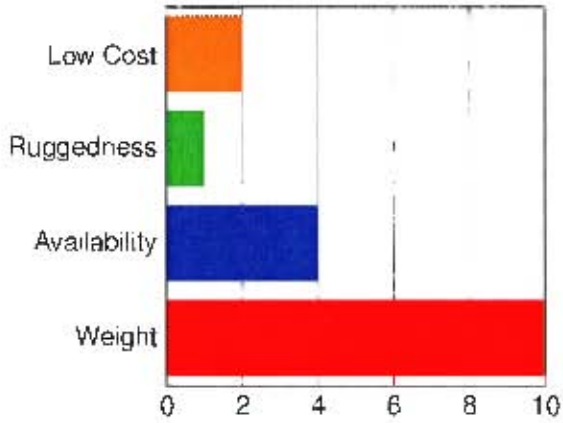

Figure 4.9: The weighting to the factors considered for each battery technology.

4.2.5 Comparison

To aid in the comparison, the relative strengths and weaknesses of each battery technology are combined and each battery technology compared. Each factor was given a weighting according to the perceived importance of that particular factor.

Weight This was deemed to be the most important factor for consideration as it effects the portability, speed and motor requirements for the platform.

Availability This was decided to be slightly less than half as important as low weight.

Ruggedness As the platform is still in development this was chosen as the least important factor providing that the battery chosen was sufficiently rugged.

Low Cost This was chosen as also relatively unimportant factor in comparison to the other factors as the budgetary constraints for this platform were flexible.

Using these weighting factors each battery technology can be relatively evaluated for use in this platform Each factor was converted to a value between 0 and 10 and had the applicable weighting factor applied. The results are shown in Figure 4.10.

This comparison would indicate that a commercial Li-Ion battery pack should be considered the primary candidate for use on the platform. Power tool batteries are ideally suited for deployment on this platform as they are designed for use in high current draw applications and also are available with their respective chargers.

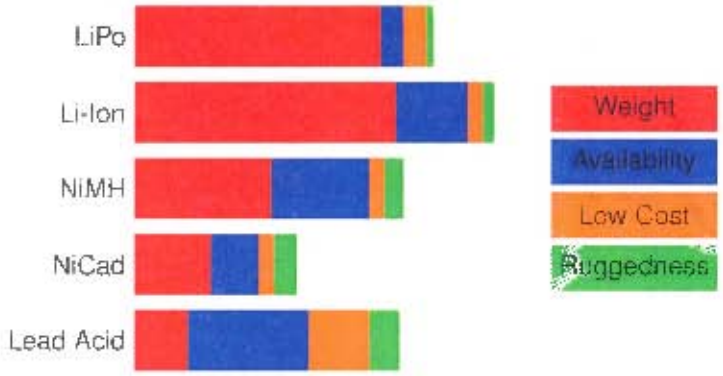

Figure 4.10: The weighted comparison for each battery technology.

Figure 4.11: The 18V 3.0Ah Makita Li-Ion battery [30].

Enquiries with local suppliers indicated that there were a number of available options. Batteries were available in 12V, 14.4V and 18V configurations. Higher voltage power supply was preferable as it would allow higher power motors to be used with lower current losses. The motors selected came in both 24V and 36V configurations, as such a decision was made to employ the 18V 3.0Ah Makita batteries in Figure 4.11. These were readily available through a local supplier.

4.3 Material Choice

In the design of the previous prototype robot in Section 2.2, the decision was made to use the polymer High Density Polyethylene (HDPE) over aluminium for the construction of the robot. HDPE while less stiff than Aluminium, was at the time significantly cheaper and also allowed for higher speed machining. During the course of manufacturing it became apparent that there were some issues with the machinability of HDPE. Internal stresses within the material resulted in parts buckling noticeably when voids were machined into them. In addition, local supplies of HDPE proved to be hugely variable with as much as 20% variation in thickness on some cast plates, this resulted in having to order substantially thicker material than desired and machining away the excess to attempt to achieve the desired size uniformity, however this only exacerbated the buckling problem. A further negative for HDPE was its price. During construction of the first prototype in 2007, HDPE was substantially cheaper than aluminium, however, over the passing months as the oil price rose, so did the price of HDPE as it is an oil based product. During that same period the price of aluminium remained approximately steady. The result was that at the time of manufacture, it cost only slightly less to make a part from HDPE than it did to make the same part from aluminium. As aluminium is stiffer than HDPE, it became possible to design aluminium parts that were stiffer, smaller, lighter and cheaper than the equivalent parts made from HDPE, with the only downside being the increased complexity of the design and machining operations.

4.4 Motor and Controller Selection

The previous prototype robot suffered from 2 problems with regards to its drive system. The large weight of the robot meant that the 65W motors (shown in Figure 4.13) were not powerful enough to achieve the required performance. The motors had also been supplied as part of an arrangement with a local firm which

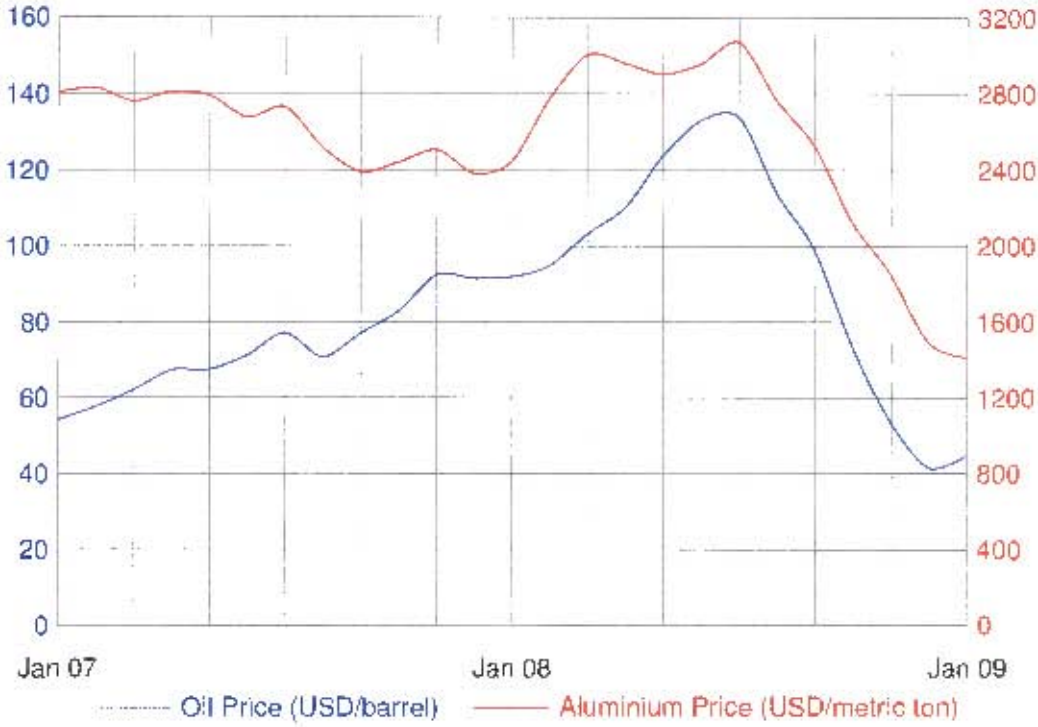

Figure 4.12: Oil and aluminium price movement[31].

Figure 4.13: The 65W Brushless DC motor and controller used in the previous explorer platform.

was importing the motors and controller integrated circuits for use in their own systems. A move away from those particular components meant that both the motors and controllers had become difficult to obtain as the suppliers were unwilling to ship the small quantities required for the platform. The motor controllers were also problematic for some other reasons. The first problem was that the controllers had a limited range of acceptable input voltages, so when the batteries were fully charged the input voltage was too high, and the input voltage sunk too low to power the controllers as the battery discharged even though the battery had not been fully discharged. The second problem which became apparent during testing was that the controllers were seemingly not allowing the motors to deliver their maximum performance at all times.

To determine the true power output of the motor and controller combination which were previously used, a Prony brake was constructed to test the motor and the available controller was used to control the motor during the test. A Prony brake measures the torque output of a motor at a particular speed. This is achieved by applying friction to the motor shaft until the motor speed begins to drop. The maximum torque applied at that speed, is then the rated torque of the motor for that speed. By performing this test multiple times at various speeds, it is possible to compare the achieved output of the motor and controller combination with the specifications supplied by the manufacturer. A test setup was constructed as shown in Figure 4.14.

A pulley was fitted to the motor. A belt with load cells on either end was coiled around the pulley and pre-tensioned. For a particular preload the motor speed was increased until it would increase no more, at this speed readings were taken from each load cell. As shown in Figure 4.15 the torque the motor exerts on

Figure 4.14: The Prony brake test set up.

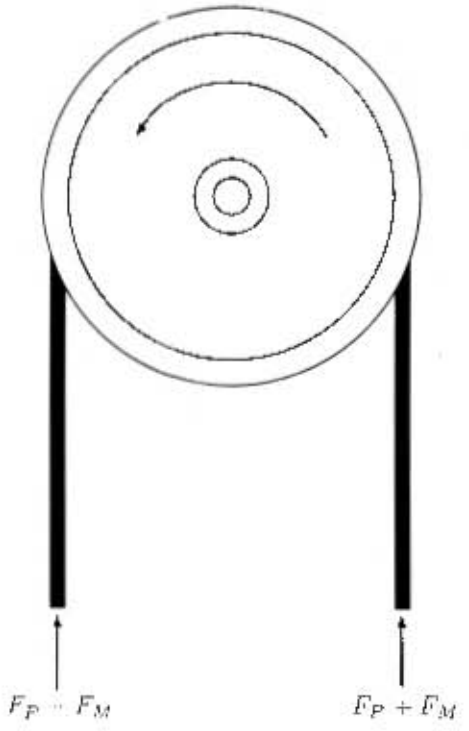

Figure 4.15: Force diagram showing Prony brake set up. F_M denotes the force applied by the motor to the belt and F_P denotes the preload force.

the belt causes one side of the belt to slacken and the other side to tighten, thus the load cell reading decreases on one side and increases on the other. By subtracting the smaller reading from the larger reading the preload on the load cells is eliminated and the result is equal to exactly double the force the motor is applying to the belt through friction. By using this force and the known pulley diameter it is possible to calculate the torque at that speed. Finally using the torque and the speed it is possible to determine the power output of the motor at various speeds.

Testing revealed that the motors were performing up to specification, but critically, upon current limiting the controller was placing the full supply current across the current sense resistor, which is what caused malfunction in the previous platform. The problems may have been possible to overcome by further developing the motor control board and trying to source the motors or equivalent motors locally, however we lacked the expertise and experience to develop a brushless DC motor controller, and even then, to be truly reliable the controller would most likely have to go through several iterations. A trip to the 2008 RoboCup showed the use of Maxon motors and controllers by many teams, additionally there existed a local agent for the motors and it was hoped that by coupling Maxon motors with Maxon controllers, a reliable drive system could be

achieved.

4.5 Concluding Remarks

Further refining the specifications in Chapter 3, the platform is to feature a central spine with tracks on each side as shown in Figure 4.4. Flipper arms at each corner of the robot can provide assistance should the robot become stuck. The platform features a stalk camera and forward and rear facing cameras housed within the spine. In order to provide space for external sensors and equipment an accessory plate is mounted onto the top of the robot onto which a piece of equipment could be fixed. Power is to be provided to the platform using a number of 18V Makita lithium-ion power tool batteries. The platform and flippers are to be driven by 36V Maxon motors and controllers. The control system should make use of a joystick or joystick-type controller, which should be intuitive to the operator. Using the broad ideas refined from this design stage, the detailed design, where the exact size, shape and performance of the robot is determined, can begin.

Chapter 5

Mechanical Systems

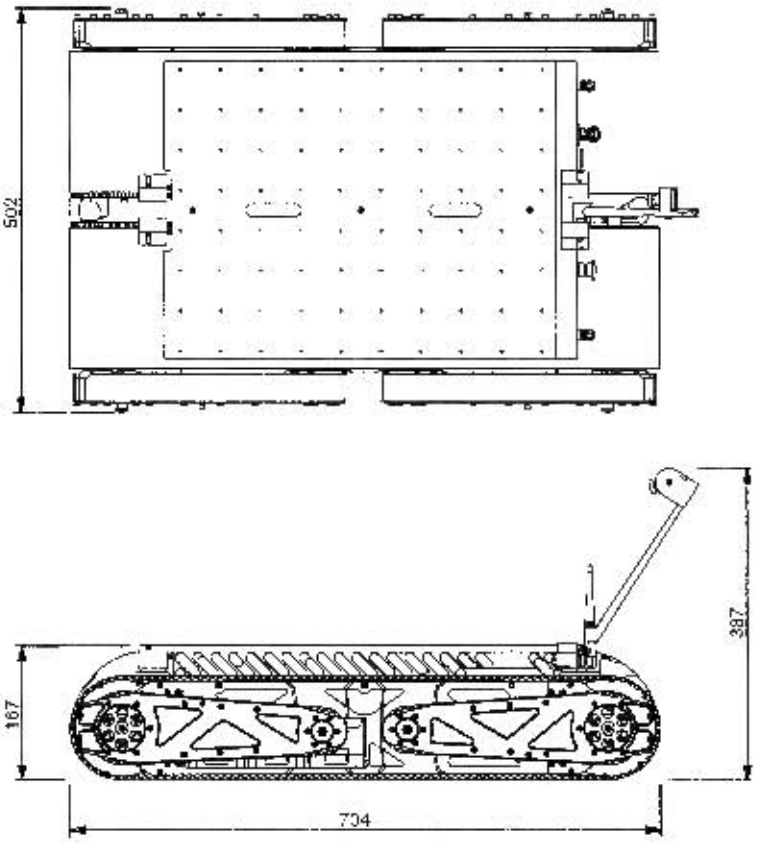

Figure 5.1: The overall dimensions of the platform.

The concept developed in Section 4.1 served as the starting point for the mechanical design. The machining facilities available are primarily manual and CNC controlled lathes and milling machines. Although it was possible to outsource manufacturing, manufacturing in-house could be performed at no cost and it was also possible to follow the part at every stage of manufacture, eliminating mistakes before the parts are made. The design of the robot was such that parts could be made using the available manufacturing technology unless it was absolutely necessary to have outside manufacturing performed.

The explorer platform (Figures 5.1 and 5.2) consists of the 3 fundamental sections in Figure 5.3, a central spine and 2 sidepods. Each sidepod is fixed to the central spine with 3mm pins and M4 Allen cap screws. In an effort to reduce the tool requirements, the robot was designed with only M3 and M4 screws.

Figure 5.4 shows how each sidepod may be further broken down. Each of these sub-assemblies is explained in further detail in the sections which follow.

The cross-section of the platform is defined by the need to fit through the entry triangle as per specifications, and the desire to enclose the flipper and drive motors within the front pulleys. The constraints brought about by this decision are shown in Figure 5.5.

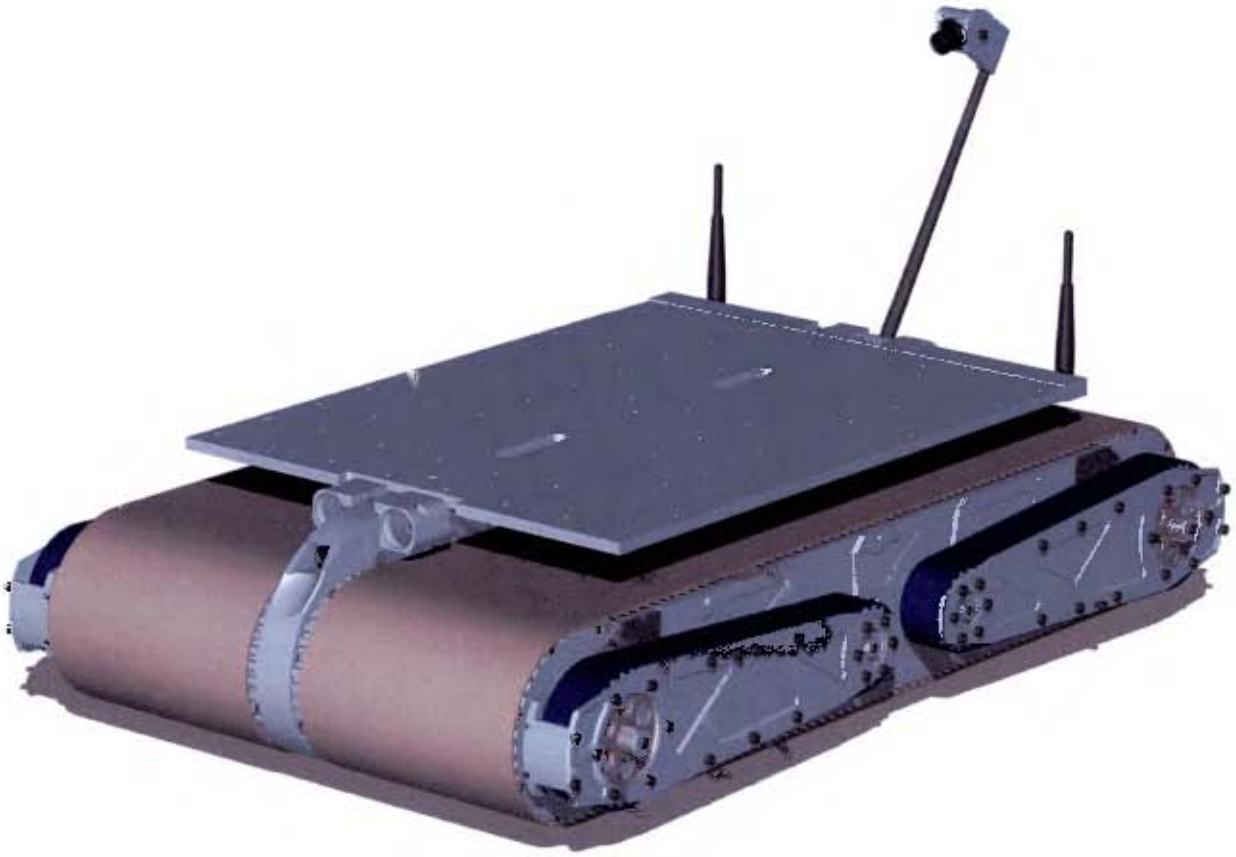

Figure 5.2: A rendering of the complete explorer platform.

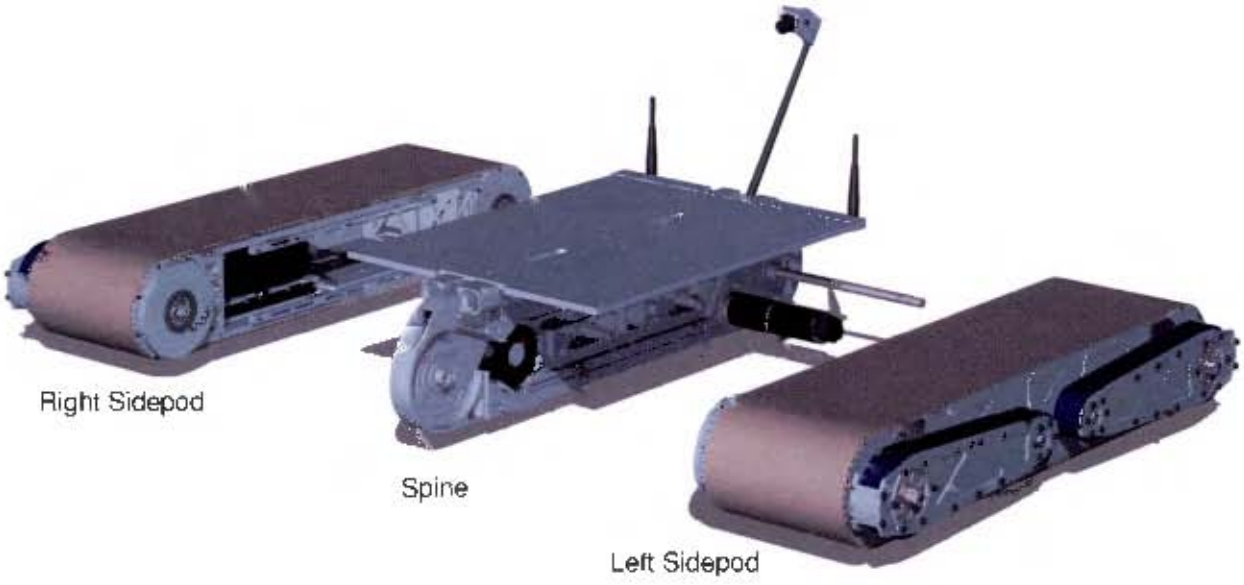

Figure 5.3: The 3 sections of the platform.

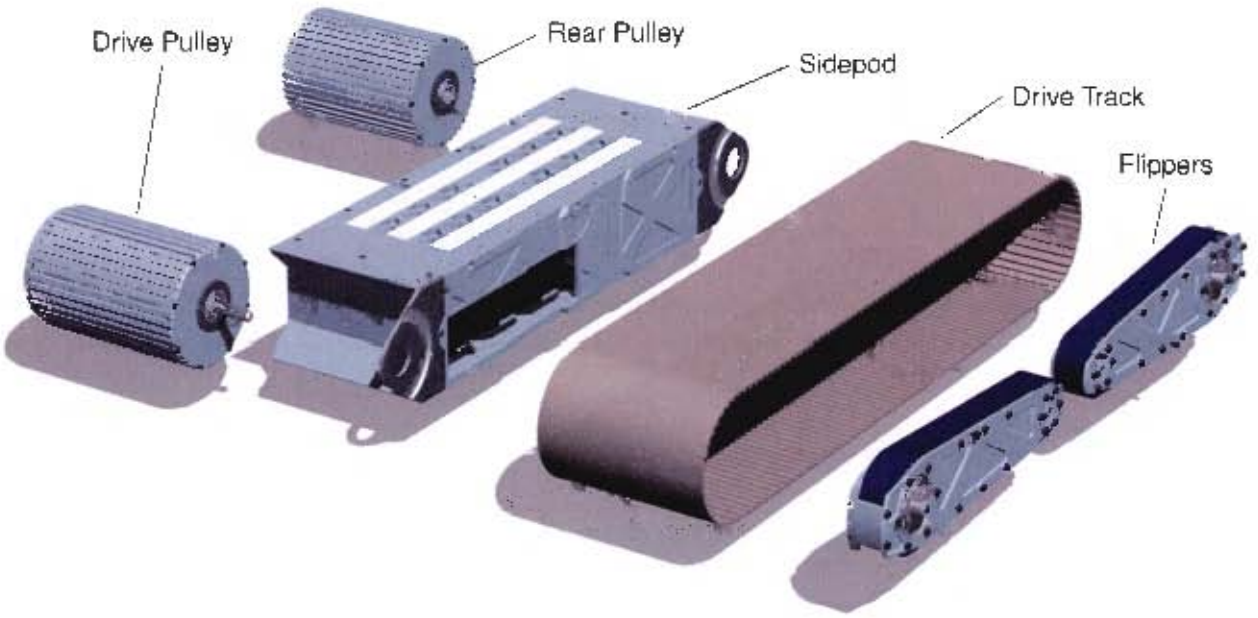

Figure 5.4: The sub-assemblies making up the left sidepod.

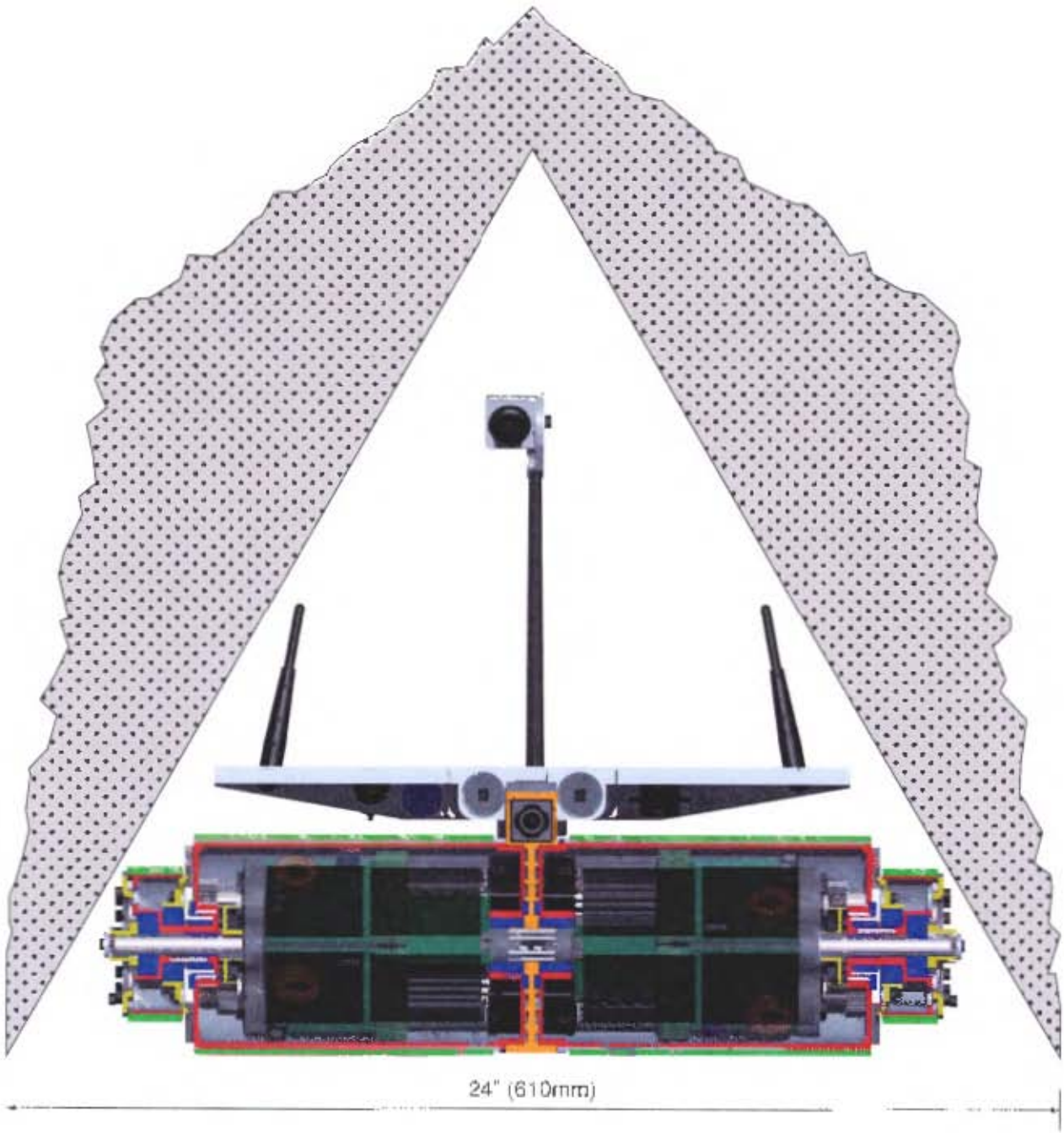

Figure 5.5: A cross-section through the drive pulleys of the platform showing the drive motors enclosed within the drive pulleys, and the space constraints resulting from having to fit through an entry triangle.

5.1 The Spine

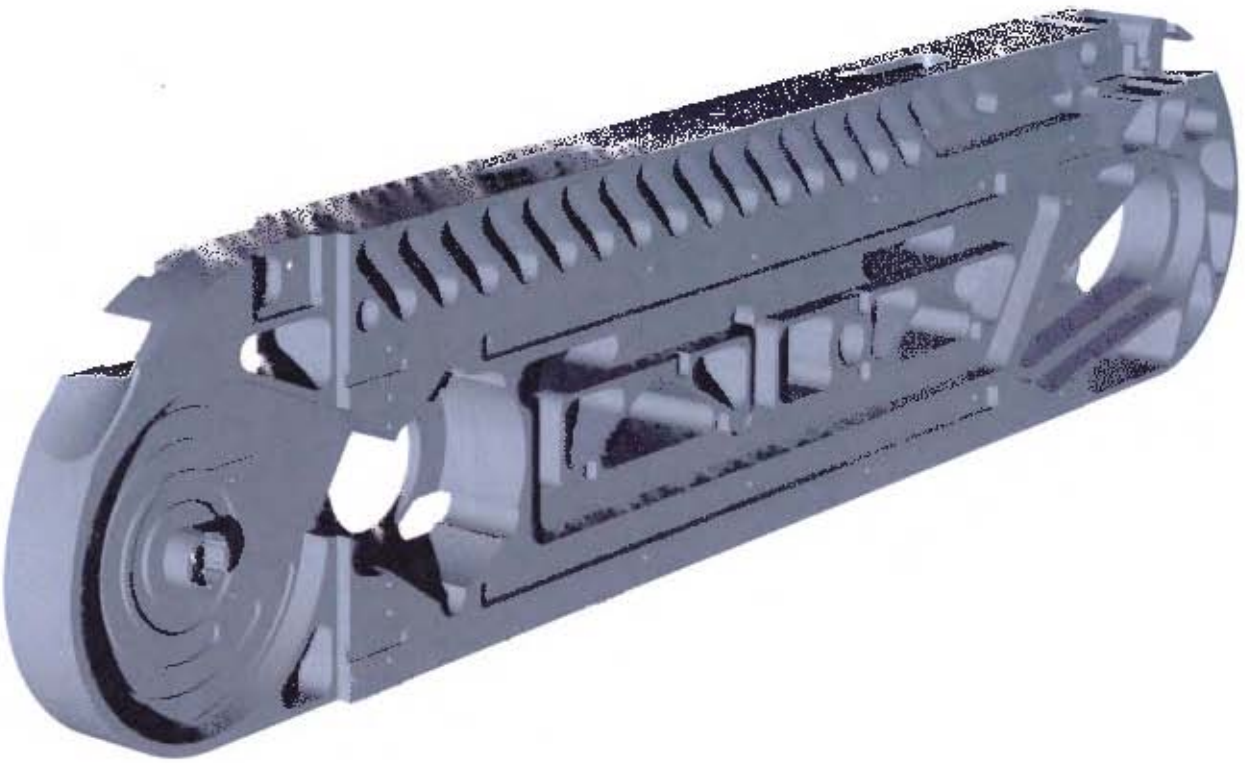

Figure 5.6: The left side of the spine.

Figure 5.7: The right side of the spine.

The spine as shown in Figures 5.6 and 5.7 is the main structural member of the robot. The axles about which the drive pulley's rotate are machined into the spine. Figure 5.8 shows the front axle on the right side. It is made in 2 parts, the main part is part of the spine. The second part of the axle is a removable cover which allows wiring to be routed into the front drive pulleys which are further detailed in Section 5.3.

The rear axle in Figure 5.9 is machined into removable covers attached to either side of the rear of the

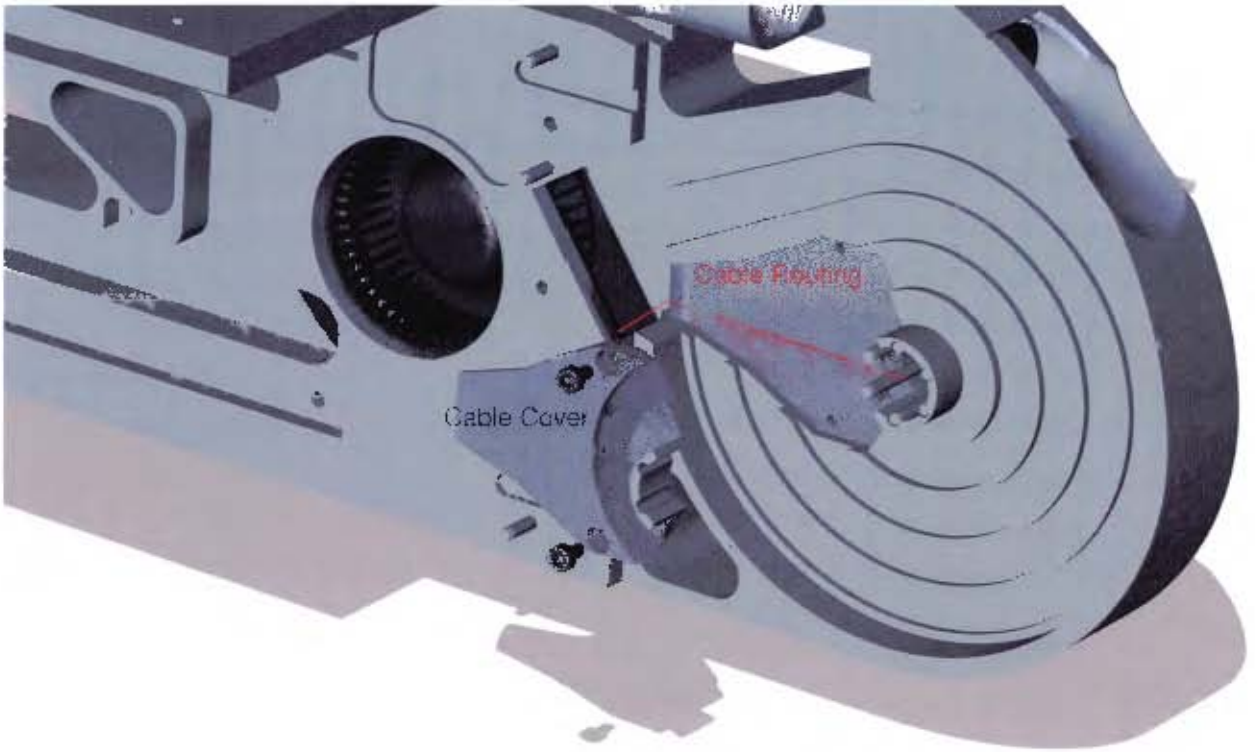

Figure 5.8: The removable cover which allows cabling to be routed from the front pulleys to the rest of the platform.

spine. Behind the covers is a gear set which provides drive to the rear flipper arms. Both rear flippers are connected to the same shaft and as such operate together.

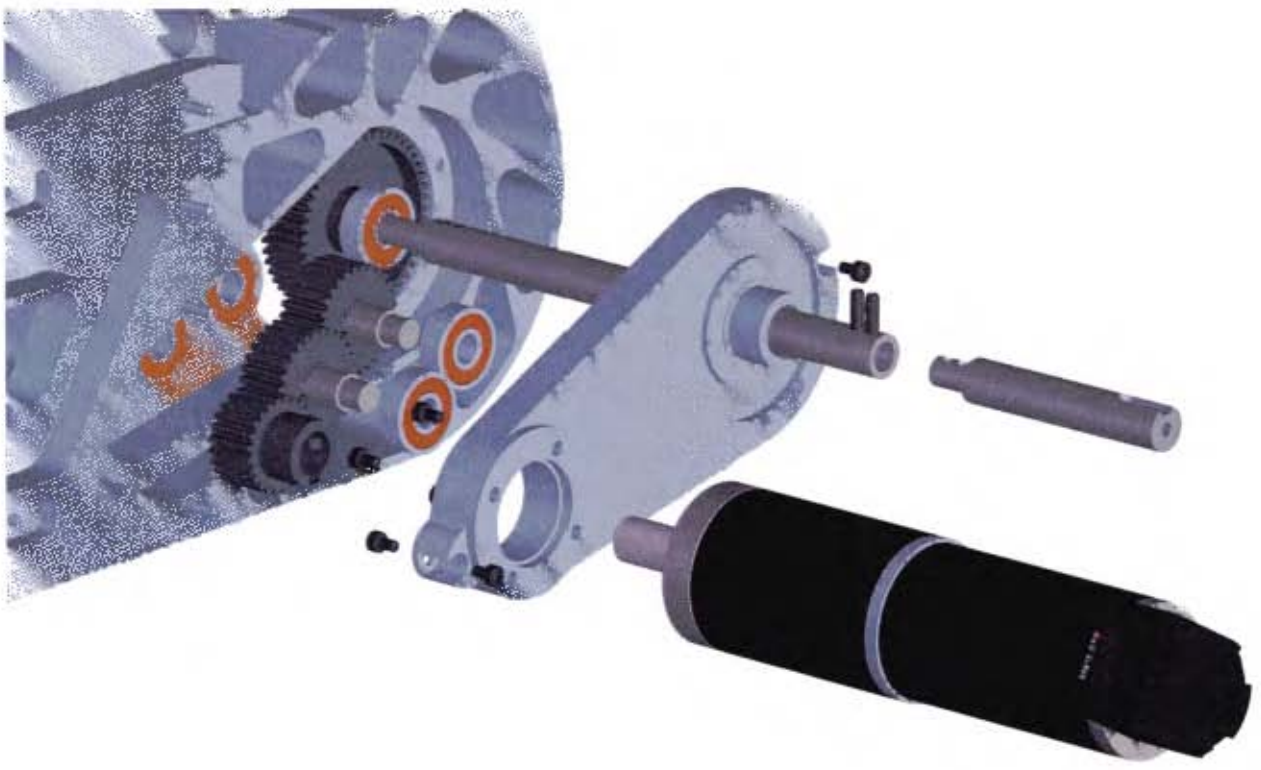

Figure 5.9: The gear system for driving the rear flippers.

The spine also comprises an accessory deck designed to provide the mechanical, electrical and communications infrastructure for further equipment to be fitted to the robot. The deck (which can be seen in Figure 5.10) is constructed of an aluminium plate. This plate has 2 oblong ports machined into them which align with ports in the spine to allow cables to be routed from the deck into the robot itself. The deck is covered with M4 tapped holes spaced at 50mm. The deck is supported at its rear by another support section. This rear section also houses the communications antennae, emergency stop button and the power and communications tether sockets as shown in Figure 5.11.

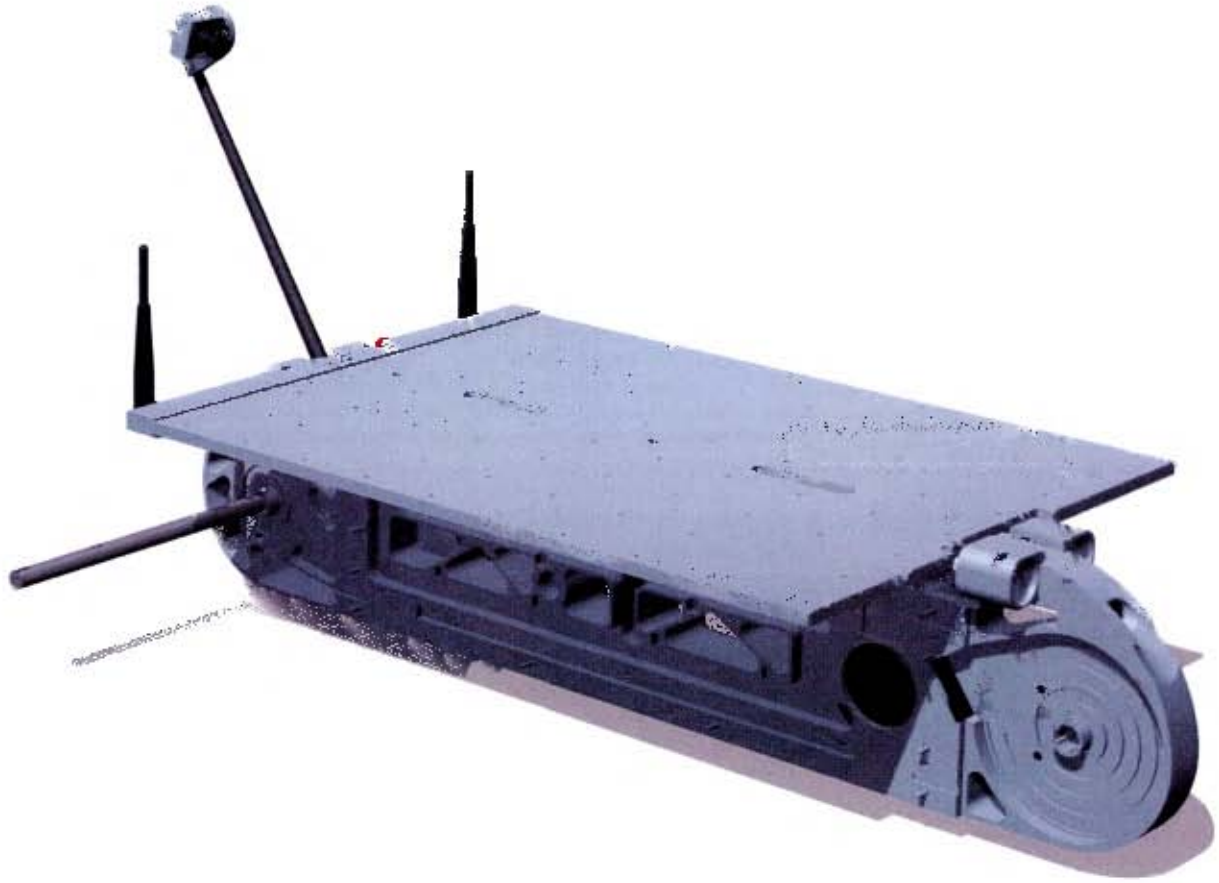

Figure 5.10: The spine with attached assemblies.

5.1.1 Lighting Modules

The spine incorporates 4 lighting modules (shown in Figure 5.12), 2 forward facing and 2 rear facing. Light is generated by 700 lumen Cree X-Lamp LED starboard modules. The lighting module incorporates a heat-sink to dissipate some of the heat generated by the LED modules which is sufficient to melt the solder joints between the power lines and LED starboard if left unchecked. Light passes through a lens which also locates the LED starboard in the housing.

5.1.2 Cameras

Three cameras are incorporated into the spine, a front facing camera, rear facing camera and a stalk camera. The front and rear facing cameras fit within recesses in the spine and are located by covers. The cover and recess for the rear camera are shown in Figure 5.13.

An exploded view of the stalk camera is shown in Figure 5.14. The stalk camera sub-assembly is designed to allow both the angle of the stalk relative to the spine and the angle of the camera relative to the stalk to be adjusted. This is to allow the view shown by the stalk camera to be adjusted after testing to that which is most useful for navigation. The base and stalk cameras utilize the same basic camera, however the stalk camera uses a wide-angle lens to maximize the amount of the platform visible from the camera. The stalk itself is a tapered graphite rod.

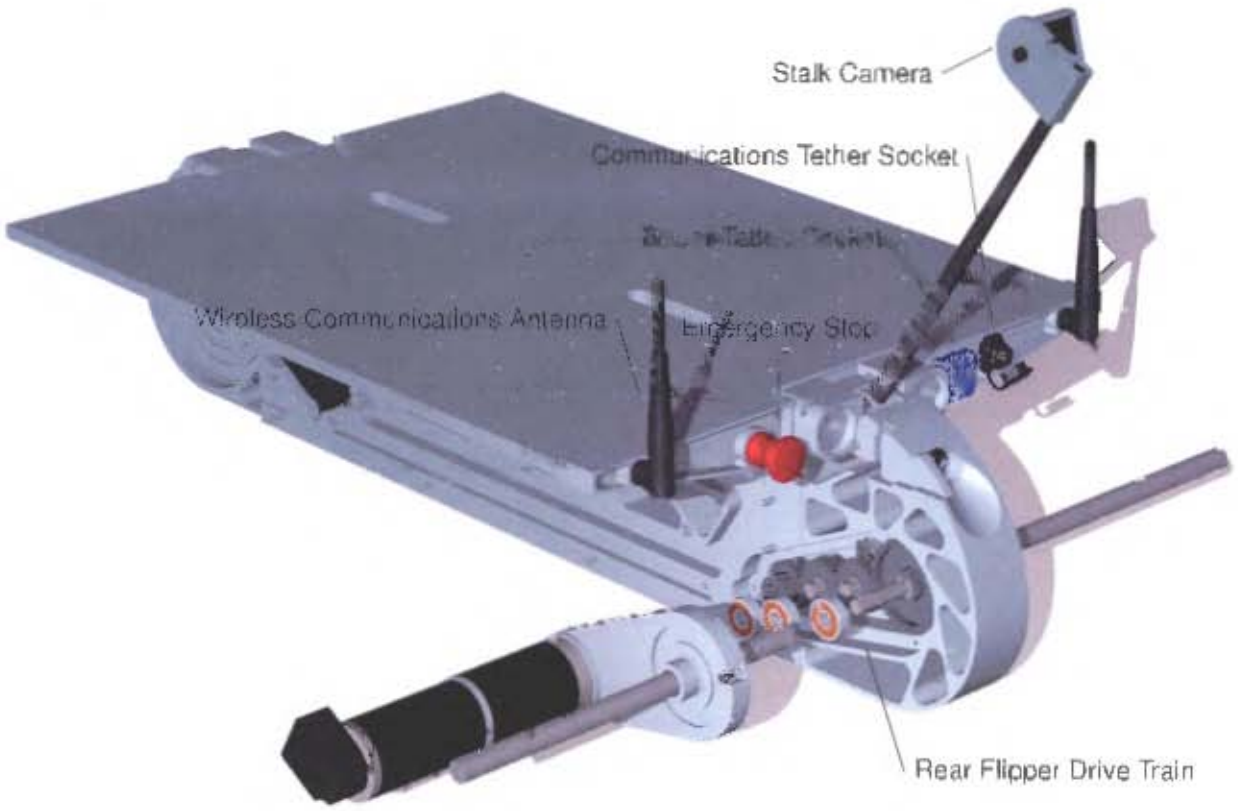

Figure 5.11: Various equipment attached on the rear of the spine.

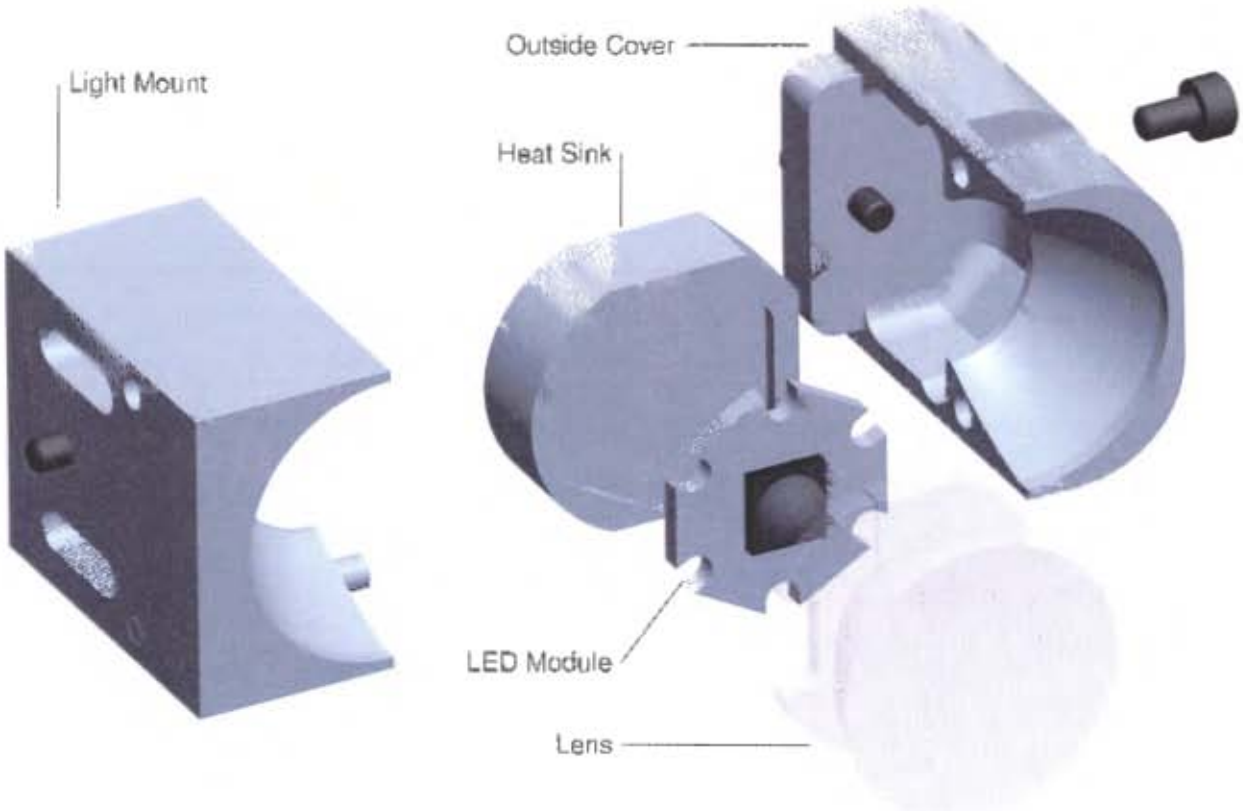

Figure 5.12: The components making up the lighting module.

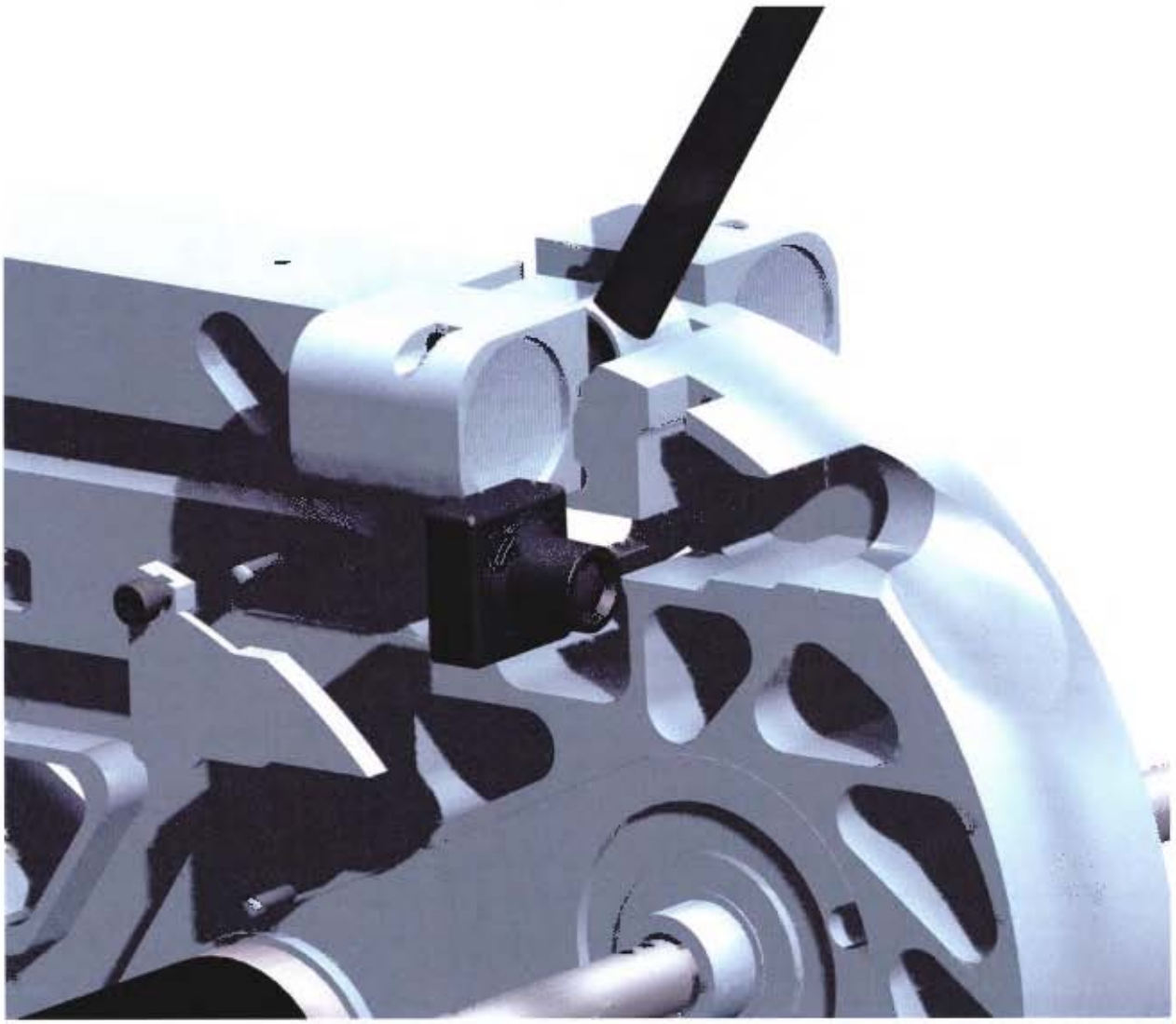

Figure 5.13: The rear facing camera and cover exploded from the spine.

Wiring for the stalk camera runs through the stalk, and then along the spine with the rear camera wiring before passing through a port in the spine and into the sidepods as shown in Figure 5.15.

5.2 The Sidepod

The primary function of the sidepods (shown in Figure 5.16) is to provide space for the batteries and electronics in addition to other equipment which may be added to the robot at a later stage. The sidepods also locate the outside of the pulleys and house the tensioning mechanism for the drive tracks.

The left and right sidepods are designed to be made of almost identical parts. Each sidepod consists of a bottom and top plate and front and rear vertical members. The only difference between the left and right sidepods being the rear vertical member of the left sidepod, which differs from all other vertical members in that it features a cutout for mounting the motor which drives the rear flippers. The parts making up the sidepod are shown in Figure 5.17.

5.2.1 The Track Tensioning System

The track tensioning system uses 3 skid plates which can be adjusted to protrude above the top surface of the top plate of the sidepod. The entire tensioning system is almost totally contained within the 8mm thick top plate.

Figures 5.18 and 5.19 show the components which make up the tensioning system. Three pieces placed upon the length of the sidepod top plate (2 of which are shown in Figures 5.18 and 5.19) capture 3 rods

Figure 5.14: The components making up the stalk camera.

along the width of the top plate. Tightening screws pulls the sliding pieces and rods outwards. 3 Skid plates are located above the rods. These skid plates have an inclined surface on their underside which rests on the rods. Thus as the rods move outwards, the skid plates move upwards.

5.2.2 Battery Clip

Each sidepod contains 3 batteries located by a battery clip as in Figure 5.20, which doubles as a terminal block for making electrical connections to the battery terminals. The batteries slide onto rails on the clip as per Figure 5.21, while spring loaded clips on the batteries themselves lock the batteries in place on the bottom of the sidepod.

The battery clip itself is comprised of 4 components which are shown in Figure 5.22. Power wires are fastened against the terminal contacts using screws to hold the wires in place and make an electrical connection

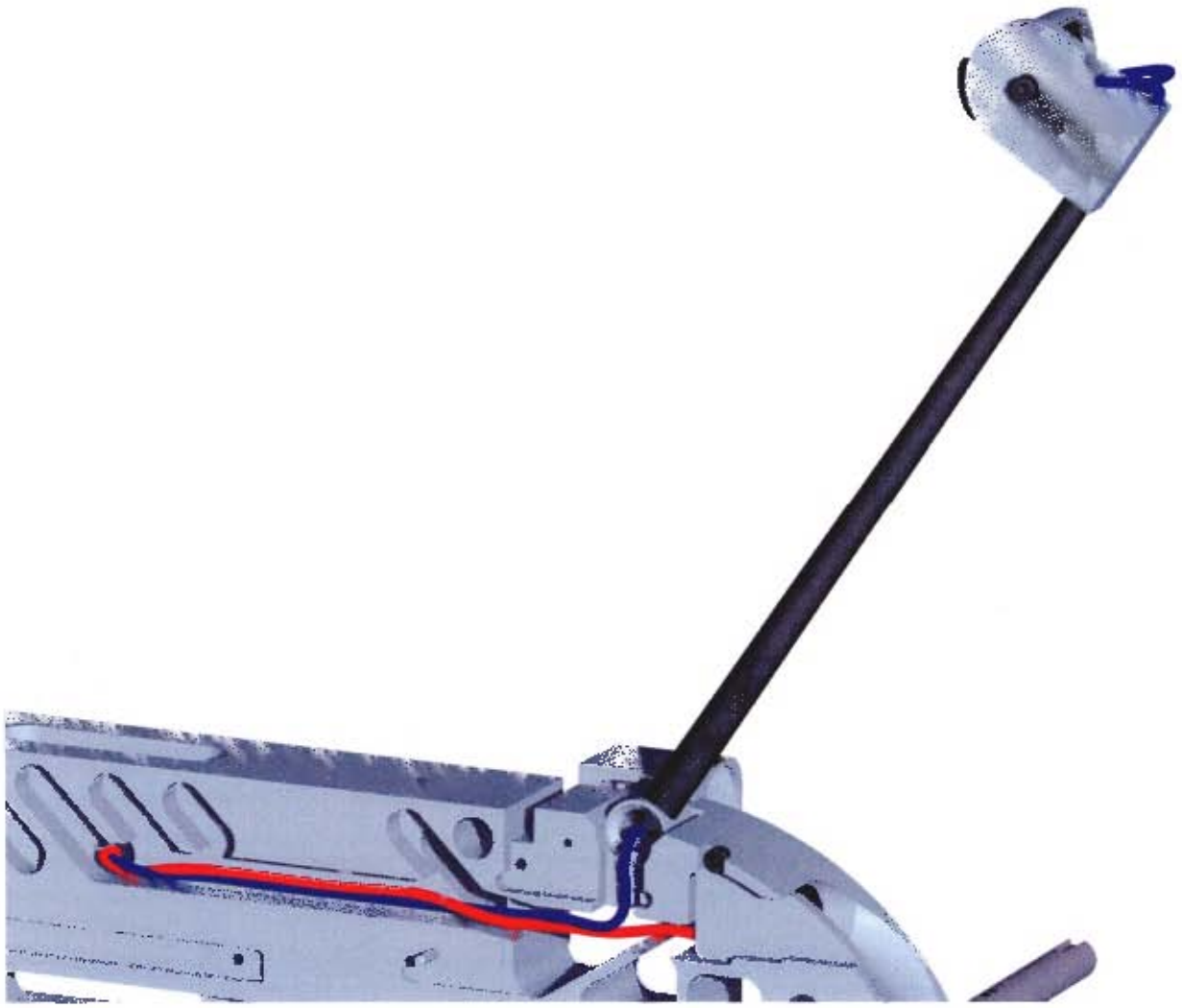

Figure 5.15: The wiring for the stalk and rear facing cameras.

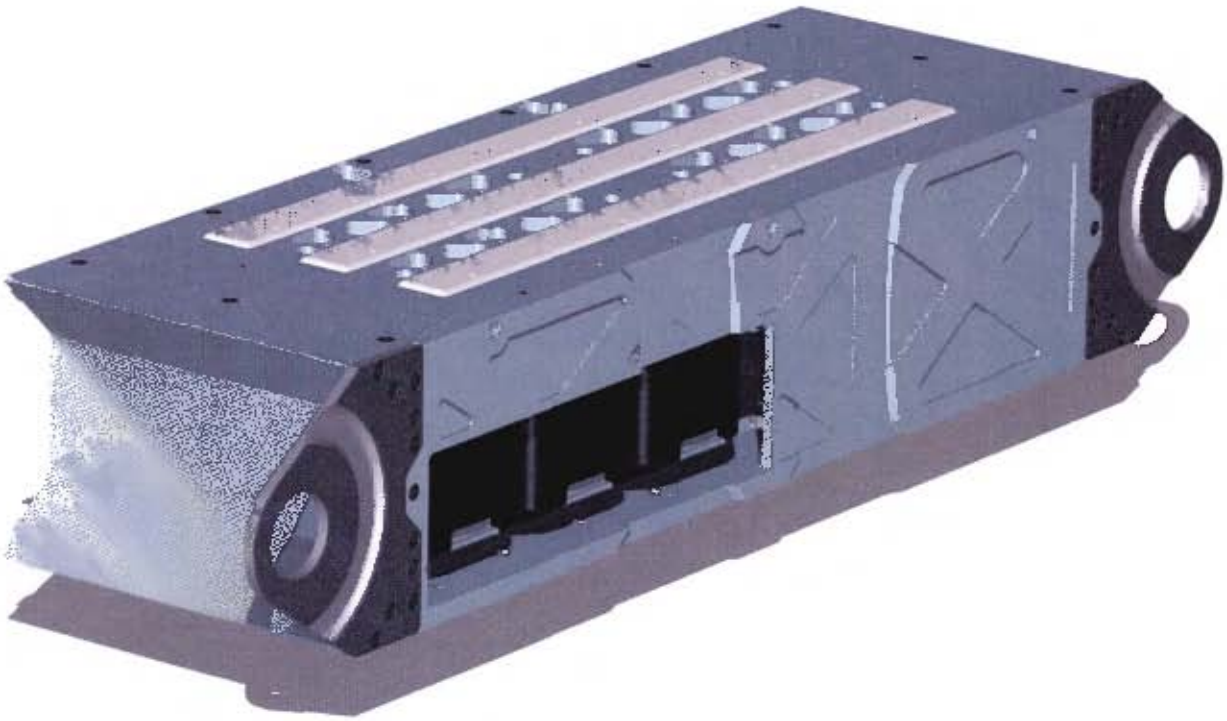

Figure 5.16: The sidepod section of the platform.

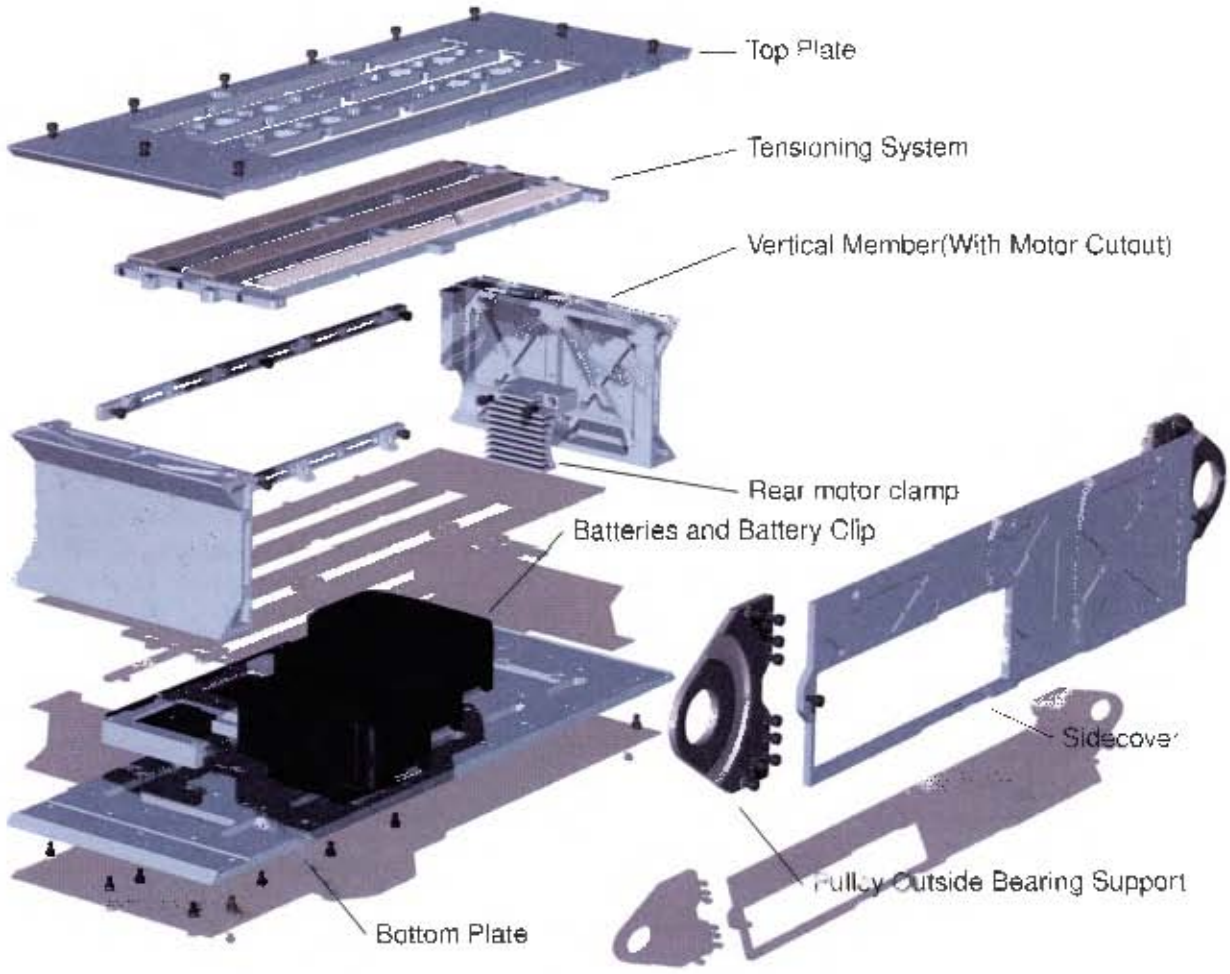

Figure 5.17: The major components making up a sidepod. This mage shows the left sidepod, with the cutout and heat-sink for the rear flipper drive motor in the rear vertical member. The right sidepod does not have this cutout in its rear vertical member.

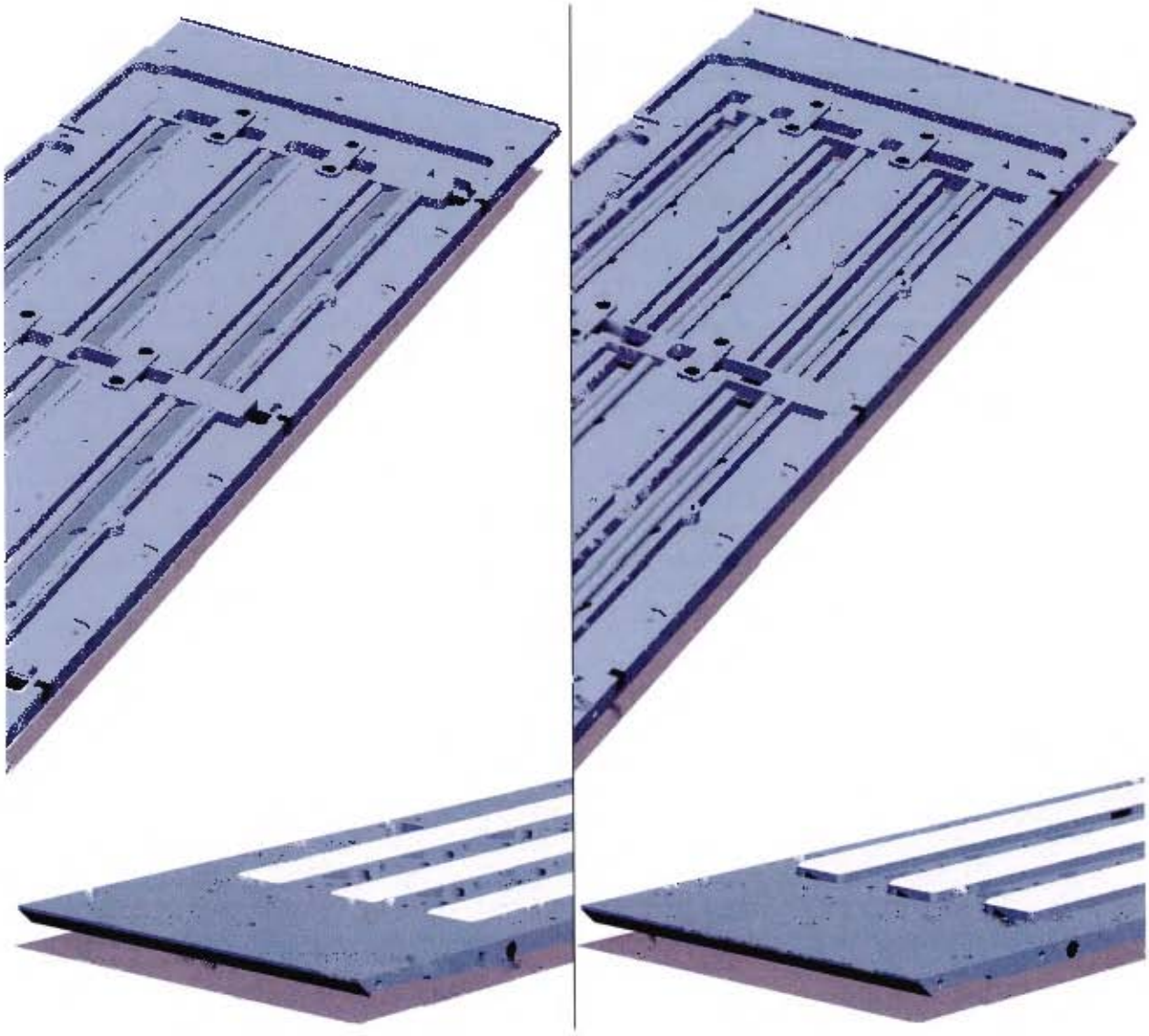

Figure 5.18: The top plate and tensioning system viewed from above and below. The skid plates are fully lowered on the left and fully raised on the right

Figure 5.19: A cut-away view of the various parts of the tensioning system shown in the raised and lowered position.

Figure 5.20: The batteries in place in the battery clip.

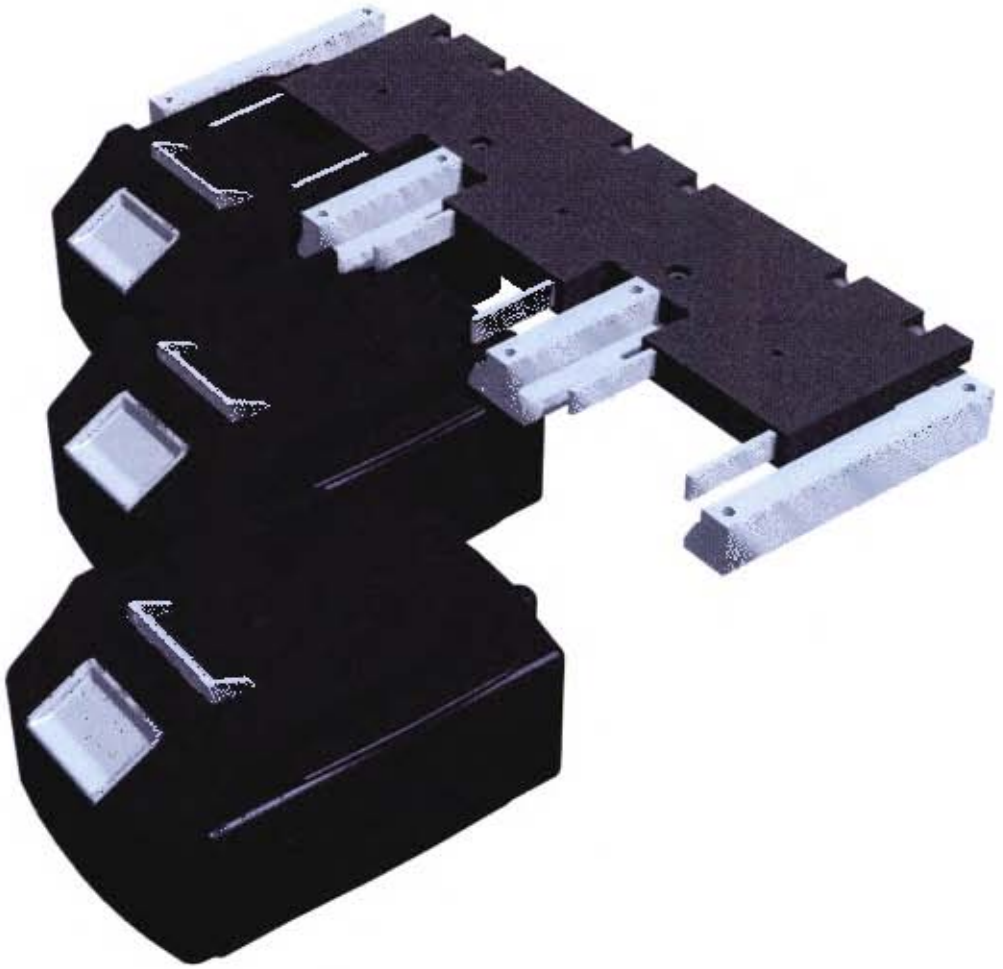

Figure 5.21: The batteries, locating rails and terminal contacts viewed from below.

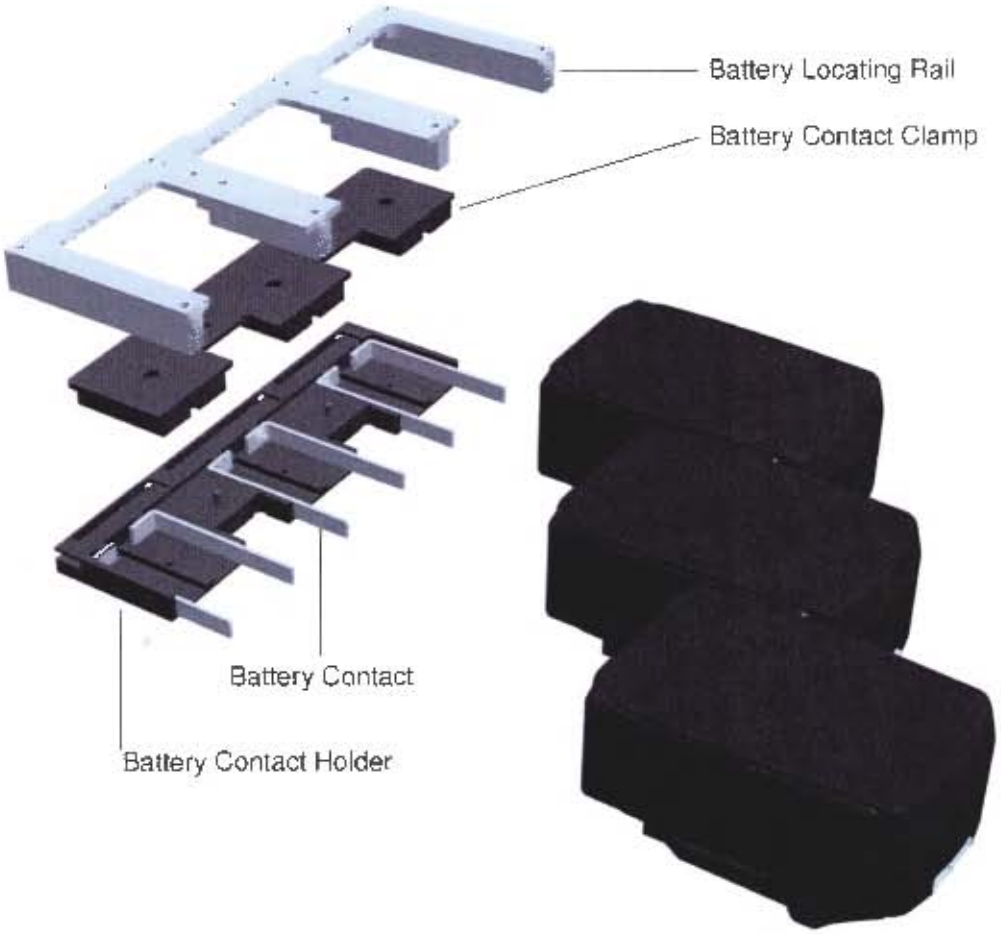

Figure 5.22: The batteries and components making up the battery clip.

5.3 The Drive Pulley

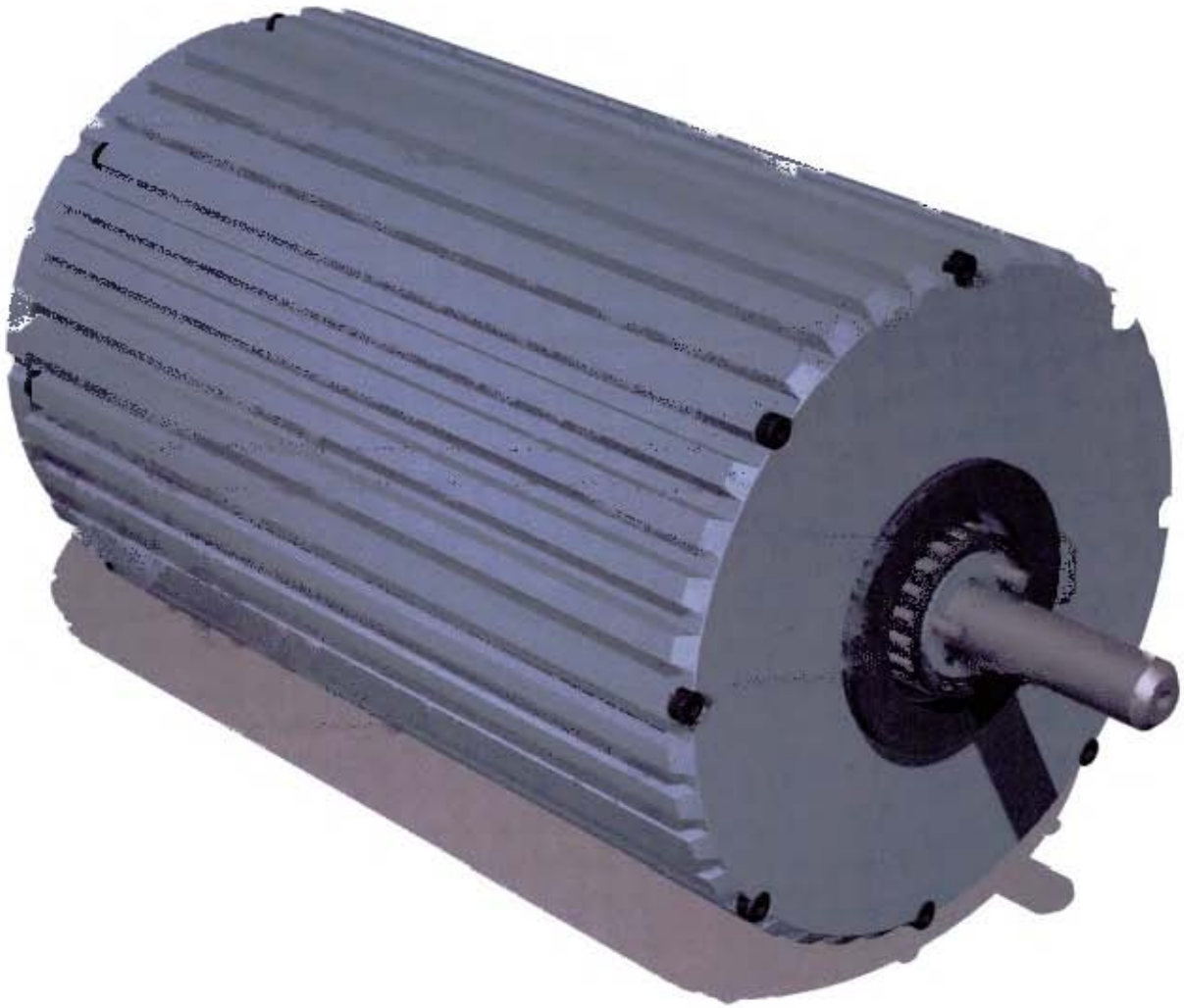

Figure 5.23: The drive pulley sub-assembly.

Using wide drive tracks results in the pulleys which drive those tracks being fairly wide. Placing the motor controllers, drive and flipper motors within the drive pulleys themselves, provides 2 benefits. Space is freed up within the robot which can be used to install more equipment, also as the motors are fairly heavy, placing them within the drive pulleys would move the centre of mass of the robot further forward which is desirable for manoeuvrability [32]. This did create some design challenges though. In addition to providing drive to the drive tracks, drive had to be provided to the tracks on the flipper arms and the flipper arms needed drive for their positioning, all of which has to move through the same axis. A complete pulley sub-assembly is shown in Figure 5.23.

The parts making up a drive pulley are shown in Figure 5.24. Both the front and rear pulleys are made up of 3 parts. An inside cover which provides the bearing interface between the pulley and the spine, a central pulley section which comprises the majority of the pulley width and an outside cover which provides a bearing interface for locating the outside of the pulley. The drive pulleys differ from the rear pulleys in that their inside cover is deeper to accommodate the length of the motors contained within the pulleys. The drive pulleys also have an outside cover which has a drive gear sandwiched between 2 aluminium parts in comparison to the rear pulley which has no drive gear and hence the outside cover can be a single piece.

The layout of the drive pulley is shown in Figure 5.25. Packaging these components within the pulleys resulted in tight clearances between the rotating drums and motor assembly as is evident in Figure 5.26.

Figure 5.27 shows a section through the spine, drive pulley and flipper with the motor assembly orientation rotated by 180° to show the layout of the drive system. The spine, the sectioned surface shown in orange, locates the motor sub-assembly using a spline-like feature created with dowel pins which fit into scallops

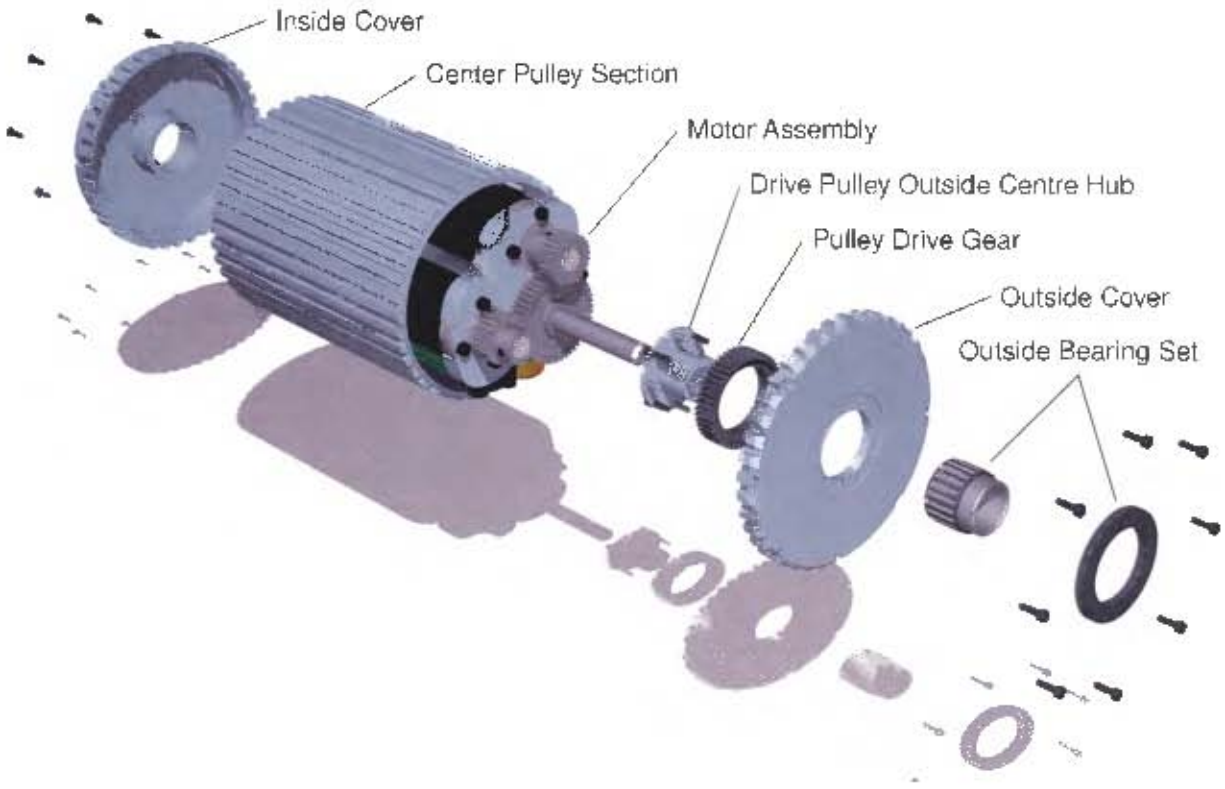

Figure 5.24: An exploded view of the drive pulley.

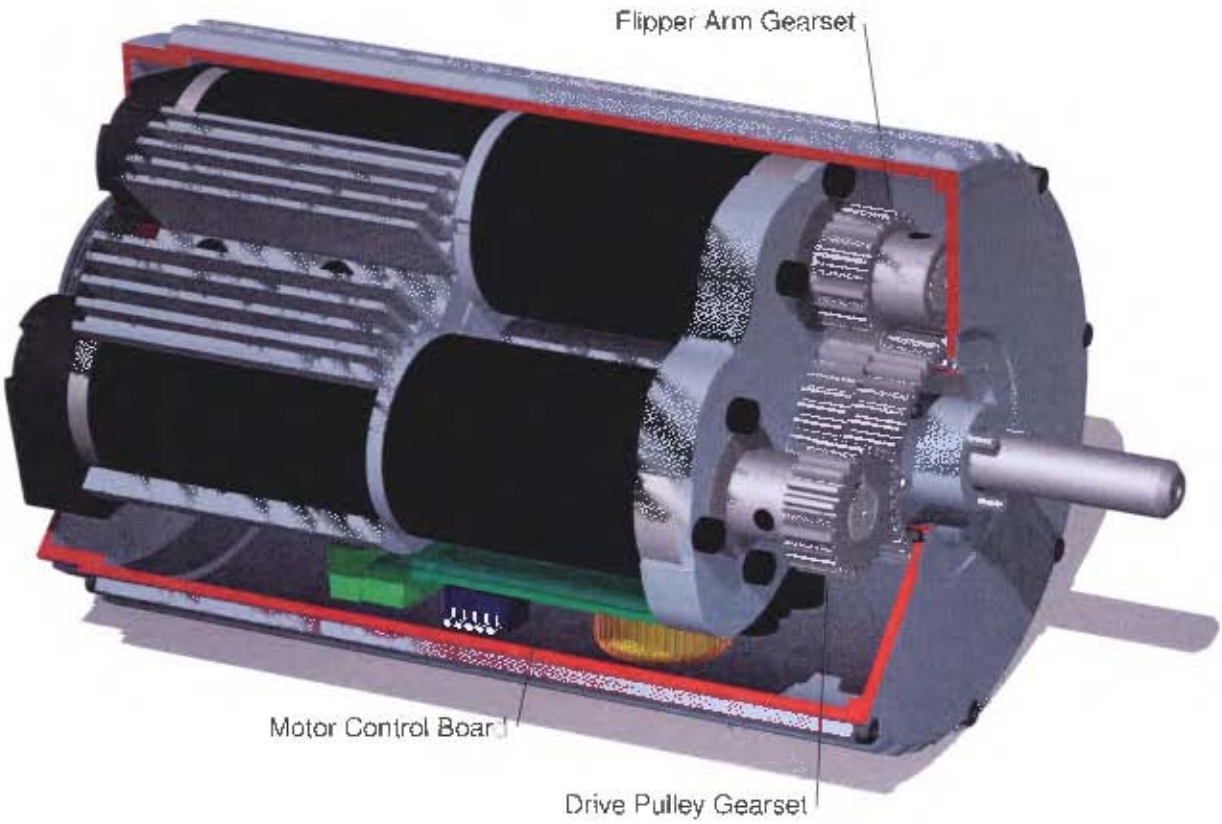

Figure 5.25: A cutaway view of the drive pulley showing the components inside the pulley.

Figure 5.26: A side view showing the components in the drive pulley and the limited clearances.

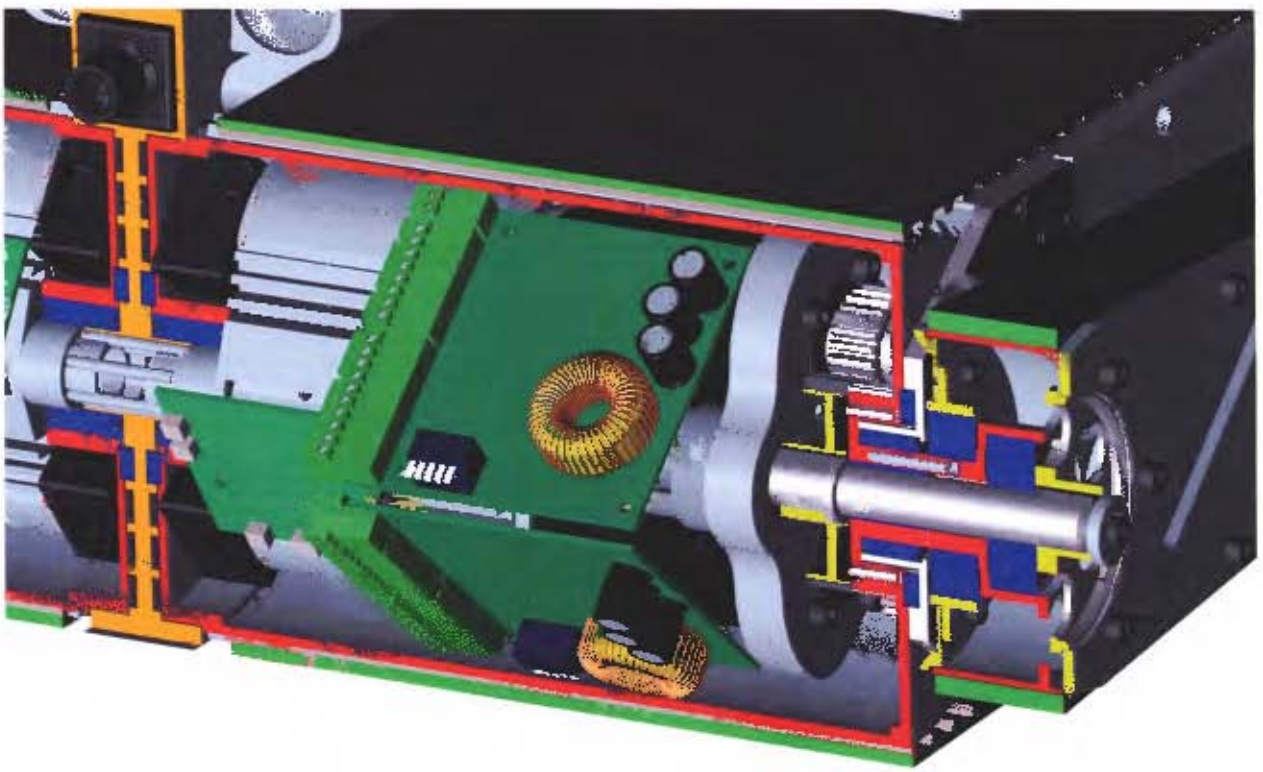

Figure 5.27: A section through the front drive train.

machined into the spine and motor assembly (see Figure 5.28). A thrust bearing and needle bearing(shown against the spine in blue) are used in combination to locate the inside surface of the drive pulley. It was necessary to use this bearing arrangement to allow enough space for wiring to pass through the center of the axle, while conserving space along the drive axis. The drive pulley, sectioned in red, is located on the outside by a similar thrust and needle bearing arrangement, which are themselves held captive in a detachable plate. The drive motor drives the pulley through a spur gear fixed with pins to the pulley itself. Drive is then transferred to the pulley driving the flipper tracks through 3 pins on the inside of the drive pulley outside cover.

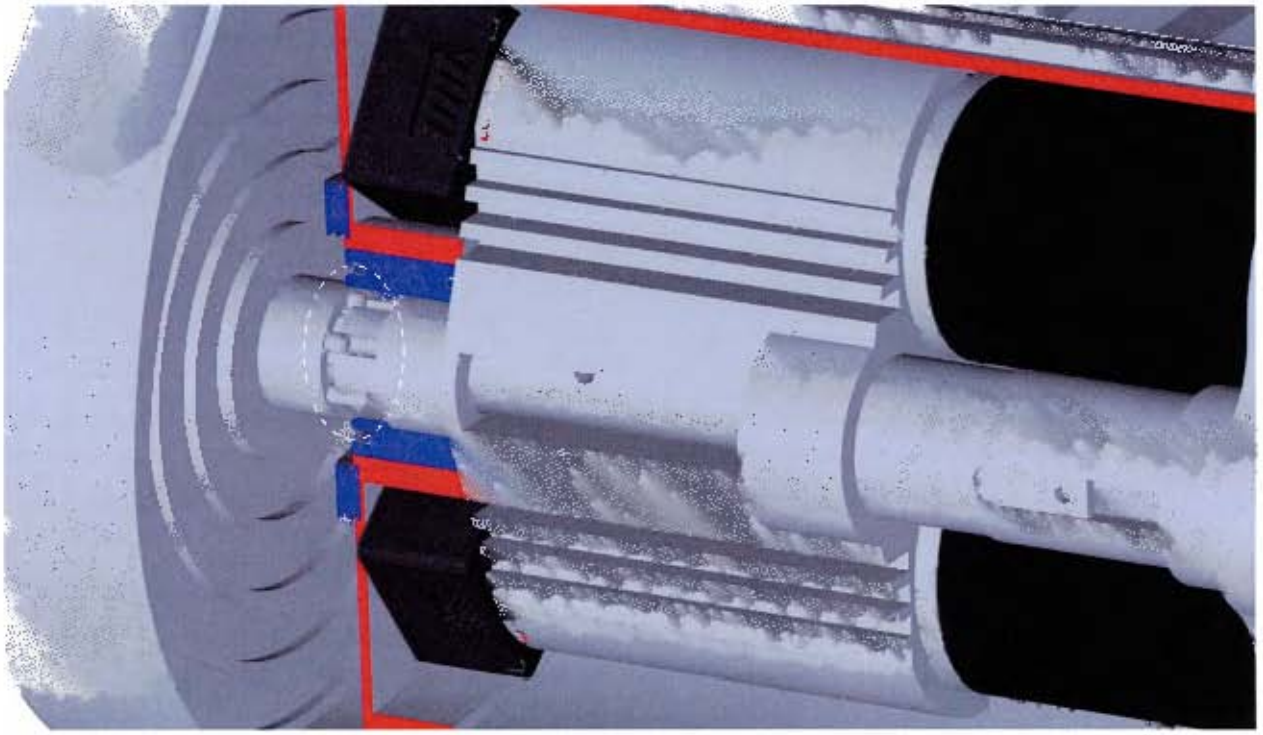

Figure 5.28: The pins fixing the motor assembly to the spine.

The motor sub-assembly of the drive pulley, shown in Figure 5.29, contains the motors, motor heat sinks, control electronics and flipper positioning shaft. The flipper positioning shaft is driven by the flipper motor through a spur gear (shown sectioned in yellow in Figure 5.27). The shaft is fixed to the arm of the flipper on its outside. The flipper arm is located on the the flipper pulley with a ball bearing, while the flipper pulley is located against the positioning shaft with another ball bearing (Both shown in blue in Figure 5.27).

5.4 The Flipper Arm

Each flipper arm is a 3 part sandwich construction with an inner and outer plate separated by spacers which enclose 2 pulleys. The various pieces making up each of the 4 flippers are shown in Figure 5.30. Drive is transferred to the flipper tracks through 3 pins on the platform's main drive pulley which can be seen in Figure 5.23. These pins fit into the holes in the drive pulley of the flipper as shown in Figure 5.31.

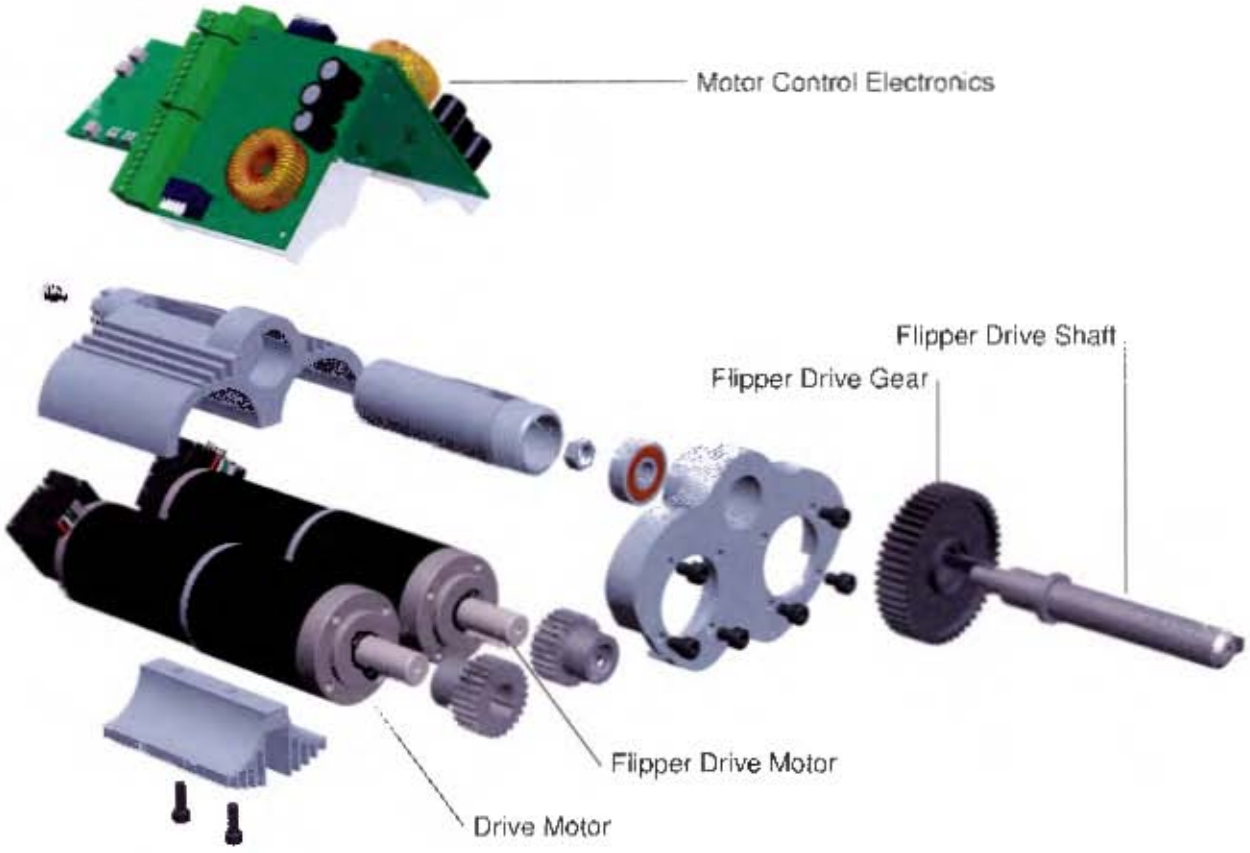

Figure 5.29: Exploded view of the motor sub-assembly.

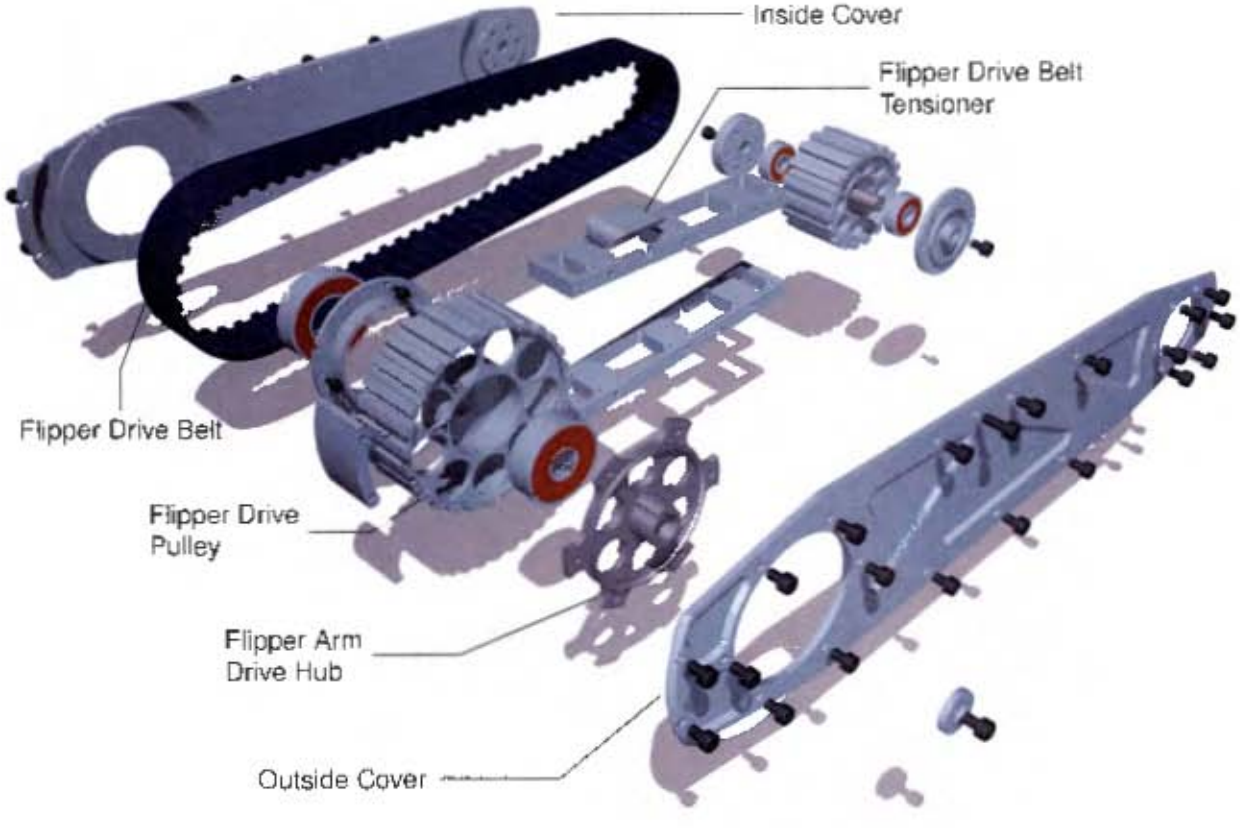

Figure 5.30: An exploded view showing the various pieces making up the flipper arm.

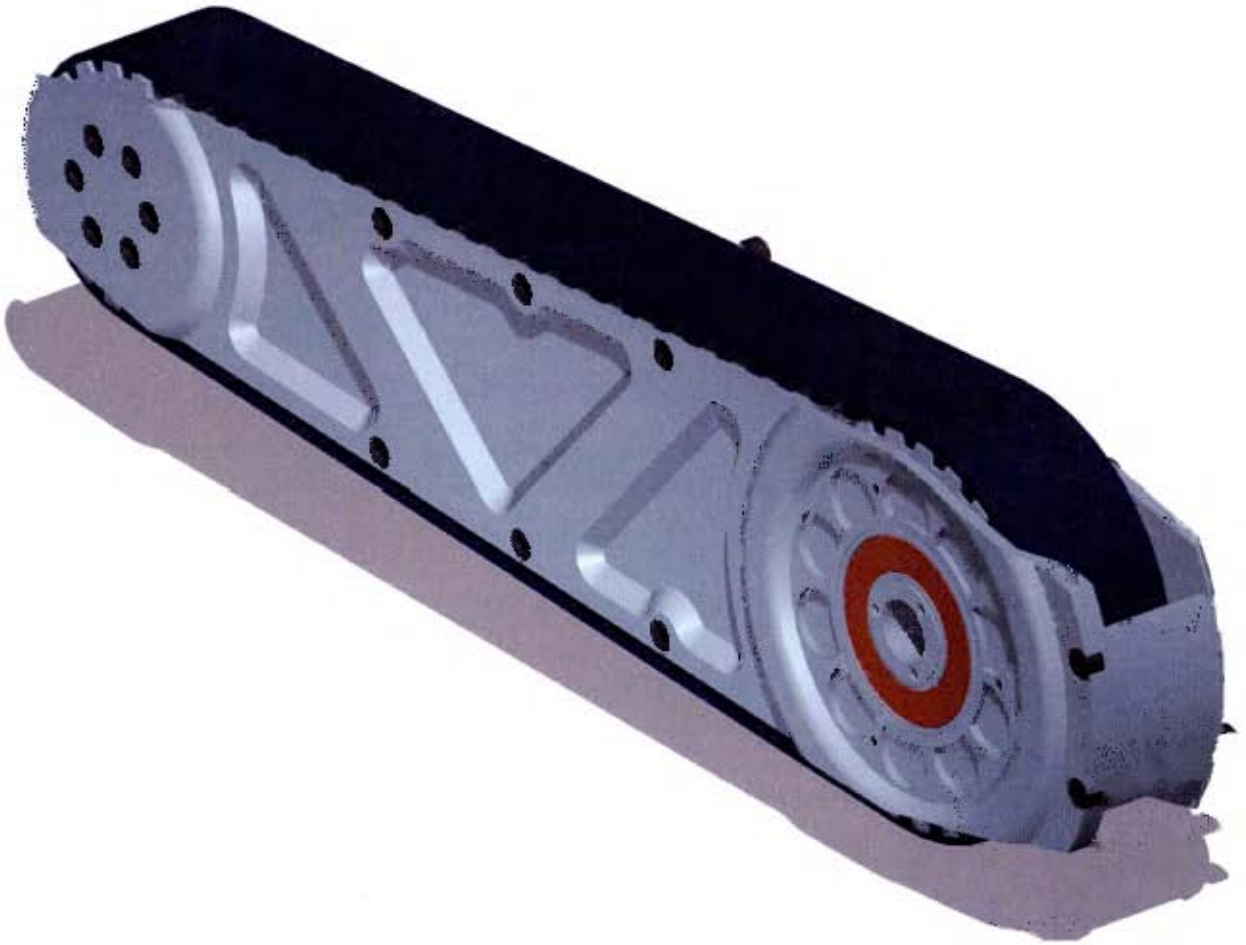

Figure 5.31: The inside face of the flipper arm.

5.4.1 Flipper Track Tensioning System

A mechanism for the adjustment of the flipper track tension is accessible on the outside face of the flipper arm, indicated in Figure 5.32.

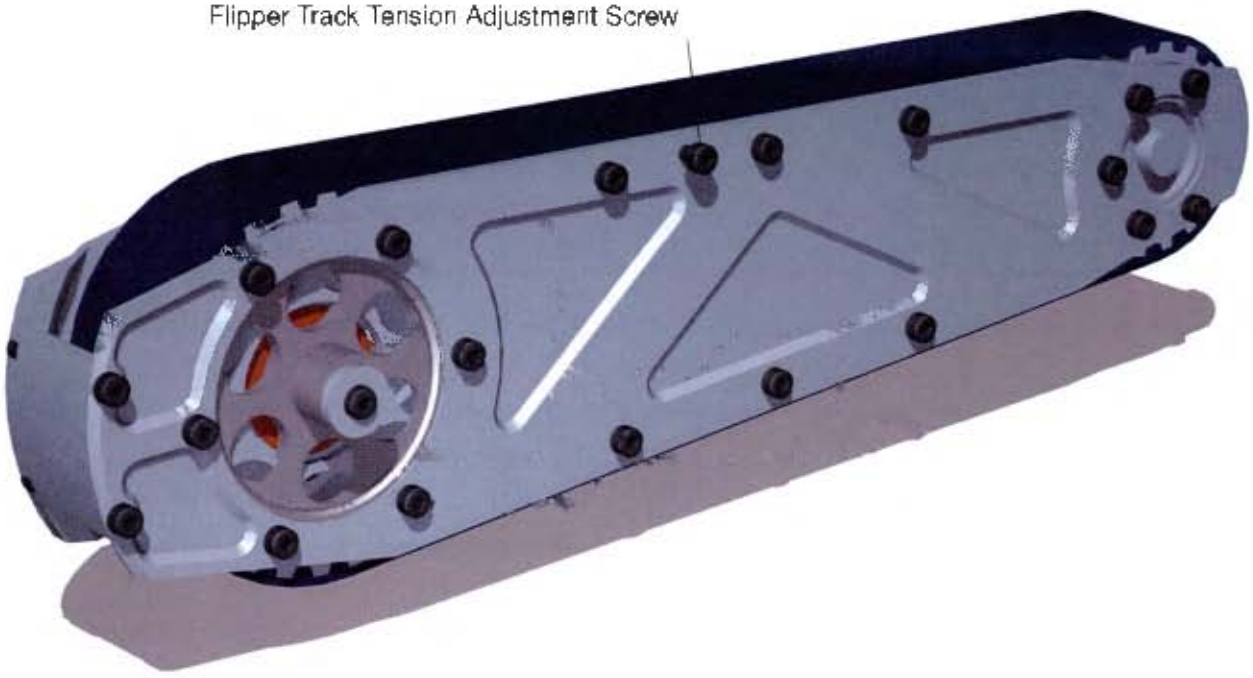

Figure 5.32: The outside face of the flipper arm.

As shown in Figure 5.33, the tensioning system for the flipper uses a set-screw which tightens against an inclined surface on a riser which causes it to move upwards. Belt tension keeps the riser in place against the set-screw.

5.5 Drive Tracks

The main drive track and the flipper tracks are both made from polyurethane T10 timing belt as shown in Figure 5.34. Each main drive belt is 175mm wide, while each flipper belt is 32mm wide. T10 belt was chosen as it is widely available and additionally can be specified with cast-in steel reinforcing. Polyurethane was chosen as the belting material of choice as through the use of solvents it would be possible to weld lugs to the outside of the tracks.

5.6 Motor Selection

The motor and gearbox combination selected for the drive and flipper motors was initially a 36V Maxon 120W Brushless DC motor fitted with a 43:1 gearbox. The decision to place the motors inside the drive pulleys necessitated reaching a compromise between size, power and cost.

The initial selection could be narrowed down to 36V brushless motors due to the choice of batteries. Motor size was the most stringent of the requirements. The length of 2 motors back to back had to be such that the platform could fit through the entry triangle (see Figure 5.5) with additional space for mounting and the structure of the platform. Motor power was a more indefinite constraint. In theory it would be possible to use gears to generate the required torque from any motor, on the other hand there are practical limitations to this approach and a large gear-train would add weight reduce efficiency and could be a potential waste of the limited available space. In general the most powerful motor which fit the other constraints would be ideal. Cost was also a somewhat flexible constraint. As the motors would be paid for out of a fixed budget for the platform, overspending on motors would leave less money available for other items, hence maximum value rather than minimum cost was sought.

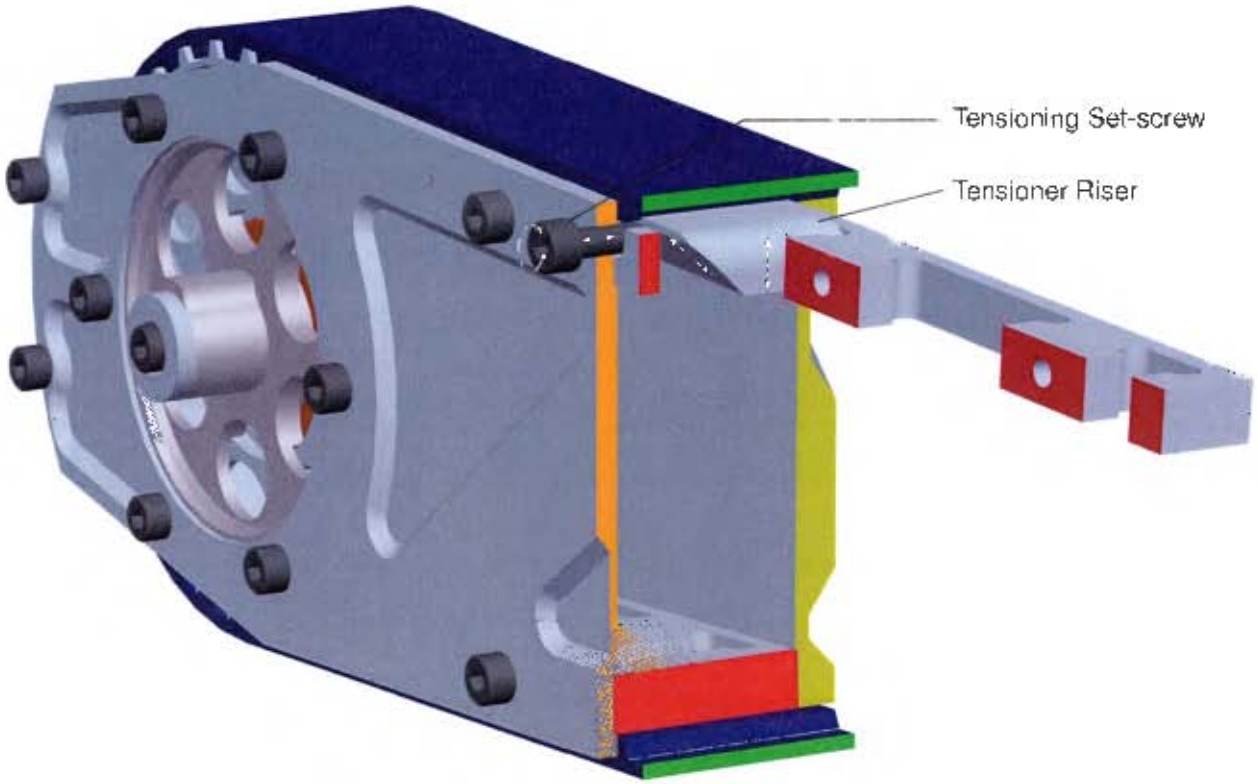

Figure 5.33: A cutaway view of the track tensioning system.

Figure 5.34: A close-up of a flipper belt.

5.6.1 Maxon Motor Ranges

At the time of selection Maxon had 4 product ranges within their brushless motor family, shown in Figure 5.35. The brushless motor family have the EC designation. The product ranges are as follows:

Figure 5.35: The various brushless Maxon motors ranges, from left to right, top to bottom; EC, EC-Max, EC-Powermax and EC-Flat.

EC The standard brushless motor range. This range provides the most selection and flexibility, not only with motors, but also with gearboxes and other accessories.

EC-max The economical brushless motor range. This range consists of a subset of the EC range which are produced in higher quantities and can thus be offered at lower cost to motors in the EC range.

EC-powermax The high performance brushless motor range. The EC-powermax range consists of motors with higher power and smaller physical size than the EC range, but importantly also with a higher cost.

EC-flat The flat motor range. This range differs from other EC motors in that the motor is laid out differently to achieve motors which are generally larger diameter but flatter than the other motors in the EC range.

The motors were compared based on the cost per Watt of power provided by the motor. The EC-powermax range performed favourably in this comparison, but was ruled out due to the high cost of the motors (typically 3 to 4 times the price of a EC motor with similar power), and also due to the fact that the 200W motor which provided the best value in the range would have required the use of larger and more expensive motor controllers. The EC-flat range was ruled out as motors which provided value and sufficient power could not be fitted with gearboxes and were too large to be realistically mounted within the platform. EC motors above 120W were ruled out due to the physical package of the motor which would be too large to package in the platform. The EC-max range motors are physically larger than the standard EC range for

Figure 5.36: A Maxon planetary gearbox.

the equivalent power, and the monetary saving was insignificant(less than R150 per motor) for the motors under consideration.

The 120W EC motor was the highest power motor available which was physically suitable. It also provided the best value of all other suitable motors.

5.6.2 Gearbox Selection

The gearbox selection was dependant on the torque required to perform certain tasks. The motors had 2 separate applications, drive motors and flipper motors.

To provide additional flexibility to the discrete gearbox ratios available from Maxon (such as that shown in Figure 5.36), an additional final drive ratio was included for both the drive and flipper motors which would take the form of a final gear reduction. The nature of operation of a platform such as this is intermittent periods of high loads, with the majority of time spent either at rest or maneuvering using low power. The motors are rated according to their capabilities to operate continuously at the rated load in still air and with no heat-sinking of the stator coils which are thermally connected to the motor housing. As such an overload factor was specified, which specifies the permissible amount beyond the rated performance a motor would have to be operated to perform a task. The maximum amount of current which it would be possible to deliver to the motors and thus the maximum power output from the motors is ultimately limited by the controllers, which had a soft limit at 5A and a hard cutoff at 10A. Considering the 3.76A rated current of the motor and the 10A limit of the controllers, a maximum overload factor of $\frac{10}{3.76} = 2.66$ was used.

The worst case scenario for the flipper arms would be one in which the entire weight of the platform would be supported on the flippers. As this is highly unlikely to occur during regular operation, specifying the motors according to this scenario should allow the platform to free itself before stalling the motors.

The worst case scenario for a drive motor would be one in which the platform is driving through irregular terrain and the entire weight of the platform would have to be lifted vertically by the drive motors. While it is unlikely that the platform would ever be in a position in which the drive tracks have to lift the entire platform vertically, using this to specify the motor should ensure sufficient torque to free the platform in the case of it becoming stuck.

As the motors and gearboxes were the first components to be specified, a number of assumptions were made about the final size and weight of the platform in order to specify the motors. Additionally to specify a gearbox, the manufacturers specifications for the motors were used. The assumptions made about the platform and motor specifications are as follows:

The final drive ratio for the drive and the flipper was chosen as a 2:1 reduction. The torque on the flipper motors is thus given by:

Item	Value	
Platform		
Platform Weight	20	kg
Pulley Diameter	150	mm
Flipper Length	250	mm
Motor		
Rated Torque	123	mNm
Rated Current	3.76	A
Maximum Current	10	A

Table 5.1: Platform and motor constants used for motor and gearbox specification

$$\begin{aligned} T_F &= \frac{Weight}{2} \times g \times Flipper\ Length \times Final\ Drive\ Ratio \\ &= \frac{20}{2} \times 9.81 \times 0.25 \times \frac{1}{2} \\ &= 12.263Nm \end{aligned}$$

The overload torque, that is the maximum torque which the controllers should allow the motor to output, should be linearly proportional to the amount of current above the rated current which the controllers can supply,

$$\begin{aligned} \frac{Maximum\ Torque}{Rated\ Torque} &= \frac{Maximum\ Current}{Rated\ Current} \\ Maximum\ Torque &= \frac{Rated\ Torque \times Maximum\ Current}{Rated\ Current} \\ Maximum\ Torque &= \frac{0.123 \times 10}{3.76} \\ Maximum\ Torque &= 0.327Nm \end{aligned}$$

Thus the required gearbox ratio is simply the ratio of the 2 torques, $\frac{24.527}{0.327} = 37.485 : 1$.

For the drive pulleys the torque required is,

$$\begin{aligned} T_D &= \frac{Weight}{2} \times g \times Pulley\ Radius \times Final\ Drive\ Ratio \\ &= \frac{20}{2} \times 9.81 \times \frac{0.15}{2} \times \frac{1}{2} \\ &= 7.358Nm \end{aligned}$$

Thus the required gearbox for the drive motors is, $\frac{7.358}{0.327} = 22.491 : 1$.

Using the same gearbox and motor combination for both the flipper and drive motors would result in it being possible to swap out a broken drive motor with a flipper motor in the field if necessary, and would reduce the number of unique spare parts required. In addition using the same motor and gearbox would yield a 10% discount from the supplier. The gearboxes most closely fitting the requirements were 43:1 and 26:1. It would thus be preferable to use a 43:1 gearbox for both the drive and flipper motors providing that this would not make the platform too slow under normal operation. The rated speed of the motor is given as 8710RPM, using a 43:1 gearbox and the estimated wheel diameter results in a platform speed of 1.6m/s. Considering that an average human walks at about 4-5km/h which equates to 1.1-1.4m/s, this platform speed was deemed more than acceptable.

5.6.3 Track Skid Forces

During testing it became apparent that the most challenging requirement of the drive motors was to perform an on-the-spot turn. The friction co-efficient between the track and the ground, μ, was measured at 0.8. Using this information and the geometry of the platform, criteria could be developed for specifying motors and gearboxes for the platform.

The friction forces acting on the tracks while performing a turn were considered. A turn about the center point of the platform would imply that all points on the tracks are moving in a circular path. Friction acts opposite to the direction of motion and as such the direction of the friction force changes at various points along the track. Figure 5.37 shows the forces as a result of friction acting upon a clockwise rotating skid-steered vehicle. The distribution of mass along the length of the track is assumed to be uniform, and as such the magnitude of the distributed frictional force can also assumed to be uniform. The direction of the force changes along the length of the track in order to oppose the direction of motion at a particular point. The cumulative effect of the forces can be summed and considered to produce a moment due to friction acting around the centroid of the vehicle, given in Figure 5.37 as M_F.

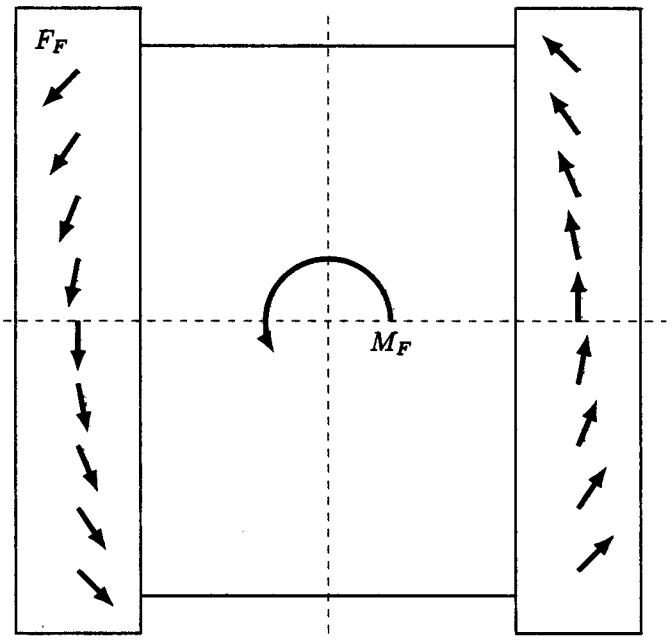

Figure 5.37: The distributed friction force F_F and resulting moment M_F, acting upon a clockwise rotating vehicle.

To calculate the magnitude of the frictional moment M_F, the product of the frictional force and its distance from the center of rotation at all points along the tracks need to be summed. Figure 5.38 shows a diagram of the vehicle and its geometry. The length of track touching the ground is given as L_T, while the distance between the two tracks is given as L_W. Looking only in the first quadrant as shown, we can say that the contribution to the frictional moment over a portion of length Δx of some point, distance x from the midpoint of the track will be given by $F_F \Delta x L(x)$. The total contribution of the first quadrant to M_F is then given by,

$$\sum_{x=0}^{\frac{L_T}{2}} F_F L(x) \Delta x$$

The length L changes as a function of x, and can be expressed as,

$$L(x) = \sqrt{x^2 + \left(\frac{L_W}{2}\right)^2}$$

The expanded form of the first quadrant's contribution to M_F is,

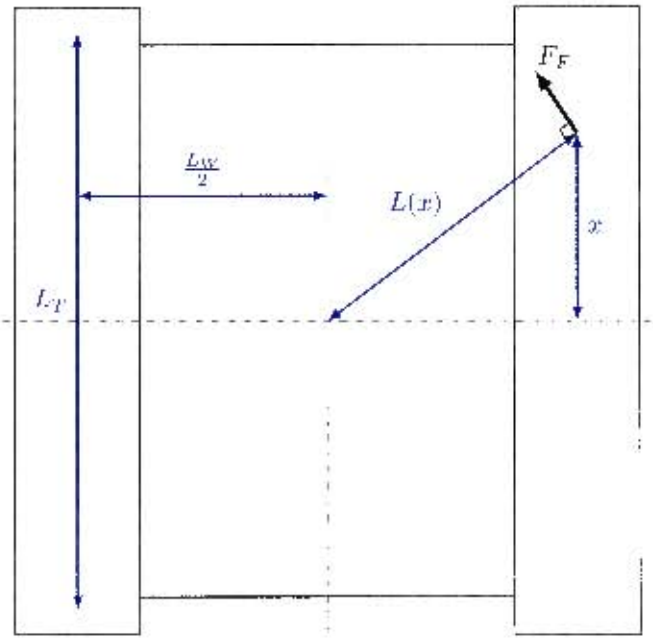

Figure 5.38: The geometric constants for the vehicle used to calculate the frictional moment caused by F_F acting at a distance L from the center of rotation.

$$\sum_{x=0}^{\frac{L_T}{2}} F_F \sqrt{x^2 + \left(\frac{L_W}{2}\right)^2}\,\Delta x$$

The vehicle is assumed to be symmetric about both its horizontal and vertical axes thus,

$$M_F = 4\sum_{x=0}^{\frac{L_T}{2}} F_F \sqrt{x^2 - \left(\frac{L_W}{2}\right)^2}\,\Delta x$$

This can be expressed in integral form as,

$$M_F = 4\int_0^{\frac{L_T}{2}} F_F \sqrt{x^2 + \left(\frac{L_W}{2}\right)^2}\,dx$$

Since the distributed frictional force, F_F, has been assumed to be constant along the length of the track, this can be removed from the integral to simplify the equation,

$$M_F = 4F_F \int_0^{\frac{L_T}{2}} \sqrt{x^2 + \left(\frac{L_W}{2}\right)^2}\,dx$$

Stewart [33] gives the integral of the general form,

$$\int \sqrt{x^2 + a^2}\,dx = \frac{x}{2}\sqrt{x^2 + a^2} - \frac{a^2}{2}\ln\left(x + \sqrt{x^2 - a^2}\right) + C$$

Thus,

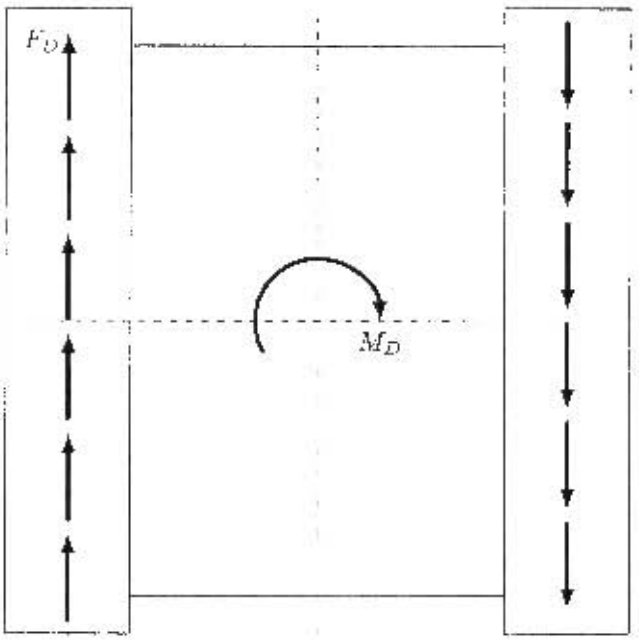

Figure 5.39: The distributed drive force F_D acting upon a clockwise rotating vehicle.

$$M_F = 4F_F \int_0^{\frac{L_T}{2}} \sqrt{x^2 + \left(\frac{L_W}{2}\right)^2}\, dx$$

$$- 4F_F \left[\frac{x}{2}\sqrt{x^2 + \left(\frac{L_W}{2}\right)^2} + \frac{\left(\frac{L_W}{2}\right)^2}{2} \ln\left(x + \sqrt{x^2 + \left(\frac{L_W}{2}\right)^2} \right) \right]_0^{\frac{L_T}{2}}$$

$$M_F - 4F_F \left(\frac{L_T}{4}\sqrt{\frac{L_T^2 + L_W^2}{4}} - \frac{L_W^2}{8} \ln\left(\frac{L_T}{2} + \sqrt{\frac{L_T^2 + L_W^2}{4}} \right) - \frac{L_W^2}{8} \ln\left(\frac{L_W}{2} \right) \right)$$

The frictional force F_F can be assumed to be directly proportional through a friction co-efficient to the mass of the platform given by M. The platform mass M, is uniformly distributed along the length of the 2 tracks $2L_T$, yielding a distributed load on the tracks of $\frac{M}{2L_T}$. The distributed frictional force can then be given by,

$$F_F = \mu g \frac{M}{2L_T}$$

Where μ is the co-efficient of friction, and g is the gravitational constant. Substituting this into the previous result gives

$$M_F = \frac{2\mu g M}{L_T} \left(\frac{L_T}{4}\sqrt{\frac{L_T^2 + L_W^2}{4}} + \frac{L_W^2}{8} \ln\left(\frac{L_T}{2} - \sqrt{\frac{L_T^2 + L_W^2}{4}} \right) - \frac{L_W^2}{8} \ln\left(\frac{L_W}{2} \right) \right) \tag{5.1}$$

The drive tracks exert drive force to create a turning moment, M_D, which is opposed by the frictional moment, M_F. For the vehicle to turn the applied moment must be at least equal to the opposing moment, so $M_D = M_F$.

The drive force acts at a distance $\frac{L_W}{2}$ from the centerline as shown in Figure 5.39. The moment exerted by one track is $F_D \frac{L_W}{2}$. The total moment due to drive forces M_D,

$$M_D = 2F_D\frac{L_W}{2}$$
$$M_D = F_D L_W$$

Equating the drive and friction moments allows F_D to be determined,

$$\begin{aligned} M_D &= M_F \\ F_D L_W &= \frac{2\mu g M}{L_T}\left(\frac{L_T}{4}\sqrt{\frac{L_T^2+L_W^2}{4}} - \frac{L_W^2}{8}\ln\left(\frac{L_T}{2}+\sqrt{\frac{L_T^2-L_W^2}{4}}\right) \quad \frac{L_W^2}{8}\ln\left(\frac{L_W}{2}\right)\right) \\ F_D &= \frac{2\mu g M}{L_T L_W}\left(\frac{L_T}{4}\sqrt{\frac{L_T^2-L_W^2}{4}} + \frac{L_W^2}{8}\ln\left(\frac{L_T}{2}+\sqrt{\frac{L_T^2+L_W^2}{4}}\right) - \frac{L_W^2}{8}\ln\left(\frac{L_W}{2}\right)\right) \end{aligned} \tag{5.2}$$

This can be used to determine the torque requirements at the motor output shaft, T_M, using the drive pulley diameter D_D and the total gear ratio between the motor output and the drive pulley g_f.

$$T_M = \frac{\mu g M D_D}{g_f L_T L_W}\left(\frac{L_T}{4}\sqrt{\frac{L_T^2+L_W^2}{4}} + \frac{L_W^2}{8}\ln\left(\frac{L_T}{2}+\sqrt{\frac{L_T^2+L_W^2}{4}}\right) - \frac{L_W^2}{8}\ln\left(\frac{L_W}{2}\right)\right) \tag{5.3}$$

The plot of Equation 5.3 in Figure 5.40 shows that as the vehicle gets relatively long and narrow, i.e. $\frac{L_T}{L_W} > 1$ the torque requirements increase and that conversely with $\frac{L_T}{L_W} < 1$ the torque requirements decrease.

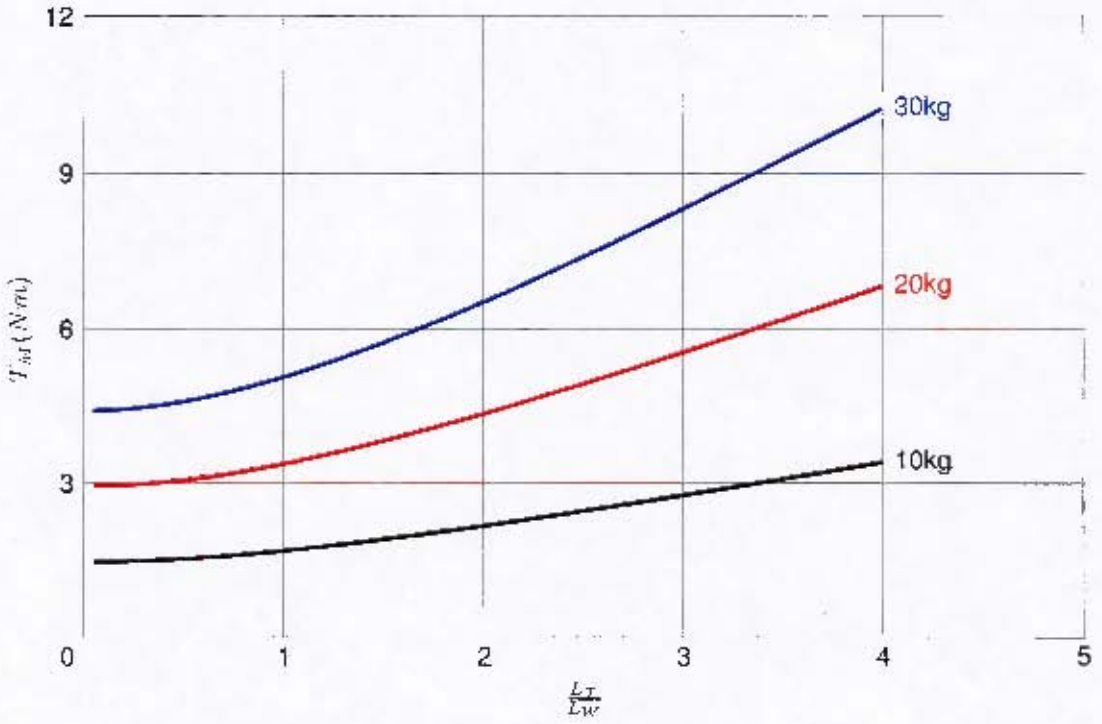

Figure 5.40: A plot showing the relationship between the geometry of a vehicle and the motor torque required to perform an on-the-spot turn. Data is shown for 3 different vehicle weights.

The weight of the platform as built is above 42kg rather than the estimated 20 kg. The increased platform weight pushed the torque requirements beyond what could be provided, even for short periods of time. The initial estimation for maximum torque allowed by the controller was based on a maximum current of 10A, testing revealed that the controller's soft limit of 5A would have been a better choice.

Using these calculations new motor and gearbox combinations for the drive and flipper motors were ordered. Space constraints limited choice to the same 120W motor with any 3 stage planetary gearbox. In addition to the increased platform mass of 42kg, a 17kg robotic arm and sensor payload shown in Figure 5.41 was fitted to the platform. This yields a new total design weight of 60kg.

Using the final platform weight and size to determine the drive torque required to perform a turn, yields,

$$\begin{aligned} T_D &= \frac{\mu g M D_D}{g_f L_T L_W}\left(\frac{L_T}{4}\sqrt{\frac{L_T^2+L_W^2}{4}}+\frac{L_W^2}{8}\ln\left(\frac{L_T}{2}+\sqrt{\frac{L_T^2+L_W^2}{4}}\right)-\frac{L_W^2}{8}\ln\left(\frac{L_W}{2}\right)\right) \\ &\quad -\frac{0.8\times 9.81\times 60\times 0.127}{\frac{45}{25}\times 0.65\times 0.5}\left(\frac{0.65}{4}\sqrt{\frac{0.65^2+0.5^2}{4}}-\frac{0.5^2}{8}\ln\left(\frac{0.65}{2}-\sqrt{\frac{0.65^2+0.5^2}{4}}\right)-\frac{0.5^2}{8}\ln\left(\frac{0.5}{2}\right)\right) \\ &= 13.595Nm \end{aligned}$$

Comparing this to the torque required to lift the platform vertically using the drive tracks yields,

$$\begin{aligned} T_D &= \frac{Weight}{2}\times g\times Pulley\ Radius\times Final\ Drive\ Ratio \\ &= \frac{60}{2}\times 9.81\times\frac{0.127}{2}\times\frac{27}{45} \\ &= 11.213Nm \end{aligned}$$

Thus the torque required to perform an on the spot turn is greater than that required to lift the platform vertically. Using 5A instead of 10A for maximum current gives a new maximum torque of 0.164Nm. Calculating the desired gearbox ratio for the motor thus yields $\frac{13.595}{0.164} = 82.896:1$. To avoid operating the motor near its limit, an additional safety factor of 1.5 was applied, this in turn yields a desired gearbox ratio of $124.345:1$. The next available size up from this is $126:1$, which was ordered.

5.6.4 Revised Flipper Torque Requirements

The additional platform weight ultimately changed the demands on the flipper motors and as such the gearboxes needed to be re-specified.

$$\begin{aligned} T_F &= \frac{Weight}{2}\times g\times Flipper\ Length\times Final\ Drive\ Ratio \\ &= \frac{60}{2}\times 9.81\times 0.25\times\frac{25}{47} \\ &= 39.136Nm \end{aligned}$$

Using the new maximum motor torque of 0.164Nm, the desired gearbox ratio is $238.632:1$. Unfortunately the largest available reduction for a 3 stage gearbox is $156:1$. This was chosen as it was the only option. The consequences of this are that the flippers have to be used with some care, and would not be able to rely on the flippers to remove the fully loaded platform from all situations.

5.7 Concluding Remarks

In total there are 68 unique parts and 170 components which were machined for the platform. The aluminium parts which make up the majority of the structure of the platform are shown in Figure 5.42.

The concept designed was successfully completed and met the desired specifications with the exception of the platform mass which, at 42kg was somewhat higher than the desired 20kg. Further investigation of how the completed platform met the specifications is given in Chapter 7. In Chapter 6 which follows, the electrical, electronic and software systems which control the platform are discussed.

Figure 5.41: The platform with robotic arm and sensor payload(Image courtesy of Richard Whittemore).

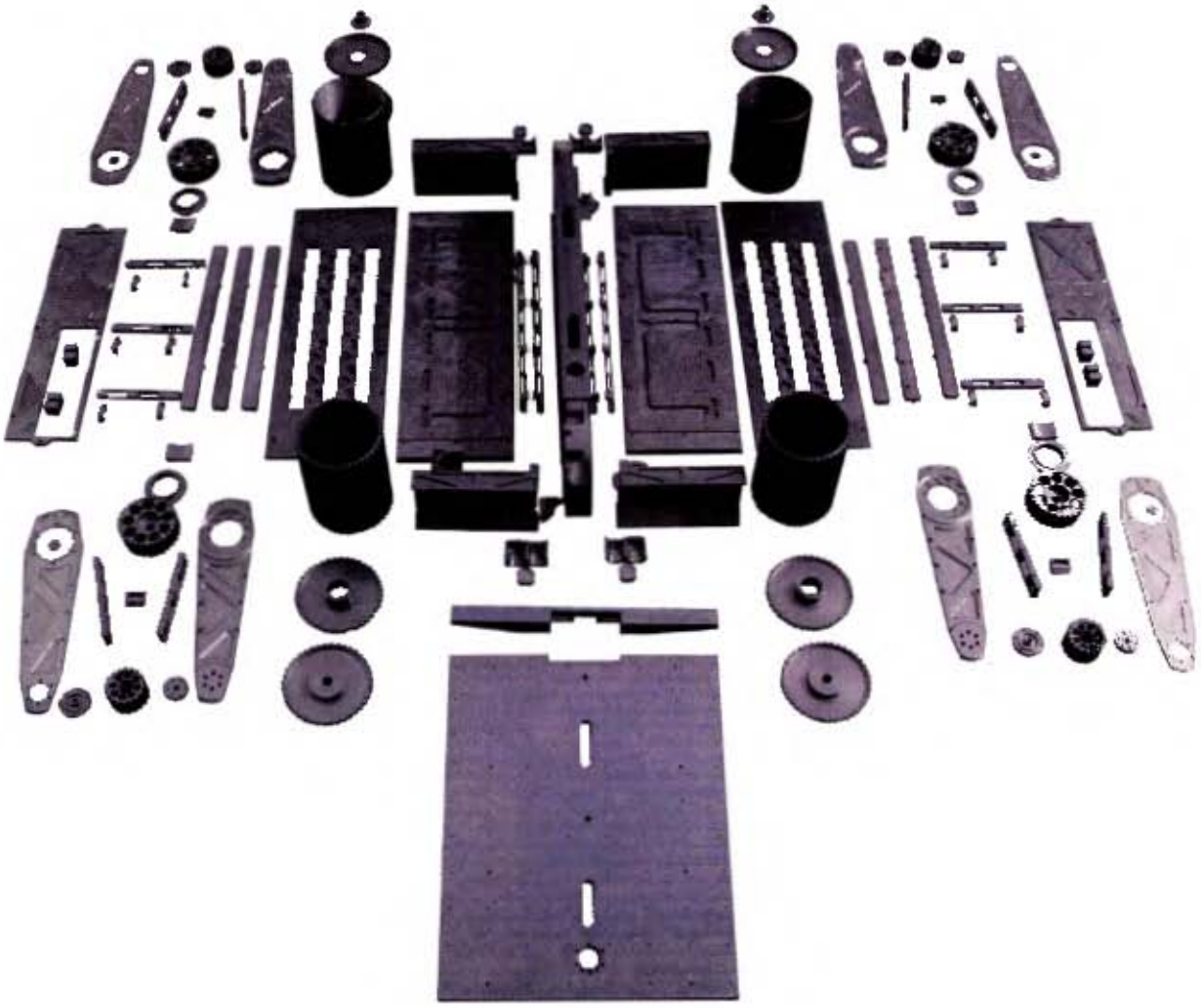

Figure 5.42: The machined aluminium parts making up the platform after anodising.

Chapter 6

Electrical, Electronic and Software Systems

In order to operate the platform's mechanical systems, power and control signals must be directed to the various subsystems of the robot. These systems can be broken down into the electrical system which is tasked with providing power to the platform, the control system, which is the electronic equipment which converts signals sent by the operator into the signals required to make the motors move, and finally the software which provides the interface between the operator and the platform.

6.1 Power Distribution

The platform makes use of 18V 3.0Ah Lithium-Ion Makita power tool batteries as the power source. The platform contains 6 of these batteries in total. The terminals of the batteries are connected to a power distribution board. The board was designed to fit upright within the sidepod, as shown in Figure 6.1. This board has a number of functions;

Power Supply The board connects 2 sets of 2 batteries in series to provide 36V, while the remaining 2 batteries are used to supply 18V. The 36V power line is used to power additional switched mode power supplies to provide both 12V and 5V which are used to power additional equipment added to the robot.

Power Tether The board uses relays which switch from battery to tether supplied power when the tether is connected.

Emergency Stop The board uses the emergency stop switch to trigger a relay which disconnects all power lines, thus shutting down all robot sub-systems.

Figure 6.2 shows the schematic of the power board, while the functional components are shown in Figure 6.3.

6.2 Control

Figure 6.4 shows an overview of the control system. The control system can be described as follows;

Interface layer The software on the operators computer converts the position of the joystick into a command to send to the robot. This software is discussed further in Section 6.3.

Communications layer The operator's computer sends the command over Ethernet to the Ubiquiti RouterStation Pro wireless router board in the control station. The router board takes the command and transmits it wirelessly to an identical router-board on the platform. The router board on the platform receives the command and outputs it through its Ethernet port.

Control Layer The command sent by the operator is extracted from the Ethernet packet and outputted over serial by the Tibbo DS1206 Ethernet-to-serial converter. The command is then broadcast to the motor control boards on the robot. The microprocessor on the motor control boards uses a Digital to Analogue Convertor (DAC) to generate an analogue signal sent to the Maxon motor controllers which is used to set the desired motor speed. Buffered IO pins control the enable and direction pins on the Maxon motor controller.

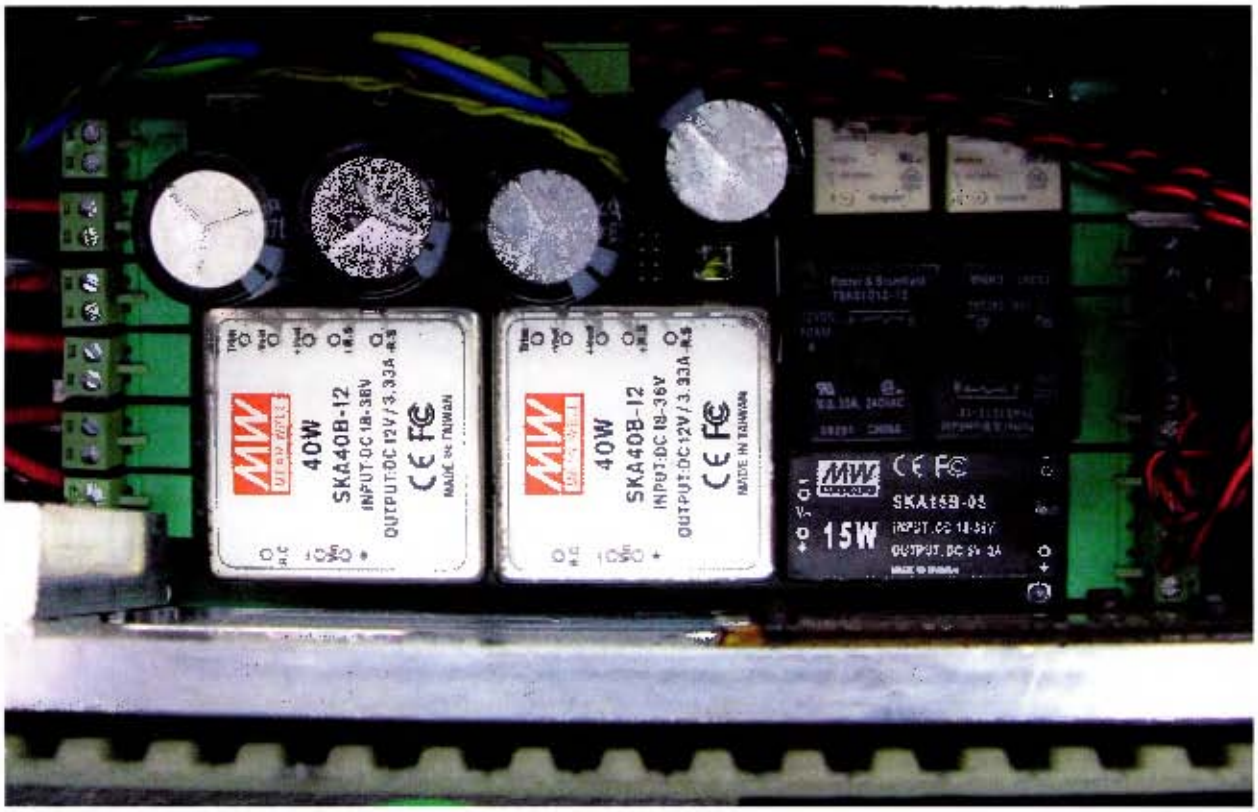

Figure 6.1: The power distribution board installed in the platform sidepod.

6.2.1 Wireless Router Board

The wireless router boards used on the operator station and on the platform are identical Ubiquiti RouterStation Pro boards. Both boards are fitted with 2 5.0GHz radios which each connect to an antenna. These router boards are fundamentally an embedded computer running a version of Linux, designed specifically for use on network routers, called OpenWRT. Setting up these boards is achieved by logging onto the boards over an SSH connection and altering configuration files on the boards. An image of one of these boards is shown in Figure 6.5.

6.2.2 Ethernet to Serial Converter

The existing motor control boards receive commands via RS232 serial communication, while the router boards communicate primarily through Ethernet. The router boards do have an on-board serial port, however this would require writing software to run on the router which would convert the Ethernet signals to serial, this would require additional setup to be done on any replacement board, and would only provide one serial port. The Tibbo DS1206 Serial to Ethernet converter shown in Figure 6.6, requires no setup, and is capable of providing 4 serial connections through one port and as such was a preferable choice to the serial port onboard the RouterStation Pros.

6.2.3 Motor Control Boards

The motor control boards shown in Figure 6.7 were designed by Robotics and Agents Research Laboratory MSc student Justin Pead and were reprogrammed for use in this application. The board features a Freescale GT16 microprocessor which interfaces with a DAC. The DAC is used to output a voltage between 0 and 5V corresponding to a received motor speed value of 0-255. This analogue signal is then connected to the speed control input on the Maxon motor controllers. The microprocessor also uses a number of buffered IO pins to control the enable and direction inputs on the Maxon motor controllers.

6.2.4 Control Command Structure

The motor control boards have a defined structure for the commands which they will accept. The structure is as follows:

255 A B C

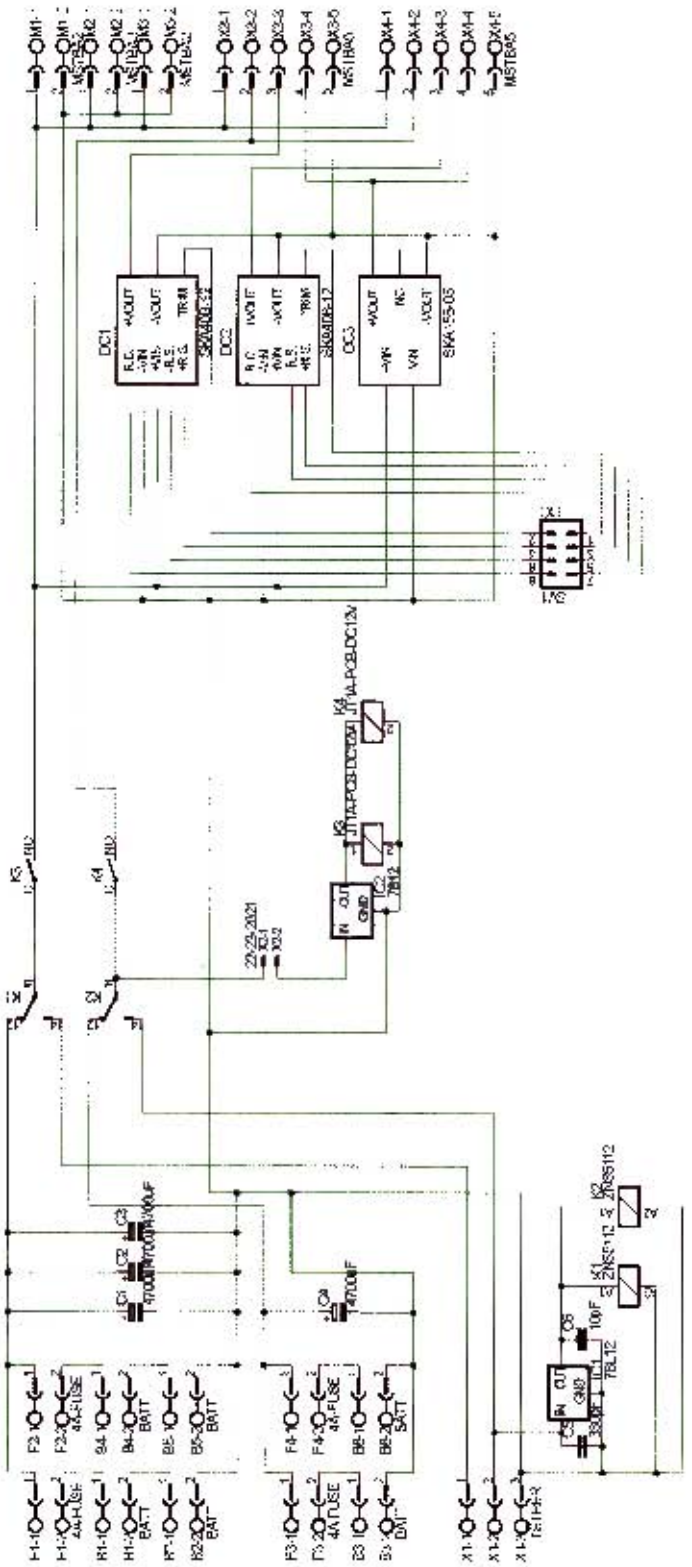

Figure 6.2: The schematic of the power distribution board.

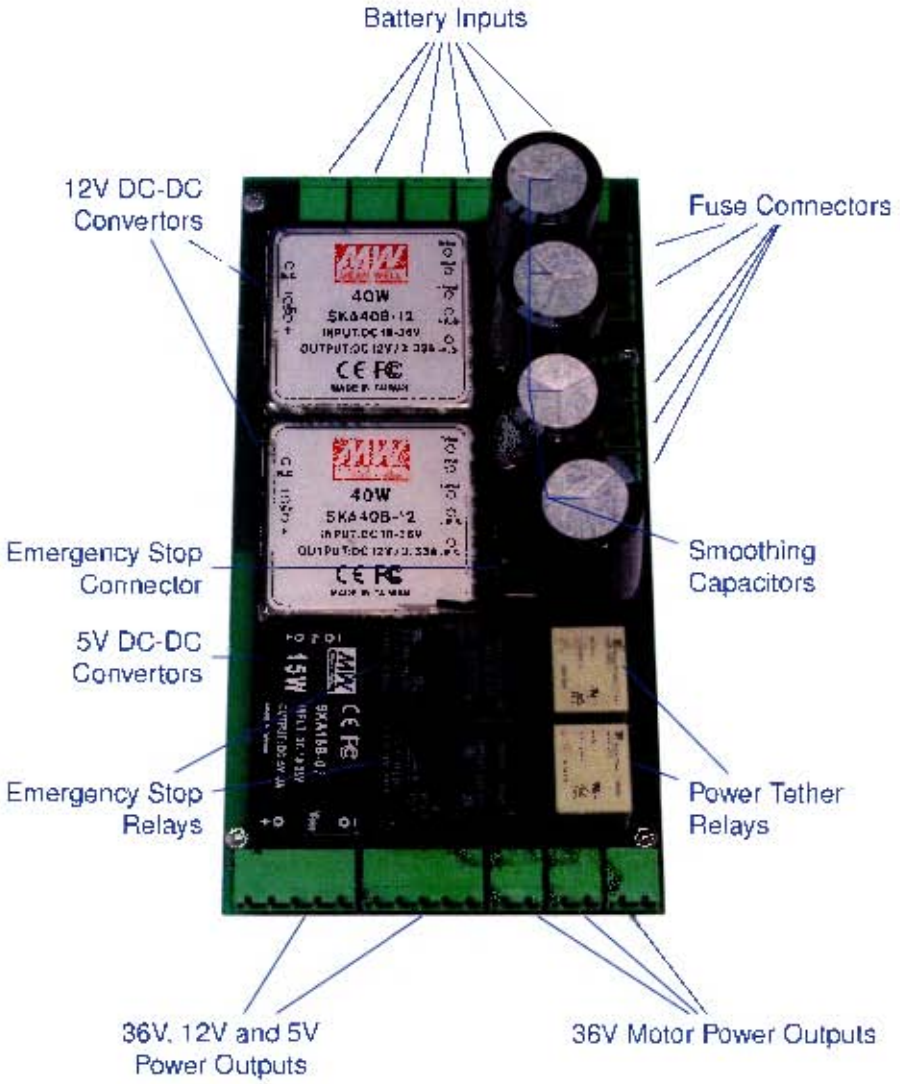

Figure 6.3: The various components on the power distribution board.

255 Initiate Each command starts with 255 as a method for signalling the start of a command to prevent errors in the event of corrupted communications.

A Motor select This is a number between 0 and 4 which specifies which motor the command is intended for (See Figure 6.8).

B Direction When 0 this command causes the motor to spin in the clockwise direction, otherwise the motor spins in the anti-clockwise direction.

C Speed This number between 0 and 255 sets the speed of the motor.

6.2.5 Motor Controllers

The controllers used are Maxon DECV50/5 controllers. These controllers are capable of supplying 5A continuously, but can provide up to 10A for short periods of time. Figure 6.9 shows the controllers as supplied in their metal enclosures and also once removed from from the enclosure to allow the board to be fitted in the drive pulleys.

6.2.6 Video Cameras

Three black and white miniature cameras are installed on the base. One of these cameras is shown in Figure 6.10. The Camera signals are encoded for transmission across the Ethernet network by the Bosch VIP X2 video encoder shown in Figure 6.11. The cameras provide a forward, rear and top view of the platform.

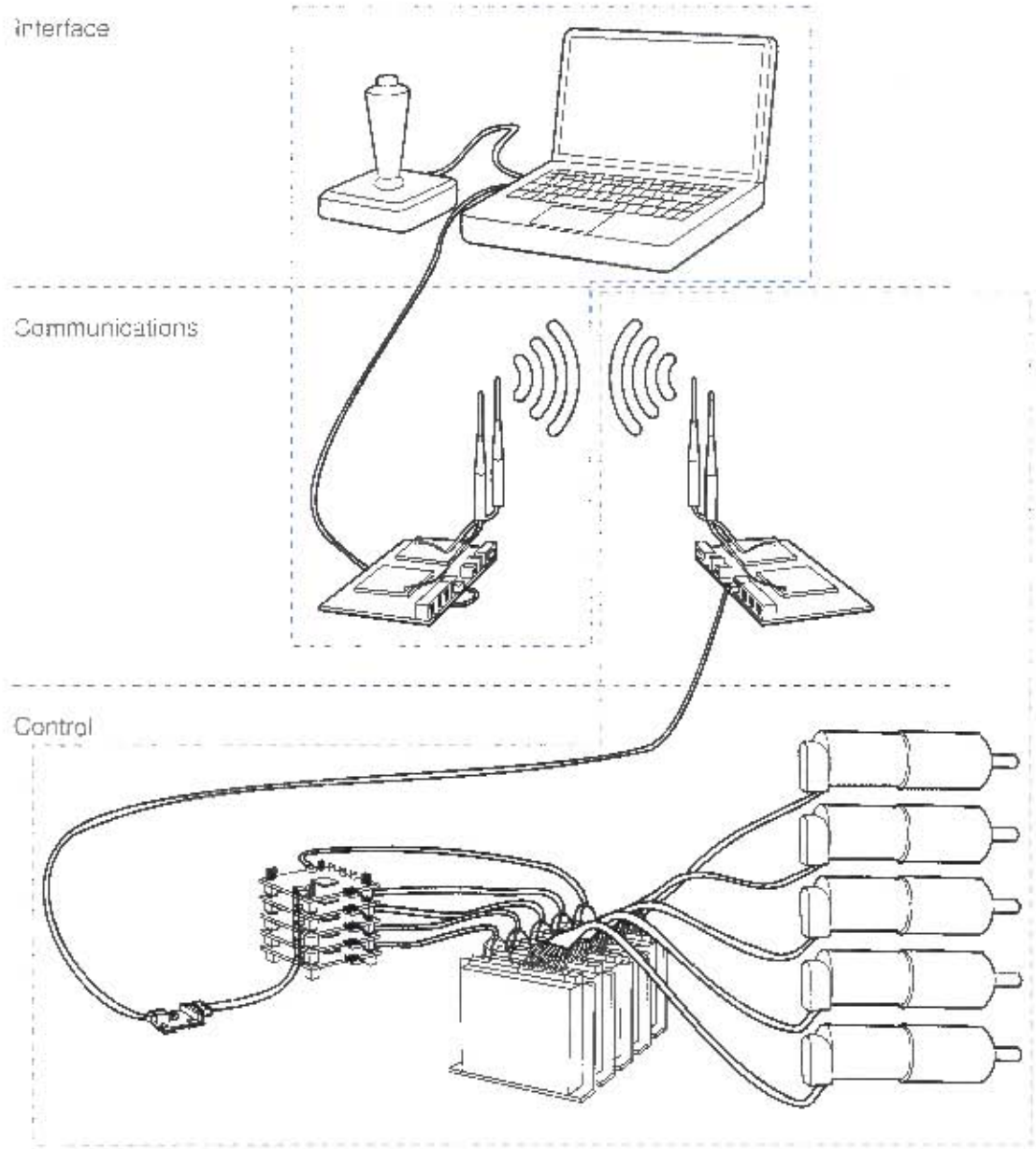

Figure 6.4: The control system of the platform. The figure shows the control system broken down into its 3 functional layers. The items enclosed by the blue dashed line are on the operator control station, while the items enclosed by the green line are on board the platform itself.

Figure 6.5: The Ubiquiti RouterStation Pro boards used to communicate with the platform.

Figure 6.6: The Tibbo DS1206 Ethernet to serial converter

Figure 6.7: The motor control boards used to provide signals to the motor controllers.

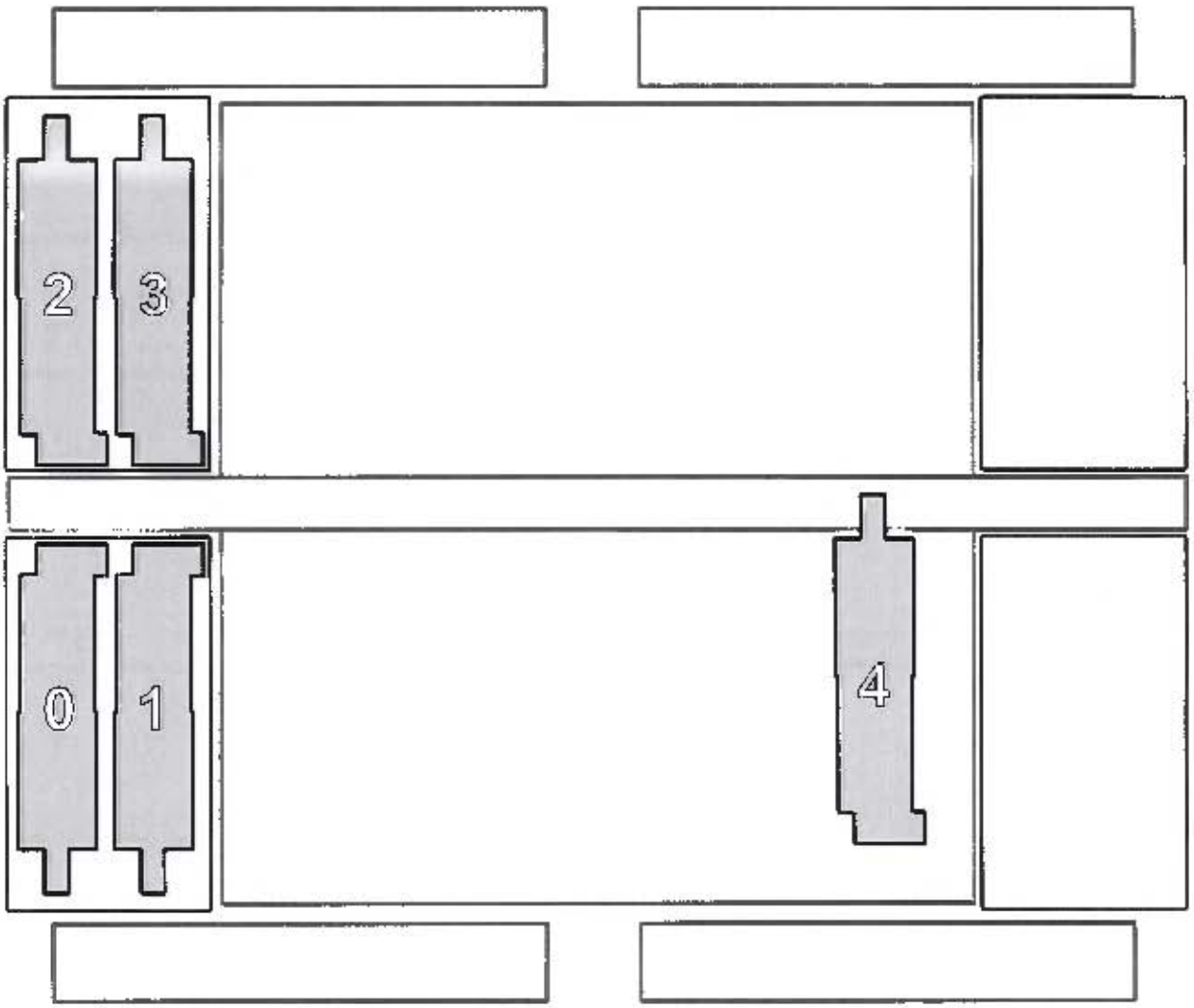

Figure 6.8: Plan view showing the positions of the various motors on the platform.

Figure 6.9: The Maxon DECV50/5 motor controller inside and also removed from the enclosure.

Figure 6.10: The miniature cameras installed on the platform.

Figure 6.11: The Bosch VIP X2 Ethernet video encoder [34].

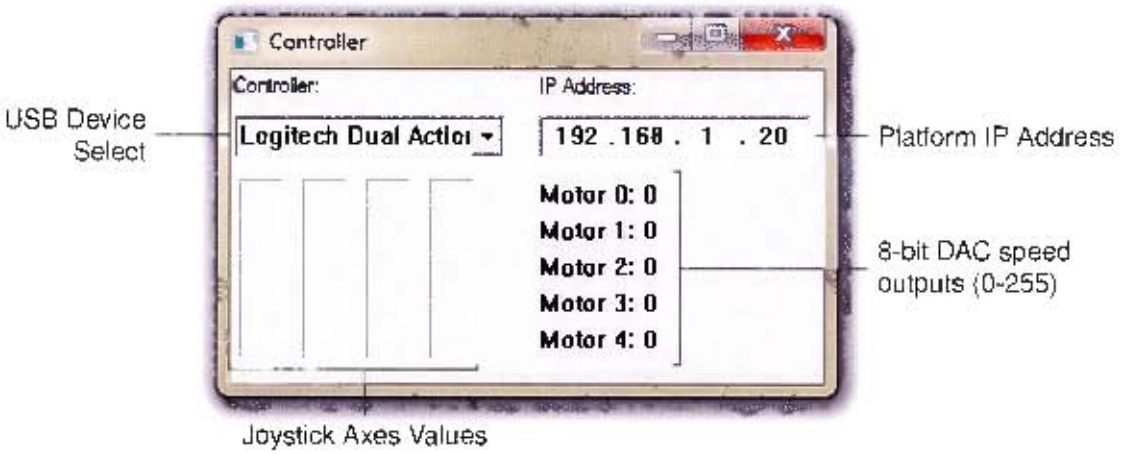

Figure 6.12: The GUI for the control software for the robot.

6.3 Software Systems

The software referred to in this section is primarily the software which runs on the operator's computer. The software running on the motor controllers onboard the robot is described above.

To control the robot, the control software takes an input from a device such as a joystick, converts this into values for motor speed and then transmits this information over the network to the platform. A screenshot of the control program is shown in Figure 6.12. It is written using the Win32 C++ libraries for maximum execution speed. This does however limit the use of the software to the Microsoft Windows™ operating system. Writing the code using a language or libraries which would allow it to be ported more easily to other operating systems was considered, but was deemed undesirable. Windows™ is by far the most popular operating system in use today and would most likely be installed by default on any computer used for the operator station. Also it is highly likely that the operator station will have to run software which will only run on the Microsoft Windows™ operating system (for example the Bosh Video encoders are designed primarily for use with Windows™).

The software communicates with the joystick as an Human Interface Device (HID) device. This choice was made as it allows the use of any generic USB device to be used as a controller. The software communicates with the device and retrieves the number of axes and buttons which the device possesses. It also retrieves the maximum values of the axes. Using these libraries it is possible to create control software which should work with any USB device. The HID code was tested with 2 different model Logitech gamepads, 3 different Microsoft Joysticks and a 3dConnexion SpaceMouse. It was able to use all devices as controllers without the need to install any drivers.

6.3.1 Joystick Input Transformation

A problem faced when trying to control the motion of a tracked vehicle with a joystick type controller, is how the values retrieved from the position of the joystick should be converted to speed inputs to the motors. It is desired that the use of the joystick should be totally intuitive and require no or minimal operator training. As such we wish to consider what motion would be expected from any particular joystick input and try and create a system that generates the required motor values from those inputs, with smooth transitions between them.

The particular device and software driver being used for receiving input values from the input device will effect the raw data, but for the sake of this example, the initial state is considered where each axis of the joystick has possible values from $0 \rightarrow J_{max}$ and in the rest position the axis would have the value of $\frac{J_{max}}{2}$. This arrangement for a 2 axis joystick is shown in Figure 6.13.

It would be desirable for the joystick to have a rest position of $(0,0)$ and a maximum magnitude of 1, this would allow for the direction vector to be easily scaled. The space and hence the direction vector $\vec{D}$ is transformed to produce the space shown in Figure 6.14 and the transformed direction vector $\vec{D'}$. It is

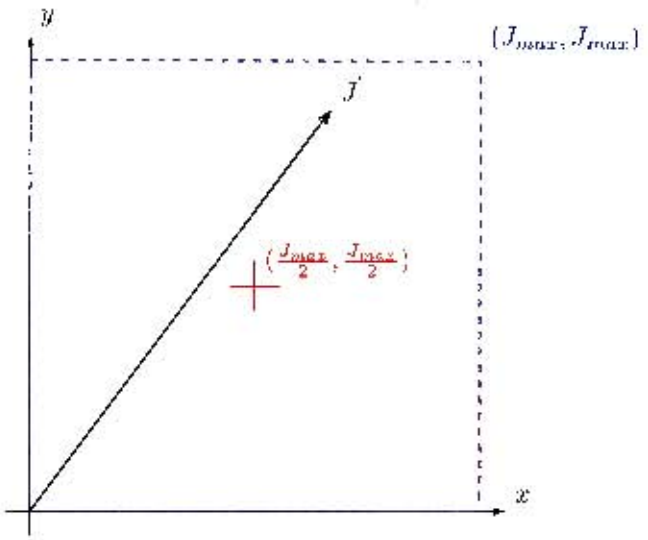

Figure 6.13: The initial space raw data from a joystick may be received in. The red cross-hairs in the center indicates the rest position of the joystick, the blue bounding box shows the limits of joystick values and vector $\vec{J}$ shows an example vector of the joysticks position.

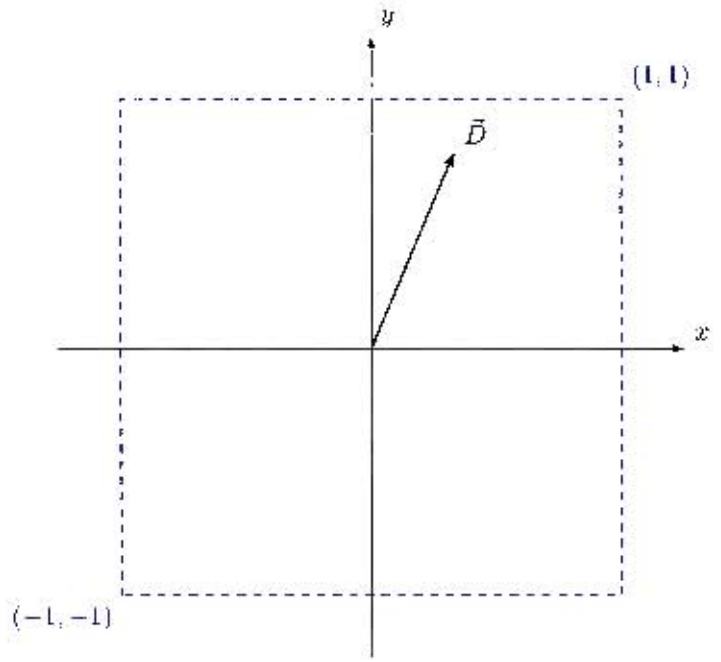

Figure 6.14: The transformed joystick space and direction vector.

possible to find $\vec{D}$ using the following formula,

$$\vec{D} = \frac{2 \times \left(\vec{J} - \frac{J_{max}}{2} \begin{bmatrix} 1 \\ 1 \end{bmatrix} \right)}{J_{max}}$$

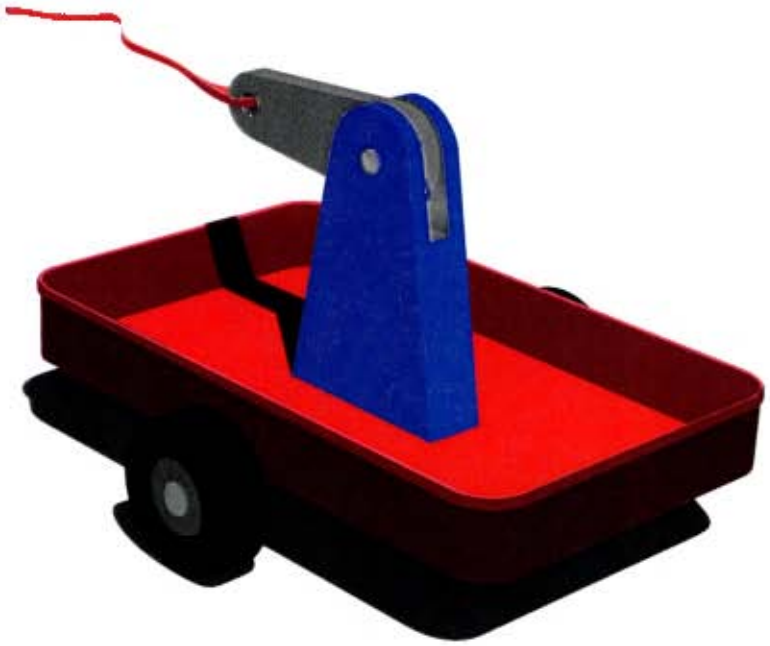

Figure 6.15: A visual representation of the control metaphor.

6.3.2 Control Metaphor

The input from the joystick ultimately is being used to derive values to send to the drive motors on-board the platform. The aim of the control system was for it to be as intuitive as possible. With this in mind, thought was given to what platform motion could be expected from various joystick motions.

Joystick pushed forward
The platform should move forward.

Joystick pulled backward
The platform should move backward.

Joystick pushed left or right
The platform should perform an on-the-spot turn in the anti-clockwise and clockwise direction respectively.

Joystick pushed in a direction between the x and y axes
The platform should perform a sweeping turn.

The control metaphor chosen to simulate this behaviour is one of a two-wheeled cart being pulled by an elastic rope as shown in Figure 6.15.

This model has a number of useful features;

Steering arm
This feature provides the on-the-spot turning ability and through changing the geometry allows the steering sensitivity to be adjusted.

Elastic rope
The joystick controls both the direction and the speed of the platform. In most vehicles separate controls would be used for speed and direction, the accelerator pedal and steering wheel in a car for instance. If possible, it would be desirable to use one control for both speed and direction. The distance from the rest position of the joystick could be viewed as the magnitude of the speed, while the direction the joystick is pointing in could be viewed as the direction the robot is travelling. This can be visualised as an elastic rope pulling the cart, the direction the rope is pulled in controls the direction of the cart, and the extension of the rope would relate to the speed the cart travels at.

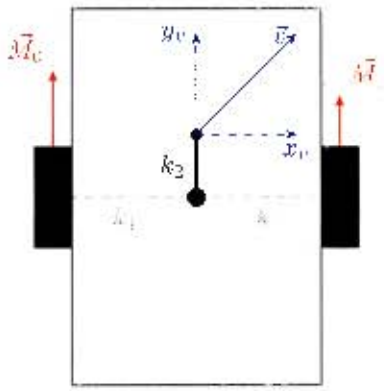

Figure 6.16: The geometry of the cart used as the control metaphor.

Dead band

This can be thought of as the elastic rope being slack, when the joystick is moved small distances around the center point, nothing will happen. A dead-band helps to combat unwanted movements due to vibration, or due to the joystick not returning precisely to its zero position after being released.

Figure 6.16 shows the layout of the cart. The speed of the steering arm end due to the operator applied force is represented by $\vec{v}$ while the motor speeds are represented by $\vec{M}_0$ and $\vec{M}_1$.

The combined effect of the wheel speeds, $\vec{M}_0$ and $\vec{M}_1$, should equal that of $\vec{v}$, which has components $(x_v\ y_v)$. The rotational and translational velocities can be summed to find the resultant wheel velocities. Summing the rotational velocities around the center of the the cart,

$$\frac{M_{0rot}}{k_1} = \frac{x_v}{k_2}$$
$$M_{0rot} = x_v \frac{k_1}{k_2} \tag{6.1}$$

$$\frac{-M_{1rot}}{k_1} = \frac{x_v}{k_2}$$
$$M_{1rot} = -x_v \frac{k_1}{k_2} \tag{6.2}$$

The translational velocities of the wheels must be equal to that of the cart,

$$M_{0trans} = M_{1trans} = y_v \tag{6.3}$$

The ratio between the width of the cart and the the steering arm $\frac{k_1}{k_2}$ is combined into a single geometry constant k_g. In total,

$$M_0 = M_{0trans} - M_{0rot}$$
$$M_0 = y_v - k_g x_v \tag{6.4}$$

and

$$M_1 = M_{1trans} + M_{1rot}$$
$$M_1 = y_v - k_g x_v \tag{6.5}$$

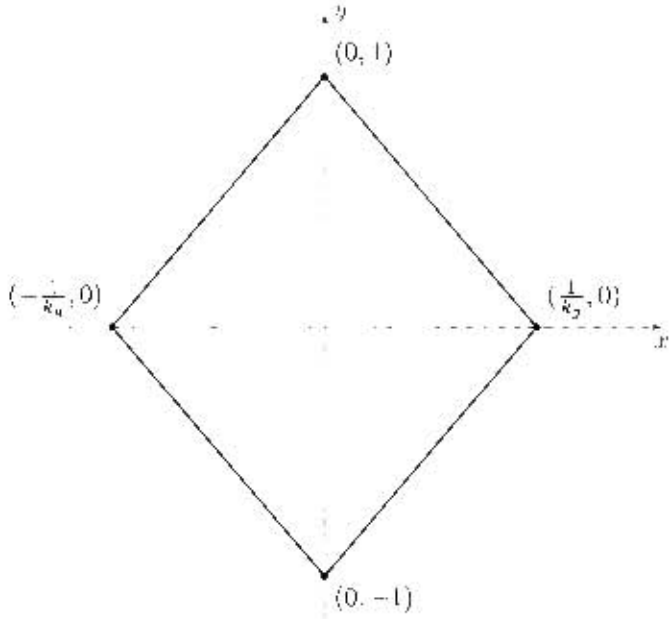

Figure 6.17: The region of acceptable velocity vectors.

Both M_0 and M_1 have a maximum magnitude, which for the sake of convenience can be set to 1. This places limits on acceptable values for x_v and y_v.

$$\begin{aligned} |M_0| &\leq 1 \\ |y_v + k_y x_v| &\leq 1 \end{aligned} \tag{6.6}$$

$$\begin{aligned} |M_1| &< 1 \\ |y_v - k_y x_v| &\leq 1 \end{aligned} \tag{6.7}$$

This creates a region of acceptable values for y_v and x_v as shown in Figure 6.17.

What is now required is some method of transforming the space and joystick inputs shown in Figure 6.14 to that shown in Figure 6.17. The direction of the joystick input vector needs to be preserved, while its magnitude needs to be scaled. This leads to a transformation scheme similar to that shown in Figure 6.18.

Considering a generic situation as shown in Figure 6.19 the proposed method for transformation is to consider,

$$\frac{\vec{v}}{v_{max}} - \frac{\vec{D}}{D_{max}} \tag{6.8}$$

The line $f(x)$ defined by $\vec{D}$, has the equation,

$$f(x) = \frac{y_D}{x_D} x$$

while the equation for the line $g(x)$ in any quadrant is given by,

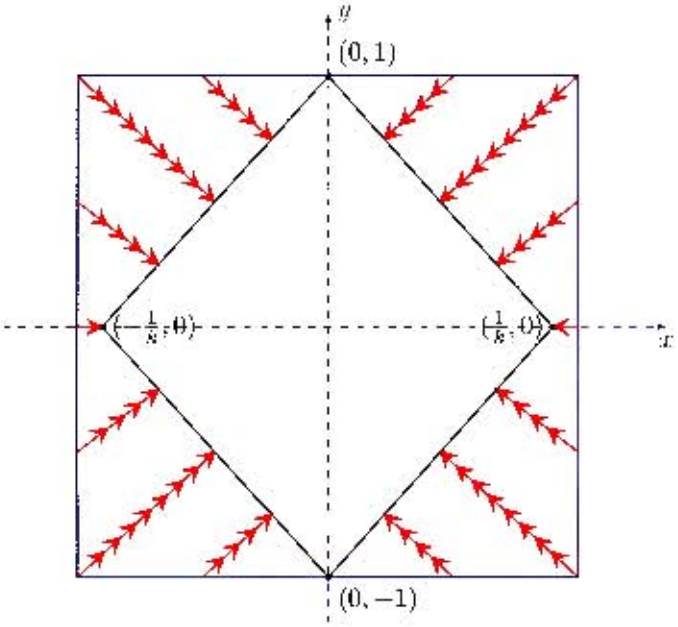

Figure 6.18: The transformation from joystick input to vehicle speed vector.

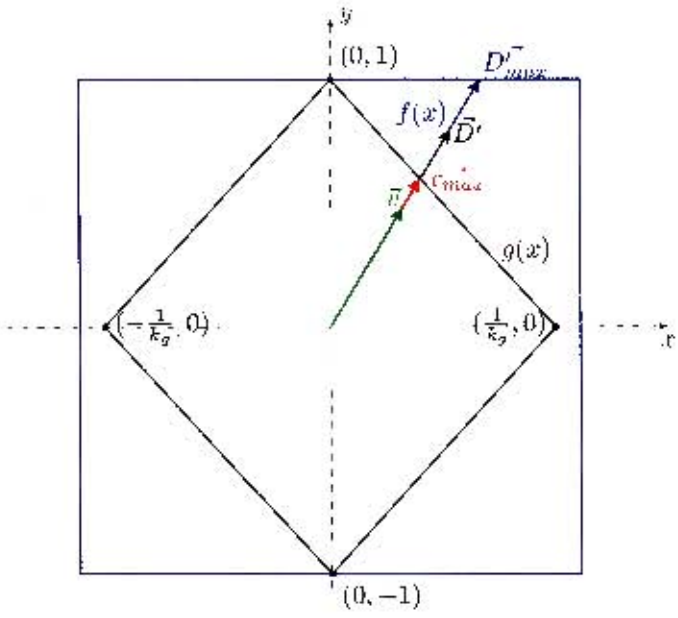

Figure 6.19: The joystick space and direction vectors before and after transformation.

$$g(x) = \frac{y_D}{|y_D|}\left(1 - \frac{x_D}{|x_D|}k_g x\right)$$

The point of intersection between $f(x)$ and $g(x)$ allows v_{max} to be found,

$$\begin{aligned} x_{v_{max}} &= \frac{x_D}{|y_D| + k_g|x_D|} \\ y_{v_{max}} &= \frac{y_D}{|y_D| + k_g|x_D|} \end{aligned} \tag{6.9}$$

From 6.8,

$$\begin{aligned} \frac{\vec{v}}{\vec{v_{max}}} &= \frac{\vec{D}}{\vec{D_{max}}} \\ \therefore \frac{x_v}{x_{v_{max}}} &= \frac{x_D}{x_{D_{max}}} \\ x_v &= x_{v_{max}}\frac{x_D}{x_{D_{max}}} \end{aligned} \tag{6.10}$$

Depending on where along the boundary $\vec{D_{max}}$ is, $x_{D_{max}}$ can be found, then used to find the motor speed values M0 and M1,

$|x_D| \leq |y_D|$

$$f(x) = \pm 1 = \frac{y_D}{|y_D|} = \frac{y_D}{x_D}x_{D_{max}}$$
$$x_{D_{max}} = \frac{x_D}{y_D}$$

Using 6.10 *and* 6.9

$$x_v = \frac{x_D|y_D|}{|y_D| + k_g|x_D|}$$
$$y_v = \frac{y_D|y_D|}{|y_D| + k_g|x_D|}$$

Substituting back into 6.4 *and* 6.5

$$M_0 = \frac{(y_D + k_g x_D)|y_D|}{|y_D| + k_g|x_D|}$$
$$M_1 = \frac{(y_D - k_g x_D)|y_D|}{|y_D| + k_g|x_D|}$$

$|x_D| > |y_D|$

$$x_{D_{max}} = \pm 1 = \frac{x_D}{|x_D|}$$

Using 6.10 *and* 6.9

$$x_v = \frac{x_D|x_D|}{|y_D| + k_g|x_D|}$$
$$y_v = \frac{y_D|x_D|}{|y_D| + k_g|x_D|}$$

Substituting back into 6.4 *and* 6.5

$$M_0 = \frac{(y_D + k_g x_D)|x_D|}{|y_D| + k_g|x_D|}$$
$$M_1 = \frac{(y_D - k_g x_D)|x_D|}{|y_D| + k_g|x_D|}$$

The maximum value of M_0 and M_1 is 1. Thus to generate integer values to send to the motor, a scaling factor needs to be applied. To achieve intuitive operation, another factor $\frac{y_D}{|y_D|}$ is applied to the $k_g x_D$ term. This can be physically thought of as reversing the direction of the steering arm when the vehicle is put in reverse.

$|x_D| \leq |y_D|$

$$M_0 = k_s \left(\frac{(y_D + \frac{y_D}{|y_D|} k_g x_D)|y_D|}{|y_D| + k_g|x_D|} \right)$$

$$M_1 = k_s \left(\frac{(y_D - \frac{y_D}{|y_D|} k_g x_D)|y_D|}{|y_D| + k_g|x_D|} \right)$$

$|x_D| > |y_D|$

$$M_0 = k_s \left(\frac{(y_D + \frac{y_D}{|y_D|} k_g x_D)|x_D|}{|y_D| + k_g|x_D|} \right)$$

$$M_1 = k_s \left(\frac{(y_D - \frac{y_D}{|y_D|} k_g x_D)|x_D|}{|y_D| + k_g|x_D|} \right)$$

Where,

x_D The x co-ordinate of the joystick input in the range -1 to 1.

y_D The y co-ordinate of the joystick input in the range -1 to 1.

k_g The geometry factor of the vehicle. The vehicle becomes more sensitive to steering inputs as this factor tends toward 0.

k_s The speed factor. This factor is equal to the maximum value which one wishes to send to the motor.

6.4 Concluding Remarks

The systems described in this chapter function as required for evaluation of the platform. Development is necessary in most systems to ruggedise the platform. The design of the electrical systems should be expanded to include additional desirable features (e.g current monitoring and switching capabilities on the power board and position control of the flippers) . These systems also require additional testing to ensure robust operation outside of the controlled environment present during testing.

The following chapter goes on to test the performance of the platform. From the results of the tests, conclusions are drawn as to how any problems may be rectified and where improvements may be made.

Chapter 7

Testing and Results

The specifications in Chapter 3 defined the desired performance of the platform. Testing the actual performance of the platform helps to determine a set of operating guidelines and also uncovers areas in which future development might improve performance. A set of test procedures was drawn up which would test the performance of the platform.

7.1 Test Procedures

The testing procedures for the platform were as follows:

Turning Perform clockwise and counter-clockwise 360°on-the-spot turns at various motor speeds.

- Measure current
- Measure speed

Driving forwards Drive forward over a distance of 1m at various motor speeds.

- Measure current
- Measure speed

Driving in reverse Drive backward over a distance of 1m at various motor speeds.

- Measure current
- Measure speed

Ramp climbing Climb 30°and 45°inclines at various motor speeds.

- Measure current
- Measure speed

Obstacle climbing Climb onto a platform using the flippers.

- Measure current

Stair climbing Climb onto and up a staircase.

- Measure current

Communications Measure the delay for a network message to reach the robot.

- Measure time using `ping` tool.

7.1.1 Measurement

The above procedures require the measurement of current and speed, the testing procedures used are described below.

Figure 7.1: Current measurements were taken from the power supplies as in this screenshot.

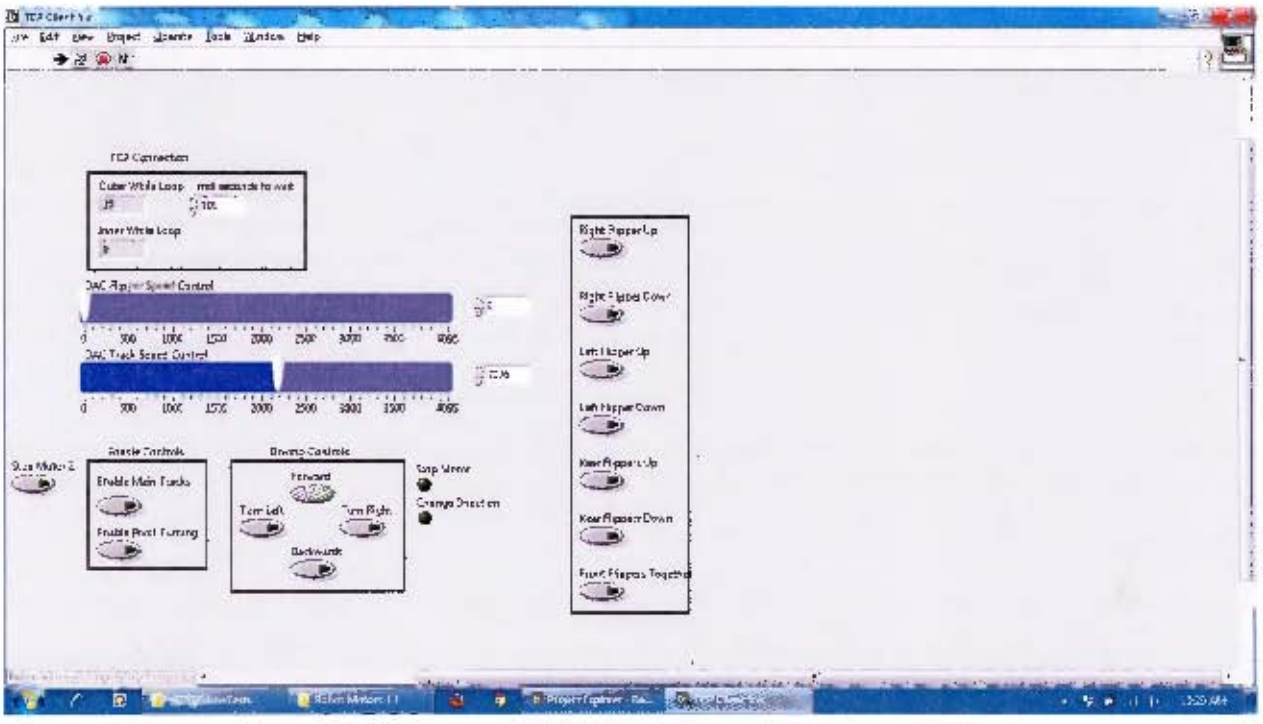

Figure 7.2: The National Instrument LabView application used for the second series of tests.

7.1.1.1 Speed

To test the speed at which the platform moved, tests were conducted over a fixed distance and timed using a stopwatch or video footage where possible.

7.1.1.2 Current

Measuring the current draw of the platform was somewhat challenging due to the electrical noise created by the motors. A dedicated current measurement module was in development by Robotics and Agents Research Laboratory MSc student David Lwabona at the time of testing. As this module would provide accurate and real-time current readings and detailed measurements were not required for this stage of testing, the decision was made to use the current read-out from the power supply (as in Figure 7.1) to give an indication of the current draw of the platform.

For the second set of tests, the control electronics on the platform had been replaced, and as such the original control program no longer worked. A National Instrument LabVIEW application was created by David Lwabona for use in testing the platform. The Graphical User Interface (GUI) for the program is shown in Figure 7.2. The test setup comprising a laptop running the control code and the power supplies from which current readings were taken is shown in Figure 7.3.

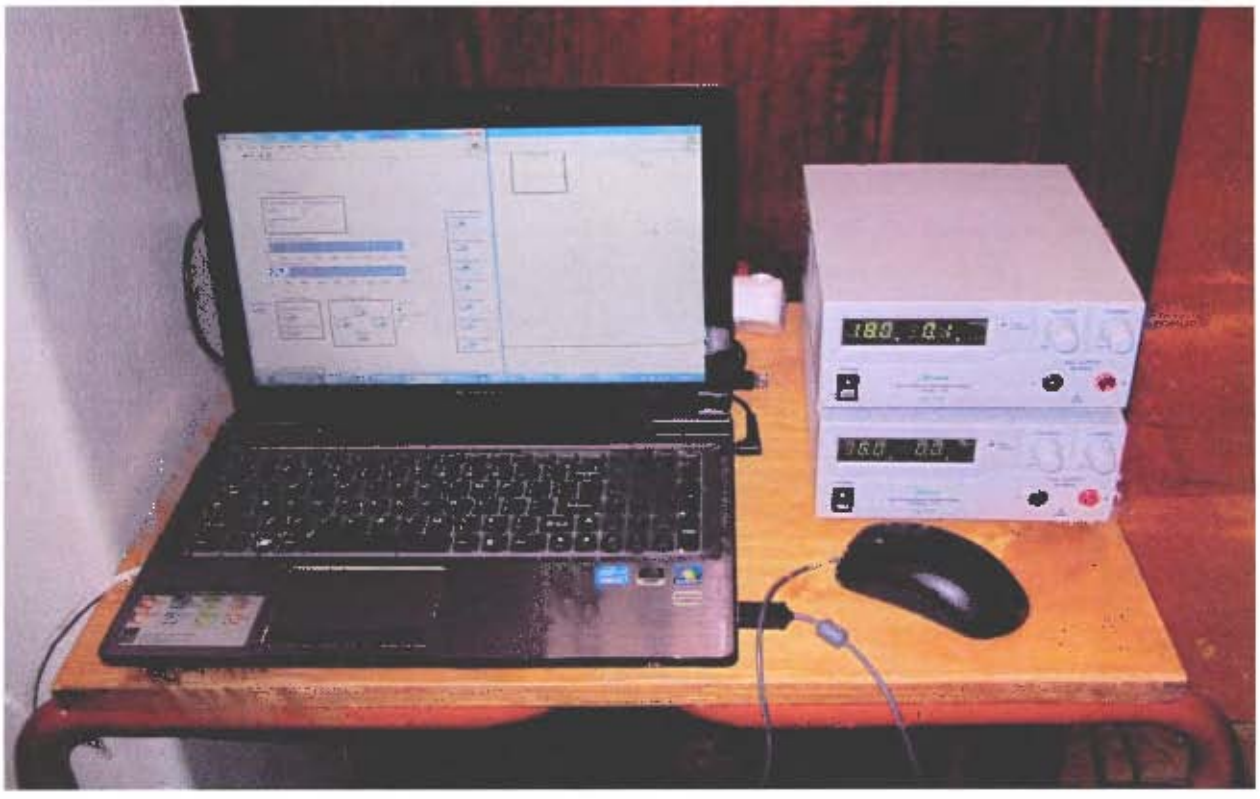

Figure 7.3: The setup of the operator control station for testing.

7.2 Test Results

Two series of tests were performed. Initial testing found that the platform lacked torque for both the drive and flipper motors. Subsequently new motors were ordered and fitted, the platform was anodised and the smooth belts used during the initial testing were fitted with polyurethane feet for additional traction. The platform was then re-assembled and taken to the 2012 RoboCup Rescue competition in Mexico City. Time constraints meant that only limited testing could occur before the RoboCup competition. Upon return from RoboCup, testing was redone using the new motor and gearbox combinations.

7.2.1 Turning

Turning on-the-spot represents a challenge as the tracks need to slip significantly to be able to complete this manoeuvre (further discussion on this is provided in Section 5.6.3 on page 60). The results of this test indicated that the motors had insufficient torque to reliably spin on-the-spot. The motor controllers occasionally went into current limiting mode and the behaviour was erratic.

Fitment of the higher ratio gearboxes allowed the platform to turn at low speeds. The current draw was similar for both the clockwise and counter-clockwise turns, although the counter-clockwise turn took 10s less with the same motor set speed. A plot of current draw over time during the turn at the lowest speed ($\frac{1}{253}$) is given in Figure 7.4.

At 20% speed the lateral forces on the drive belts were sufficient to cause one of the drive motors in each test to stall and additionally caused severe misalignment of the belts. In addition to the misalignment, the lateral forces were sufficient to cause the belt to bend along its width. The current draw and points at which each of the drive motors stalled are shown in Figure 7.5. The misalignment caused by turning at higher speeds is shown in Figures 7.6, 7.7 and 7.8.

7.2.2 Straight Line

The straight line tests involved driving the robot forward and backward over a marked distance (Figure 7.9) and measuring the time and current required to perform this task.

Initial testing ran into problems as the tracks worked off the drive pulleys as the robot drove. This behaviour

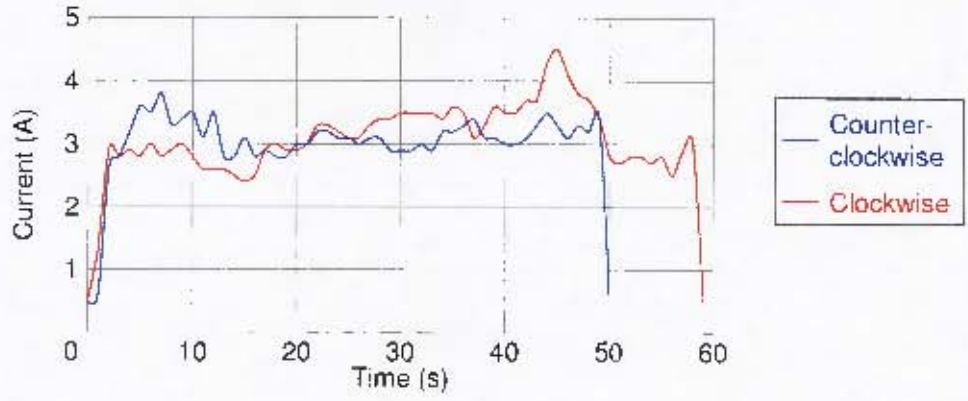

Figure 7.4: Current draw over time during platform turns at speed $\frac{1}{255}$.

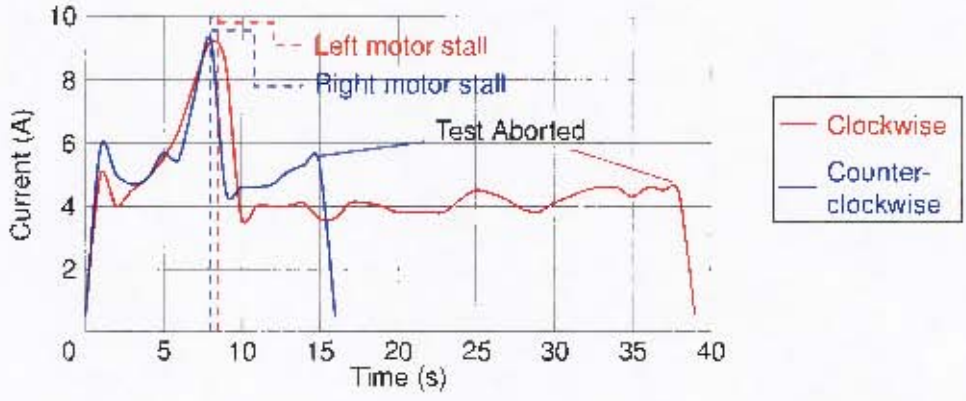

Figure 7.5: Current draw over time during platform turning at 20% speed. The points at which the motors stalled and at which the tests were aborted are shown.

was not present when the robot was run without the tracks touching the ground. The first suspicion was that the drive pulleys were not parallel to each other and perpendicular to the spine. To investigate this hypothesis, the platform was fastened to the bed of a milling machine, and a clock gauge was used to ensure the spine of the robot was parallel to one axis of the bed as can be seen in Figure 7.10. The clock gauge was then run along the width of the drive pulley to measure how much it deviated from being perfectly square. This process is shown in Figure 7.11. Measurements were taken at 4 points around the circumference of the pulley. The results showed that the pulleys were misaligned by at most 0.04mm over the entire pulley width of 180mm and in most cases were out by less than 0.01mm. This level of misalignment was deemed unlikely to cause the track to run off the pulley at the rate which was being witnessed.

The next hypothesis was that the teeth of the pulley were slightly spiralled along the width of the pulley causing the belt to be pushed off when run in one direction and drawn in when run in the other. This fit with the observations of the platform driving. To keep the belt in place, the front outside hub supports were modified to include a vertical pin on their top side which would limit the amount the belt could be pushed off the pulleys. This modification is shown in Figure 7.12. Testing this configuration resulted in the belt pushing strongly against the pin, and eventually the edge of the belt rising up and jumping over the pin. It was suspected that the weight of the platform was holding the belt firmly in place and with each revolution of the pulleys the sliding off of the belt was compounded. To combat this, a similar pin was fitted to the bottom side of the outside hub support, and the pins were replicated on the rear of the platform. This modification solved the problem and as such testing could be continued.

The robot was run in forwards and reverse and timed over a distance of 1m while the current draw was measured. The tests were performed at 6 speeds in the range of 0-255. These numbers correspond to a motor speed of approximately 0-10000rpm for an unloaded motor [35]. The results of this test are shown in Figure 7.13. Plots of the current draw during the tests are shown for the forwards direction in Figure 7.14 and for reverse in Figure 7.15. In Figure 7.16 a plot of the maximum current draw when travelling at

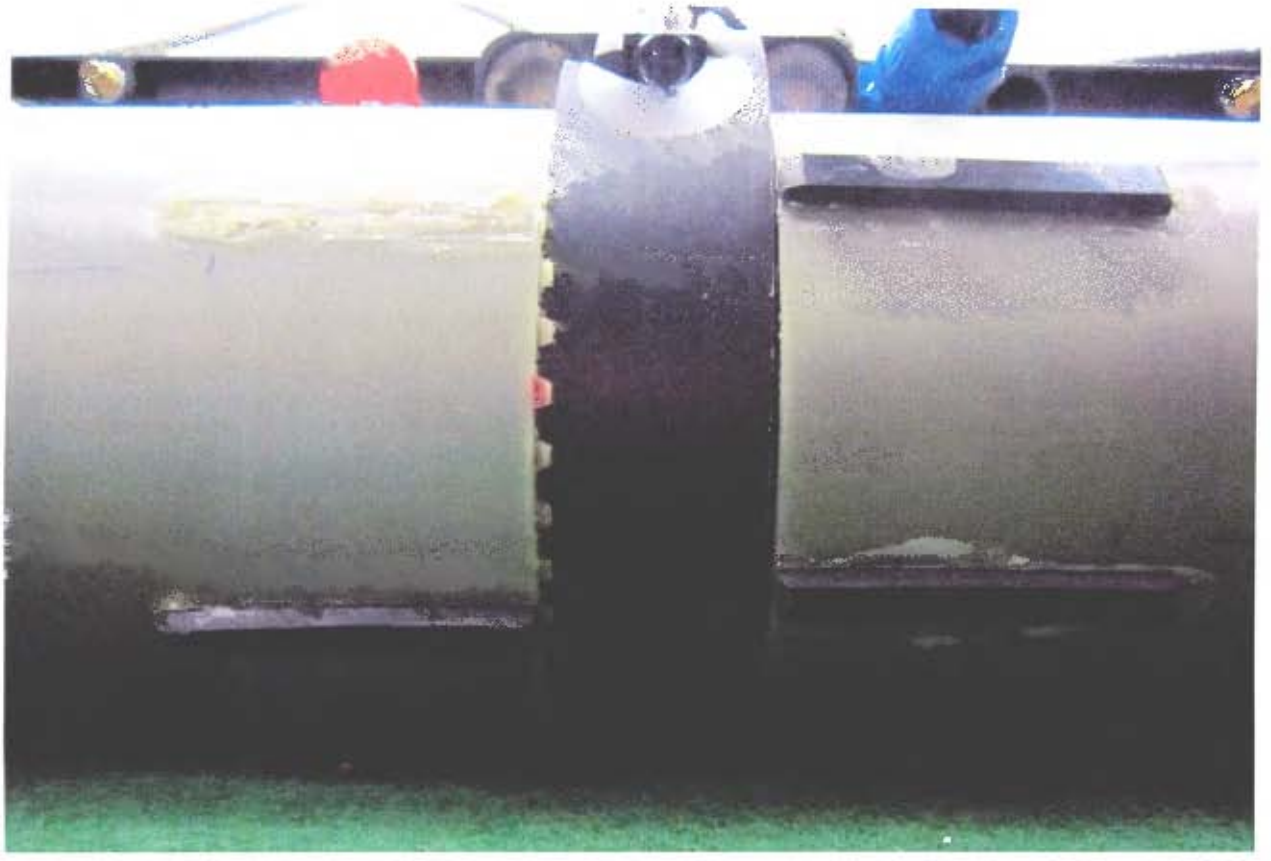

Figure 7.6: After a clockwise turn the rear end of the left track was forced against the spine with enough force to cause the track to mount the spine. The force was sufficient to cause the edge of the spine to slice the teeth of the tracks.

various speeds is shown.

The second set of tests were run with different tracks, on a different surface and with different motors. As such a direct comparison between speeds and currents in the 2 sets of tests has limited value. As with the previous tests, a distance of 1m was marked out on the floor and the platform was timed when travelling over the distance to determine its average speed. Based on the new gearbox ratios it should be expected that the platform will move at $1/3^{rd}$ of its previous speed. The tests approximately met this prediction. The results of the tests are shown in Figures 7.17, 7.18, 7.19 and 7.20.

Placing 60kg of weight on the platform increased current draw to approximately 4A at low speed while moving in a straight line.

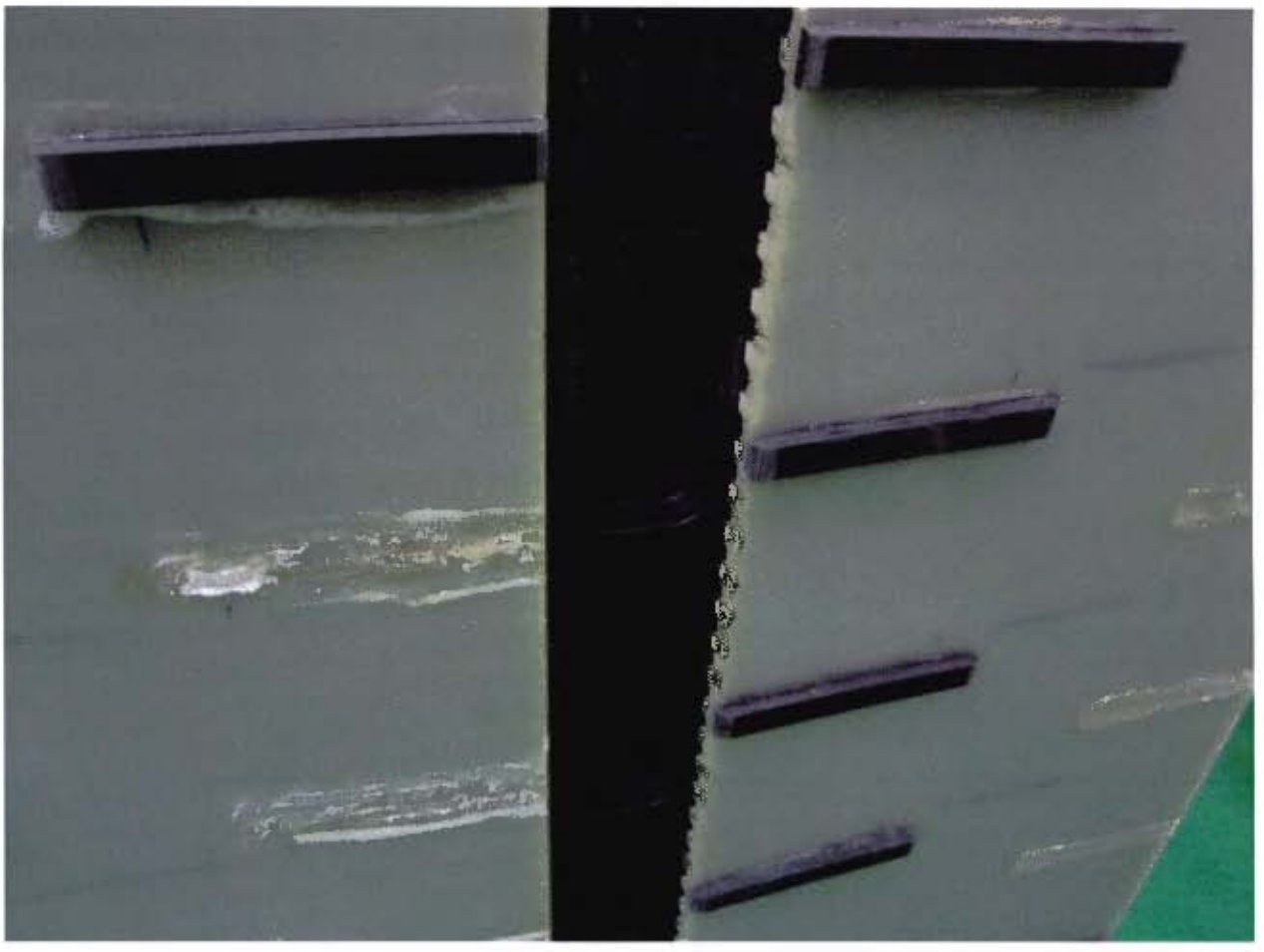

Figure 7.7: The underside of the platform after a clockwise turn at 20% speed. The front of the left track is shown having climbed over the lip of the spine. Also shown are the areas where feet have detached from the drive belts.

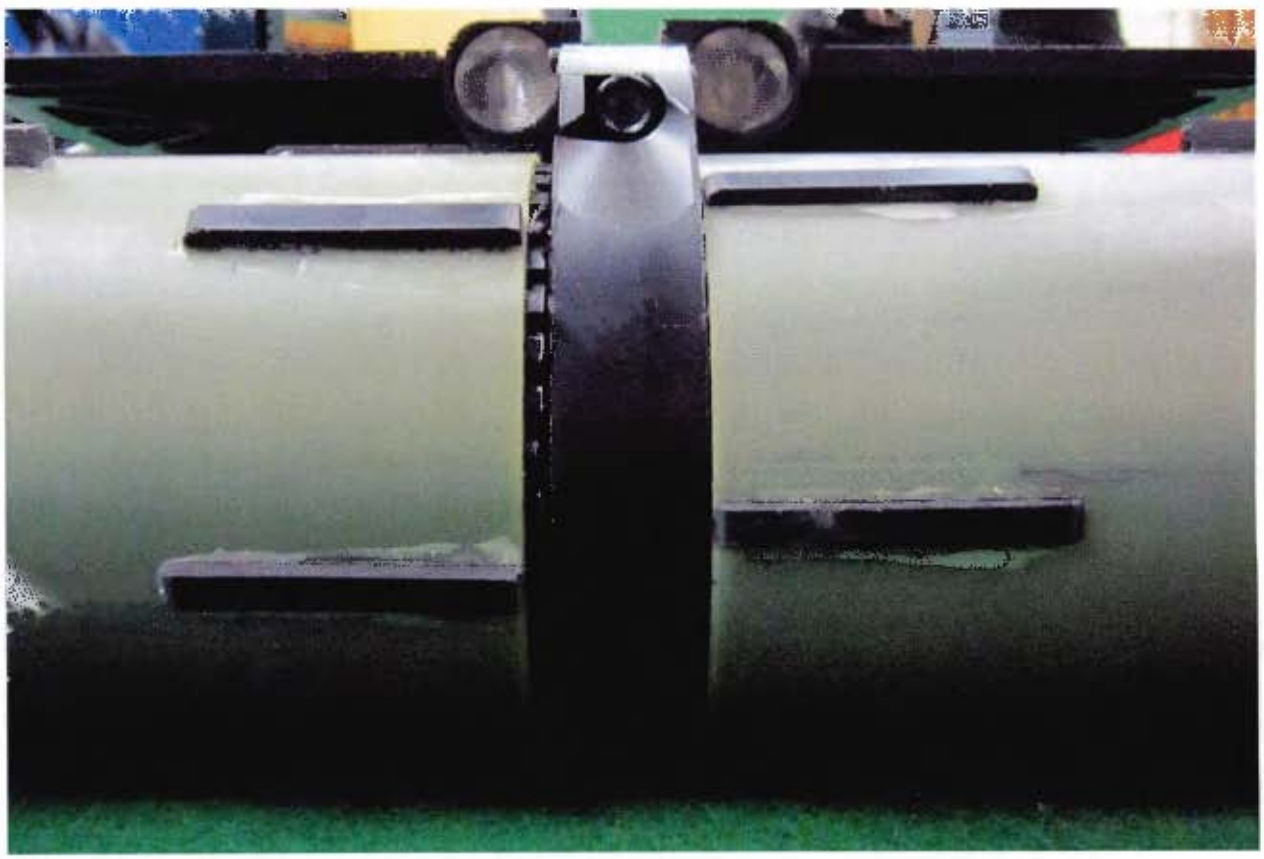

Figure 7.8: A view from the front of the platform. The left track has bent sufficiently to close the gap which should be between the track and the spine (visible on the right track) if the track was straight.

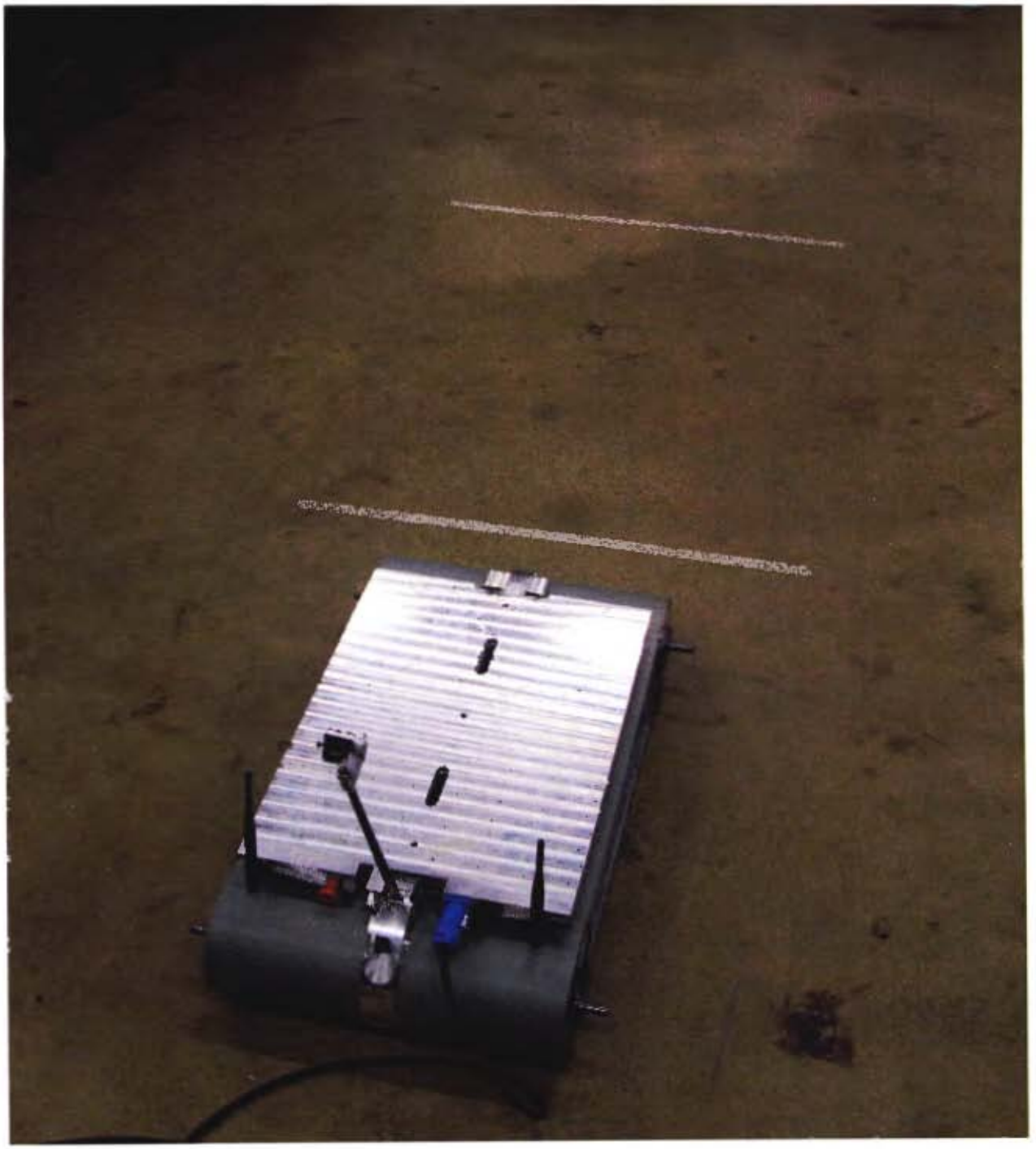

Figure 7.9: The robot and the marked distance it was timed over when traveling forward and backward.

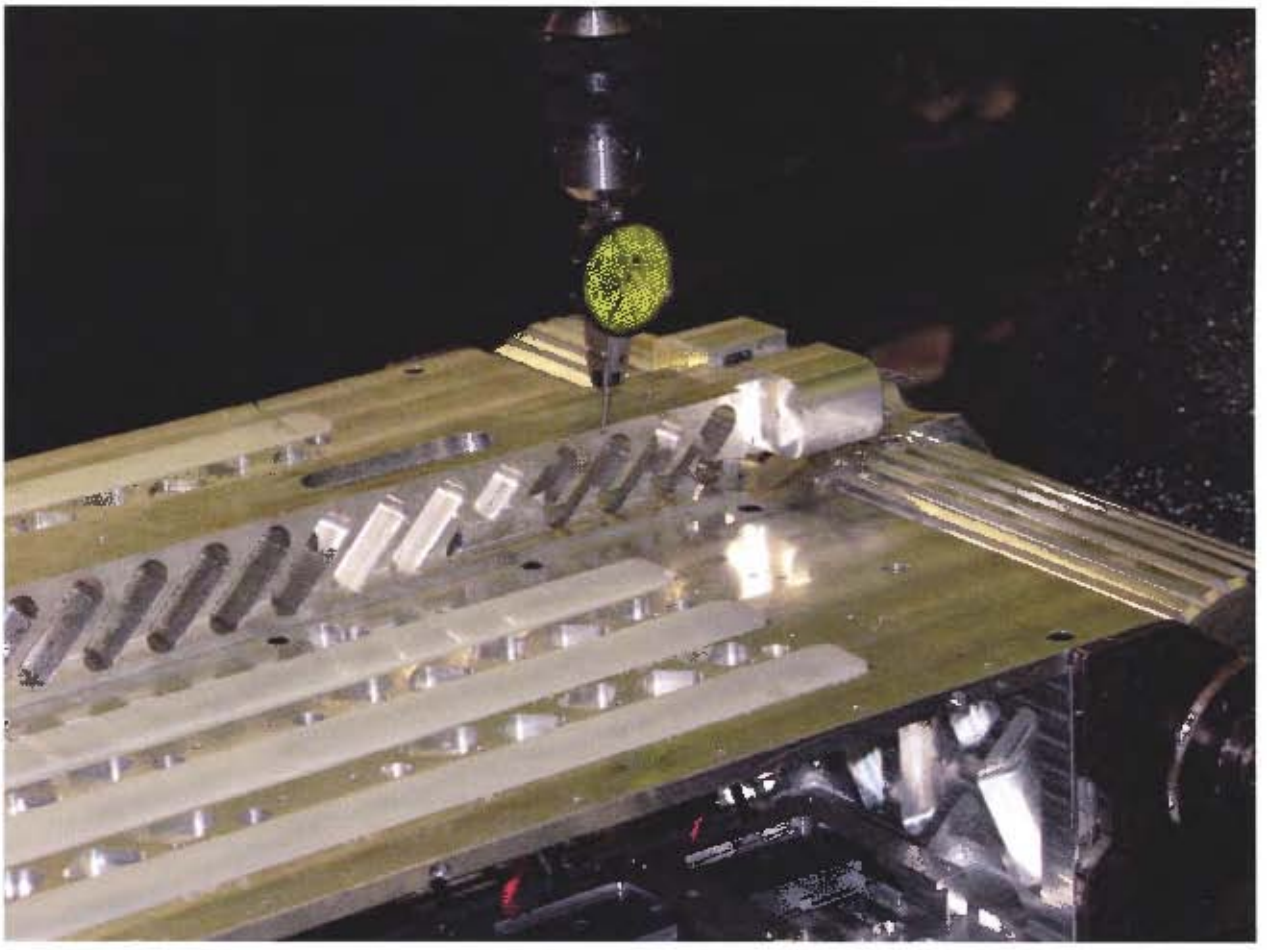

Figure 7.10: The clock gauge was run along the spine to ensure it was parallel with one axis of the mill.

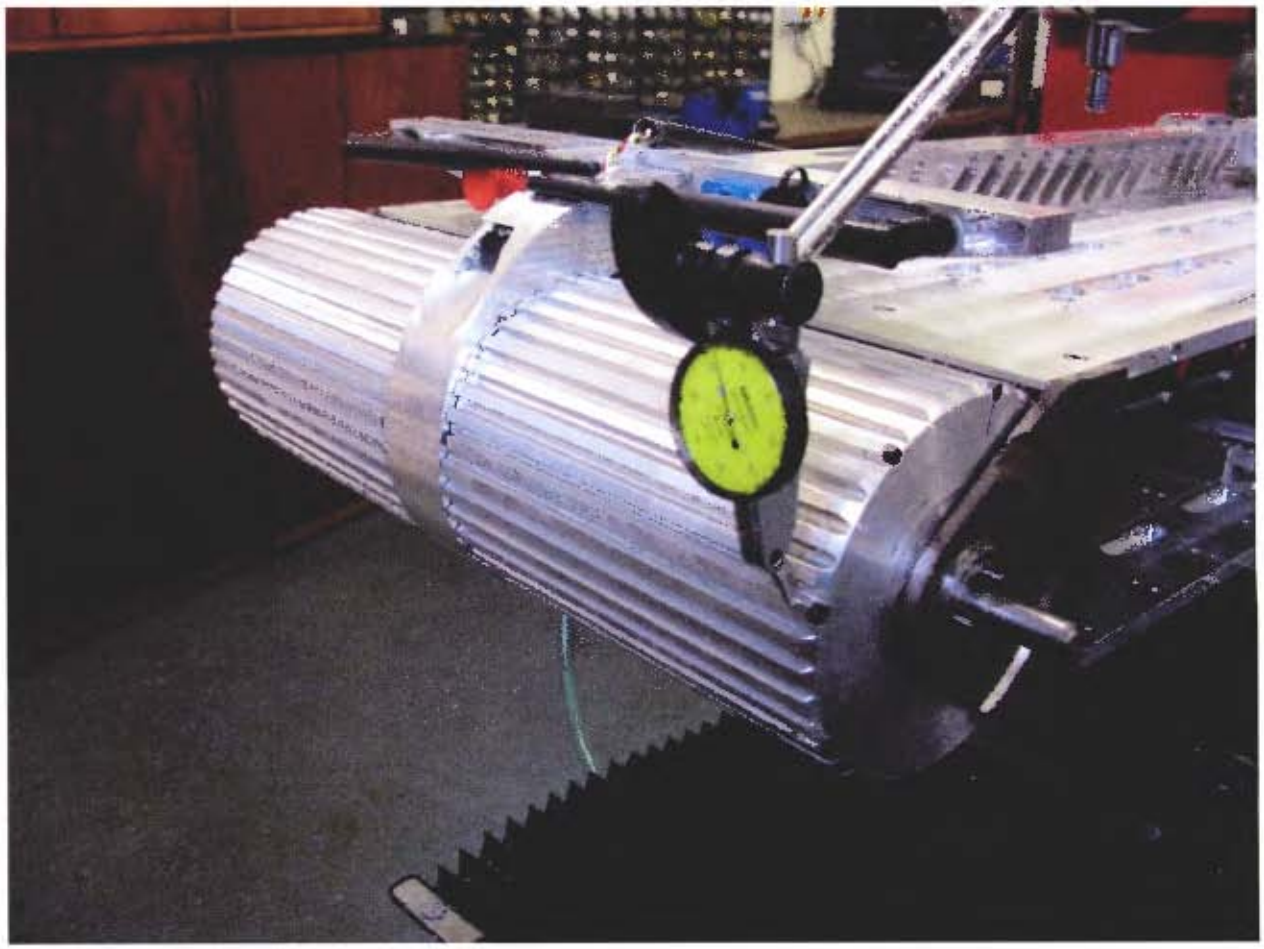

Figure 7.11: The platform secured on the table of a milling machine to determine the degree to which the drive pulleys were out of alignment.

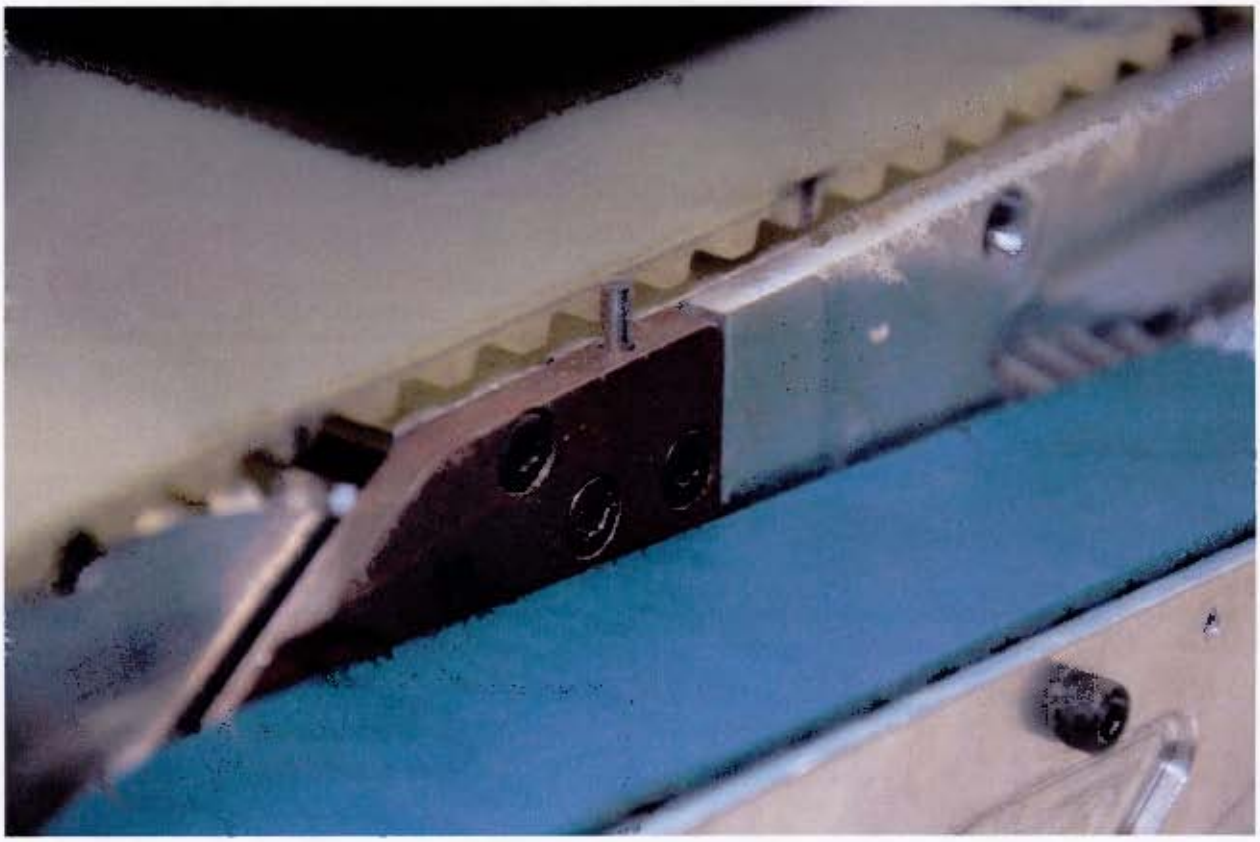

Figure 7.12: A guide pin modification to keep the drive tracks in place.

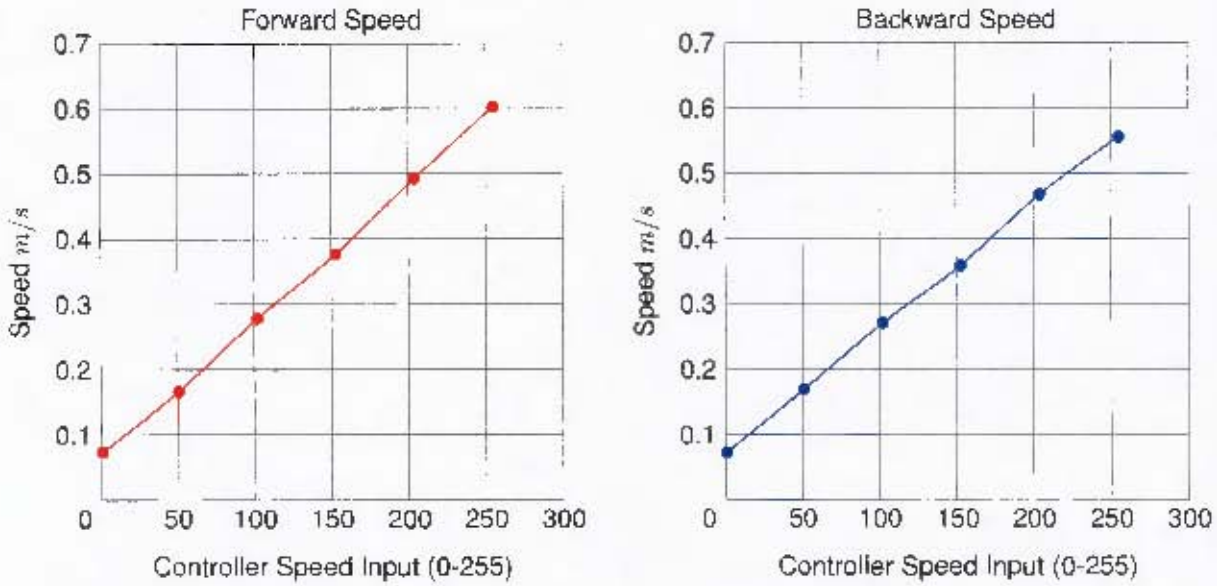

Figure 7.13: The results of the forward and reverse speed tests.

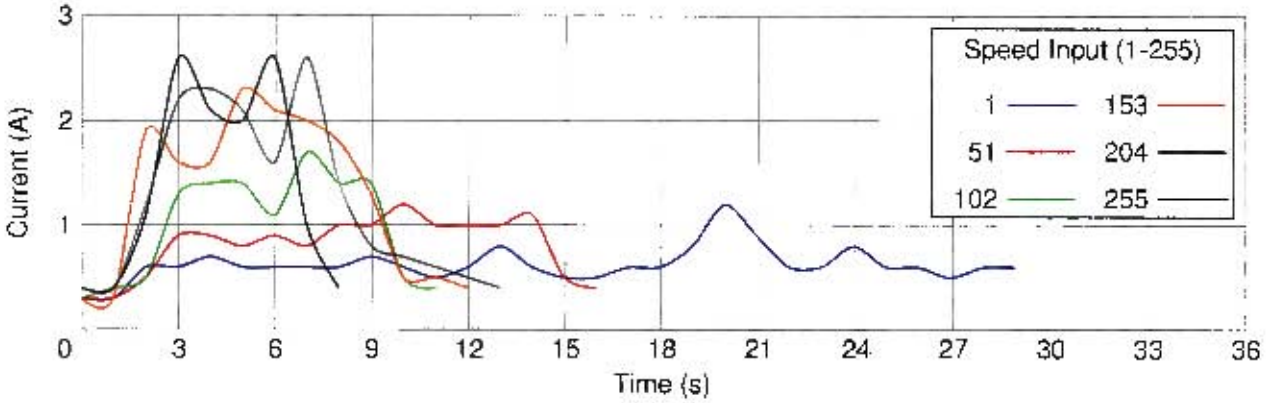

Figure 7.14: The current draw of the robot while travelling forwards at various speeds.

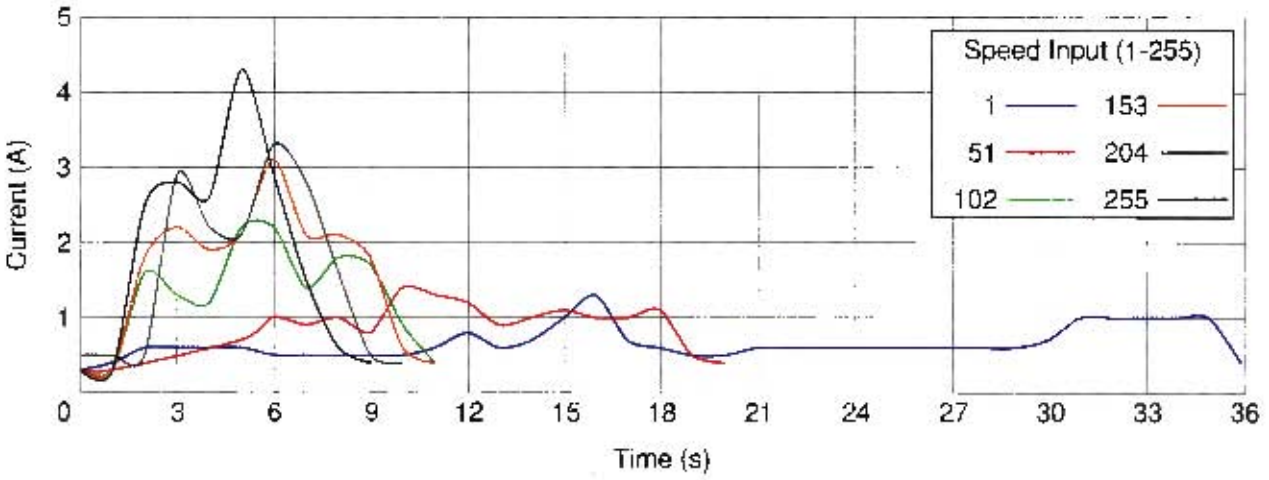

Figure 7.15: The current draw of the robot while travelling in reverse at various speeds.

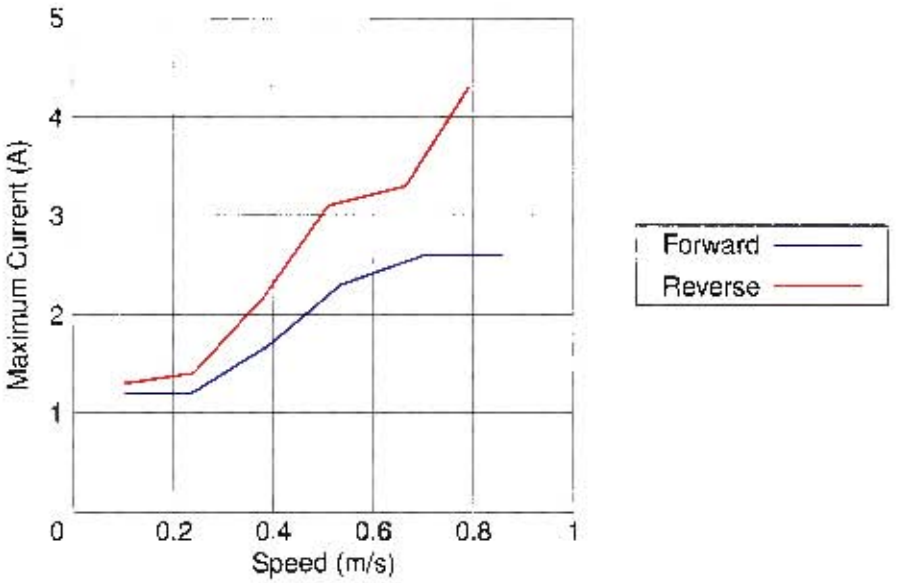

Figure 7.16: The maximum current draw of the robot while travelling forwards and in reverse at various speeds.

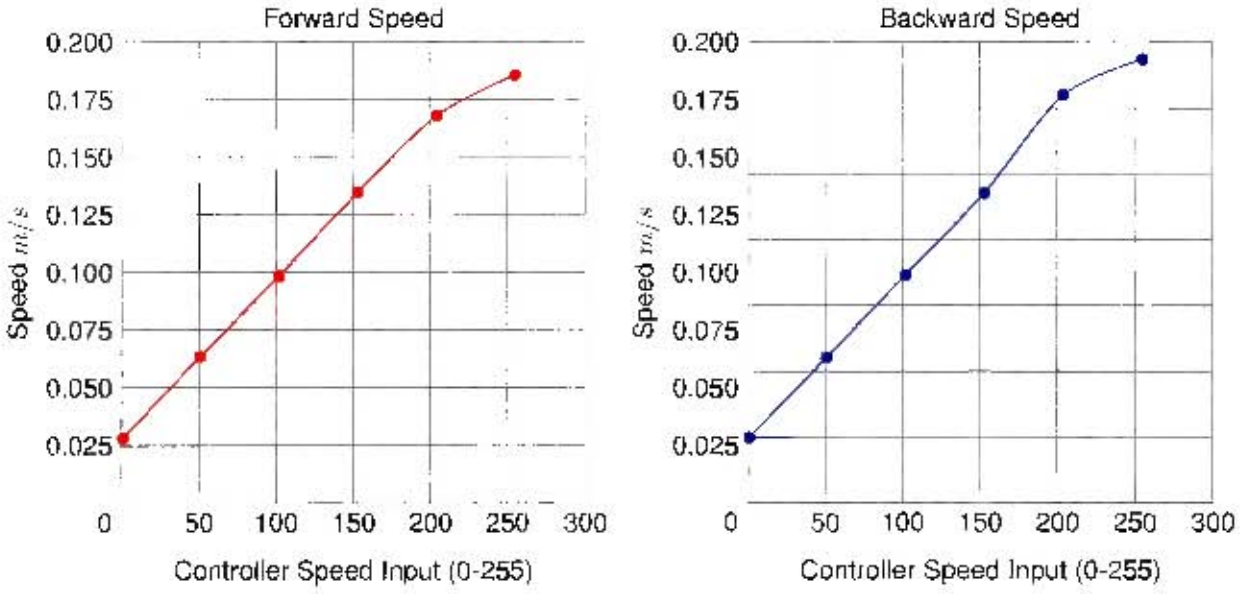

Figure 7.17: The results of the forward and reverse speed tests with new motors.

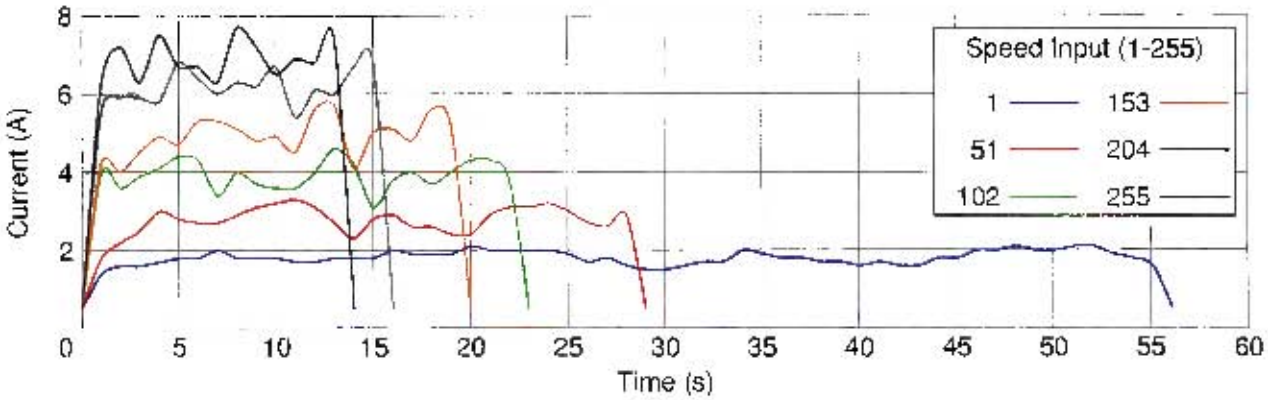

Figure 7.18: The current draw of the robot while travelling forwards at various speeds with new motors.

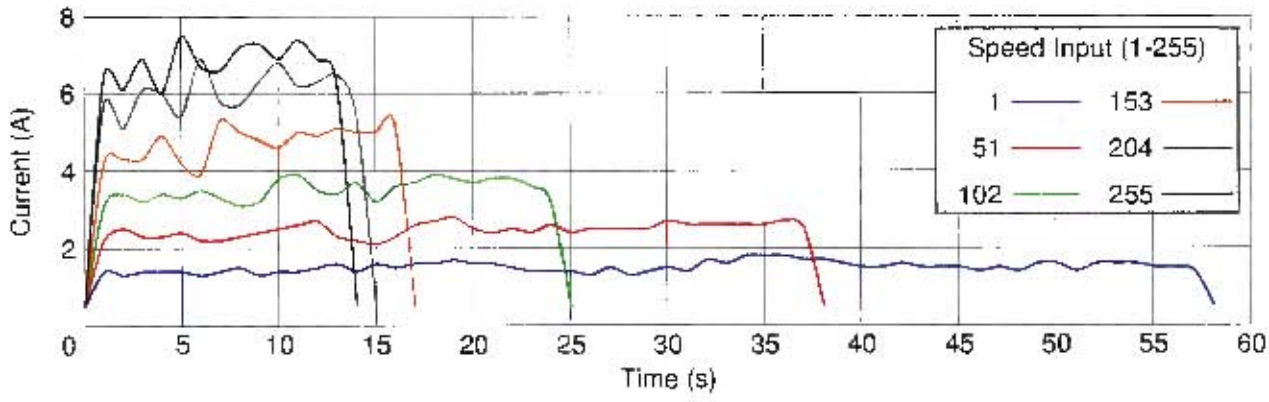

Figure 7.19: The current draw of the robot while travelling in reverse at various speeds with new motors.

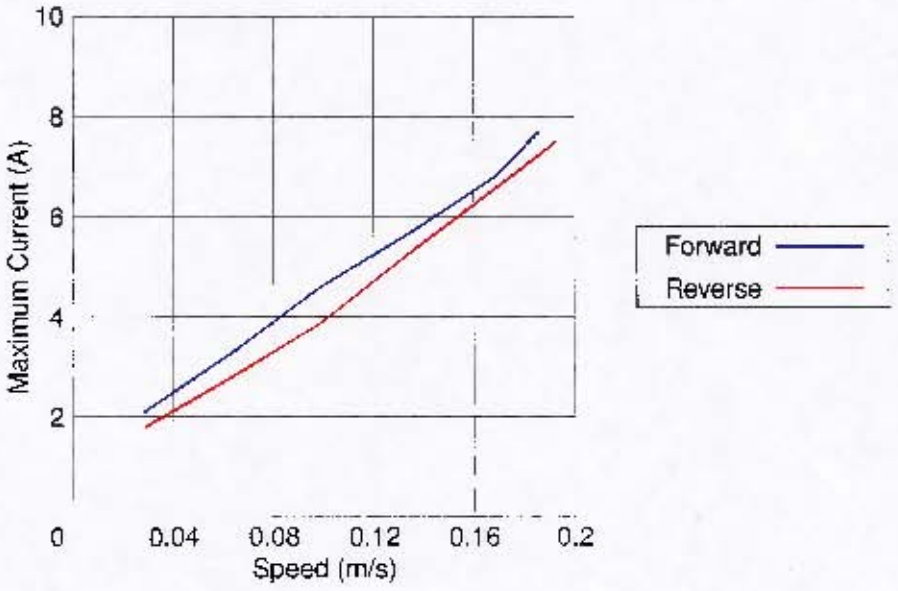

Figure 7.20: The maximum current draw of the robot while travelling forwards and in reverse at various speeds with new motors.

7.2.3 Slope Climbing

An adjustable slope was constructed and a distance was marked out on the slope. The time to move across the marked distance was measured and current draw to mount the slope and move up it was also measured. As a protection feature the motor controllers gradually slow down the motors to avoid excess energy being dumped back into the batteries. Due to this there was the risk that at higher speeds the robot might run over the top of the ramp as the motors were slowing down, so the tests were not performed over the entire range of speeds. The setup of the slope is shown in Figure 7.21, while the results of the 30° test are shown in Figure 7.22. A plot of the current draw during the test can be seen in Figure 7.23.

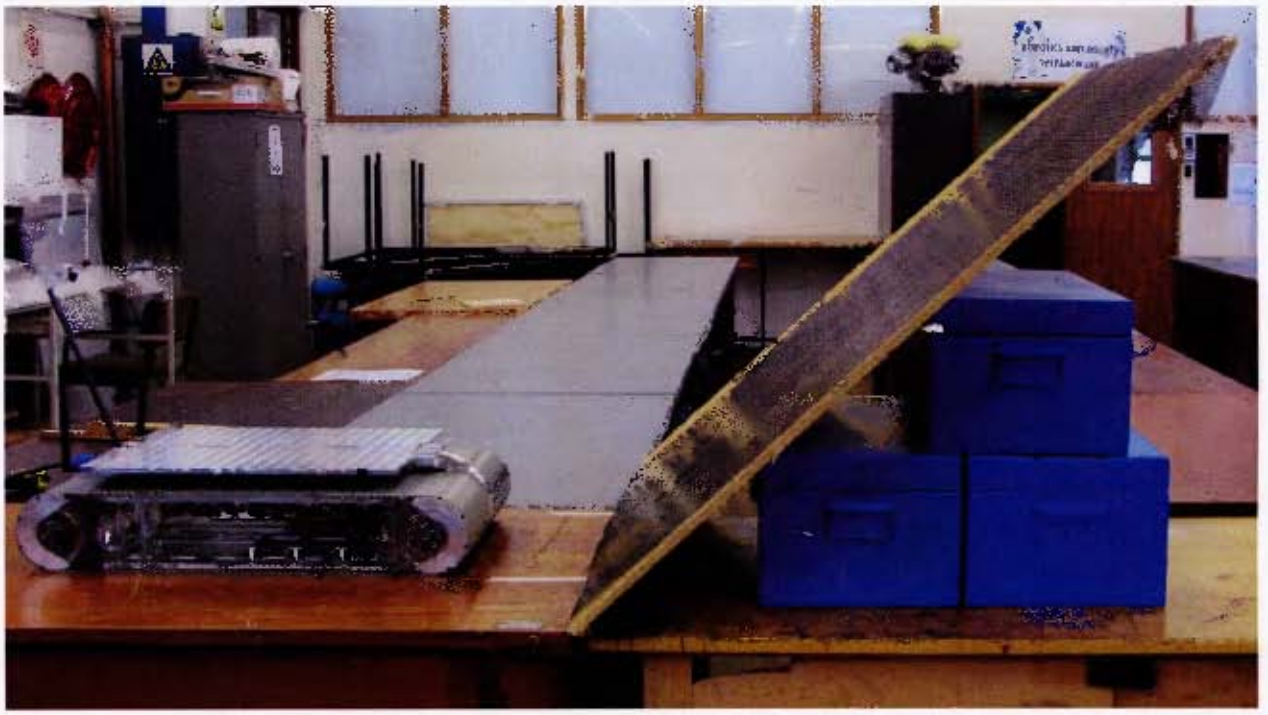

Figure 7.21: The slope used to test the slope climbing performance of the platform. The inclined surface can be seen here covered with a high friction silicon mat to attempt to provide enough traction for the platform to ascend the slope.

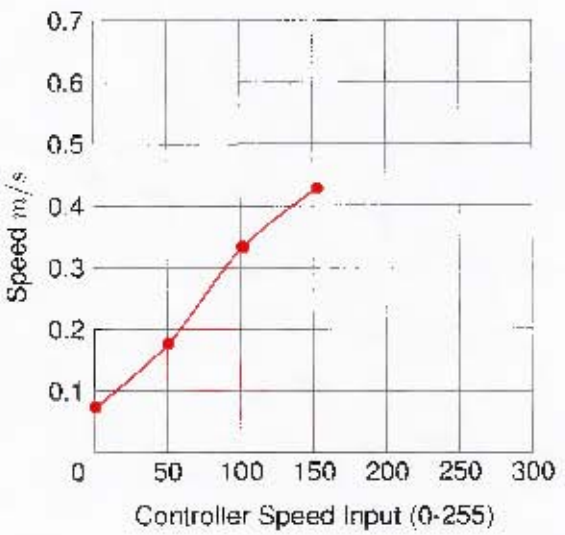

Figure 7.22: Results of the speed test performed on the 30° ramp. The tests were stopped at speed 153 due to concerns that the robot wouldn't stop before the end of the ramp.

The initial tests on the 45° ramp showed there was insufficient grip between the ramp and the tracks. The ramp was then covered with a silicon non-slip mat to improve the grip. This improved the situation somewhat

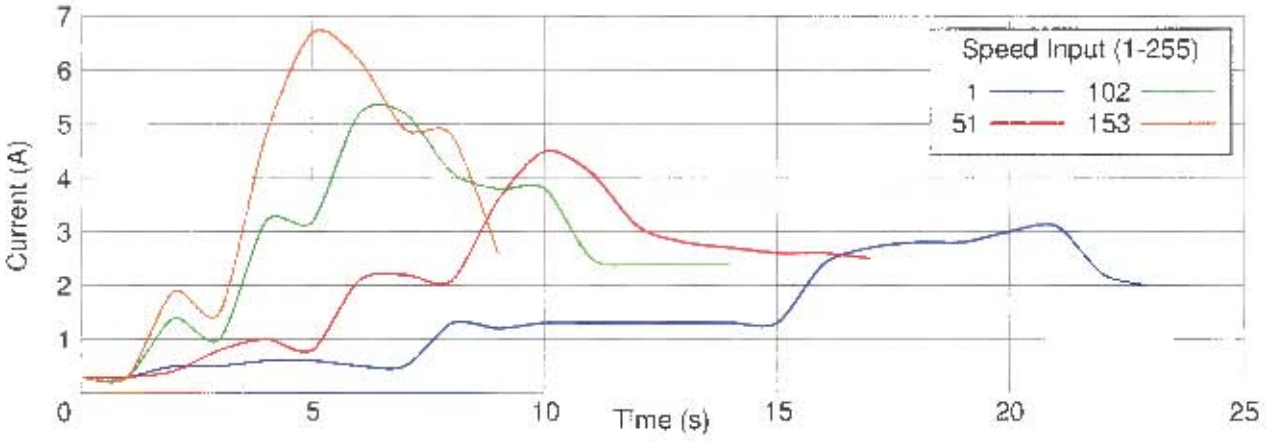

Figure 7.23: A plot of the platforms current draw during the ramp climbing tests at various speeds.

but it was still not possible to complete the test. It was noted that the drive motors were stalling by drawing too much current (5A per motor) at approximately the same time that they were losing grip.

The new gearboxes and feet fitted to the drive tracks significantly improved the slope climbing performance. In addition to this a more aggressive speed ramp was chosen for the controller so that there were no longer concerns that the platform might run over the edge of the ramp. Once the new motors were fitted the platform was able to climb both the 30° and 45° slopes. The arrangement of the ramp is shown in Figure 7.24. The results of the testing are shown in Figures 7.25, 7.26, 7.27 and 7.28.

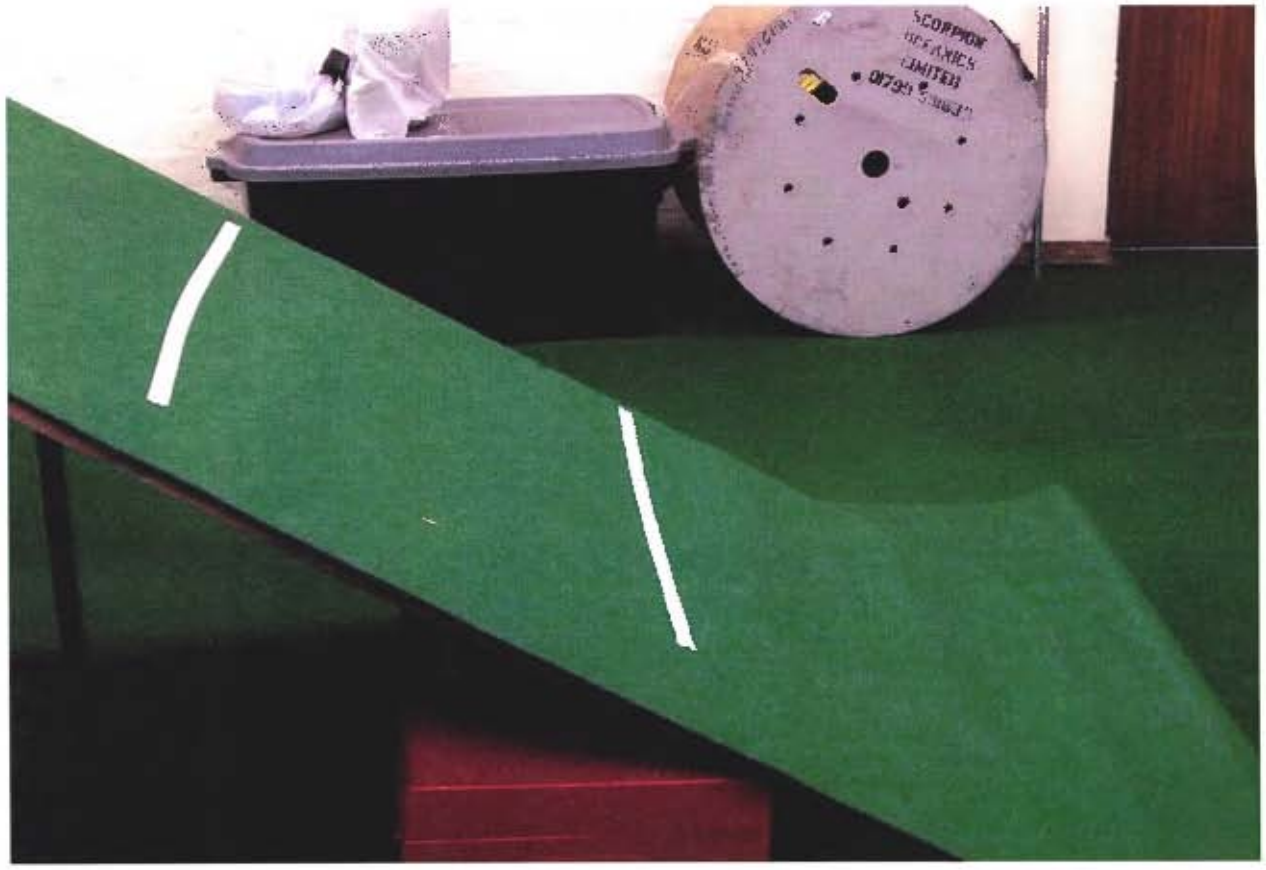

Figure 7.24: The Ramp used for the second set of slope climbing tests.

The angle of the slope was increased to 60° before the tracks began to slip on the slope. The test was performed at slow speed ($\frac{1}{255}$), while current remained below 3.2A. The slope and platform are shown in Figure 7.29. These observations would indicate that grip rather than torque is the limiting factor in determining the

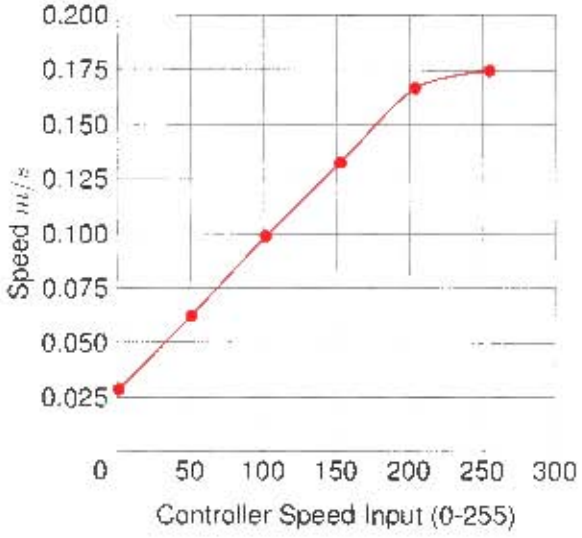

Figure 7.25: A plot of speed input against platform speed whilst climbing a 30° slope.

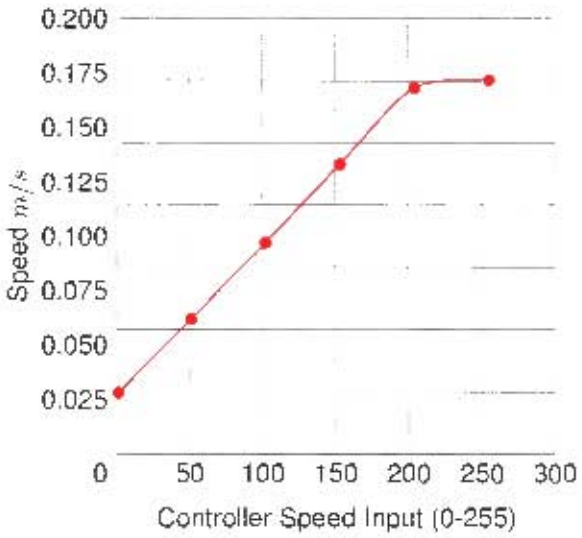

Figure 7.26: A plot of speed input against platform speed whilst climbing a 45° slope.

incline which the platform can climb.

7.2.4 Flipper Tests

Initial testing with the flippers showed that the flipper motors where unable to provide enough torque to lift the platform using the full length of the arm. There was sufficient torque to just lift the robot when the flipper arms operated with a shorter lever arm, but this did make it impossible to perform the stair and platform climbing tests.

Another issue was experienced with the control of the flipper arm motors. Drive is transferred to the belt on the flipper arm through the flipper pulley by the main drive pulley. This torque will cause the flipper arm to rotate unless it is held in place. The controllers for the motors provide a function to brake the motors to prevent them from being rotated. Unfortunately the brake function was insufficient and still allowed the flippers to be back driven by the torque applied by the drive pulley.

Once the new motors and gearboxes were fitted the platform was able to climb obstacles using the flippers. The test shown in Figure 7.30 was performed to test the functionality of the flippers in climbing over obstacles. The maximum current draw was 2.6A which was experienced while using the flippers.

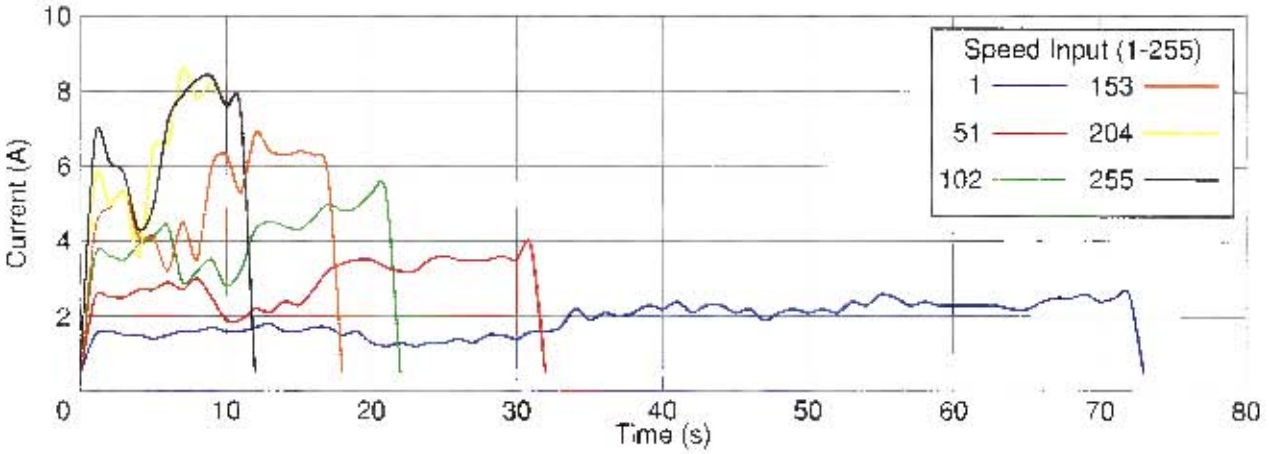

Figure 7.27: The Current draw for the platform climbing a 30° slope at various speeds.

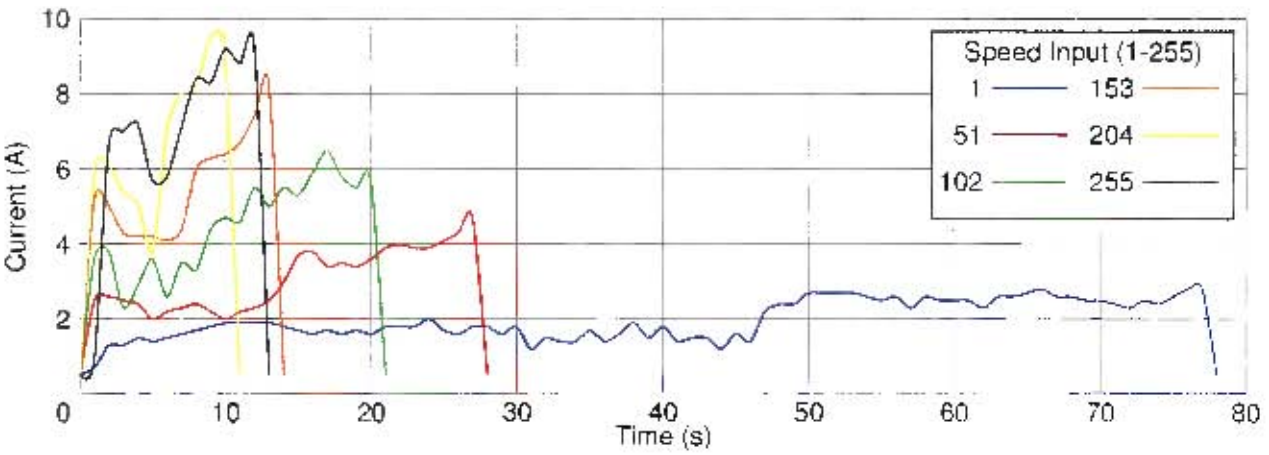

Figure 7.28: The Current draw for the platform climbing a 45° slope at various speeds.

During testing the rectangular keys attaching the flippers to the flipper drive shafts worked loose and caused a certain amount of play in the flipper drive train. This resulted in the flipper motors moving for a short while before engaging with the flippers themselves.

7.2.5 Stair Tests

Stair climbing tests could only be completed once the new motor and gearbox combinations were fitted, as mounting a set of stairs requires the use of the flipper arms. The tests were performed on the stairs shown in Figure 7.31.

The speeds and currents during the stair tests are given in Figures 7.32 and 7.33.

Figure 7.34 shows the platform climbing a set of stairs while navigating using the forward and rear facing cameras.

The stair climbing ability of the platform was also tested on steeper steps such as those shown in Figure 7.35. On steeper stairs it became necessary to use the flippers to provide additional stability. Occasionally the feet bonded to the belts slipped off the steps and caused the entire platform to slip down the incline. This became more prevalent and problematic on steeper stairs.

Figure 7.29: The platform on a 60° slope

7.2.6 Communication

The standard network diagnostic tool `ping` was used. This tool sends a small message to a network device requesting that the device return the message to the sender. The tool then measures the difference in time between when the message was sent and the reply was received to calculate the length of time taken for the round trip.

Performing tests in a 10m area around the robot resulted in pings consistently less than 5ms, with the majority of the results being less than 2ms. As these results were substantially lower than the 60-80ms ping deemed acceptable in the specifications, further testing was deemed unnecessary until more detailed communication specifications could be drawn up.

7.2.7 Entry Triangle

The most significant constraint for the design of this platform was the necessity to fit through a standard entry triangle as defined by the NIST. Fortunately during the RoboCup 2012 Competition in Mexico City, it was possible to drive the platform through a regulation entry triangle as shown in Figure 7.36.

7.3 Summary

The conclusions drawn from each test are given in the subsections which follow. A trend noticed across tests was that the platform drew more current after modifications were made than before. This is most likely due to the differences in the drive track and ground interaction as it would be expected that with higher torque motors the platform currents should decrease.

7.3.1 Straight Line Tests

These tests show that the speed value given to the motors have a linear relationship to the platform speed as shown in Figure 7.13. Figures 7.14 and 7.15 show the current draw rising to a certain level as the platform accelerates, oscillating at this level and finally dropping down when the platform slows down. As would be expected, the current draw increases with increasing speed. One unexpected result from the testing was

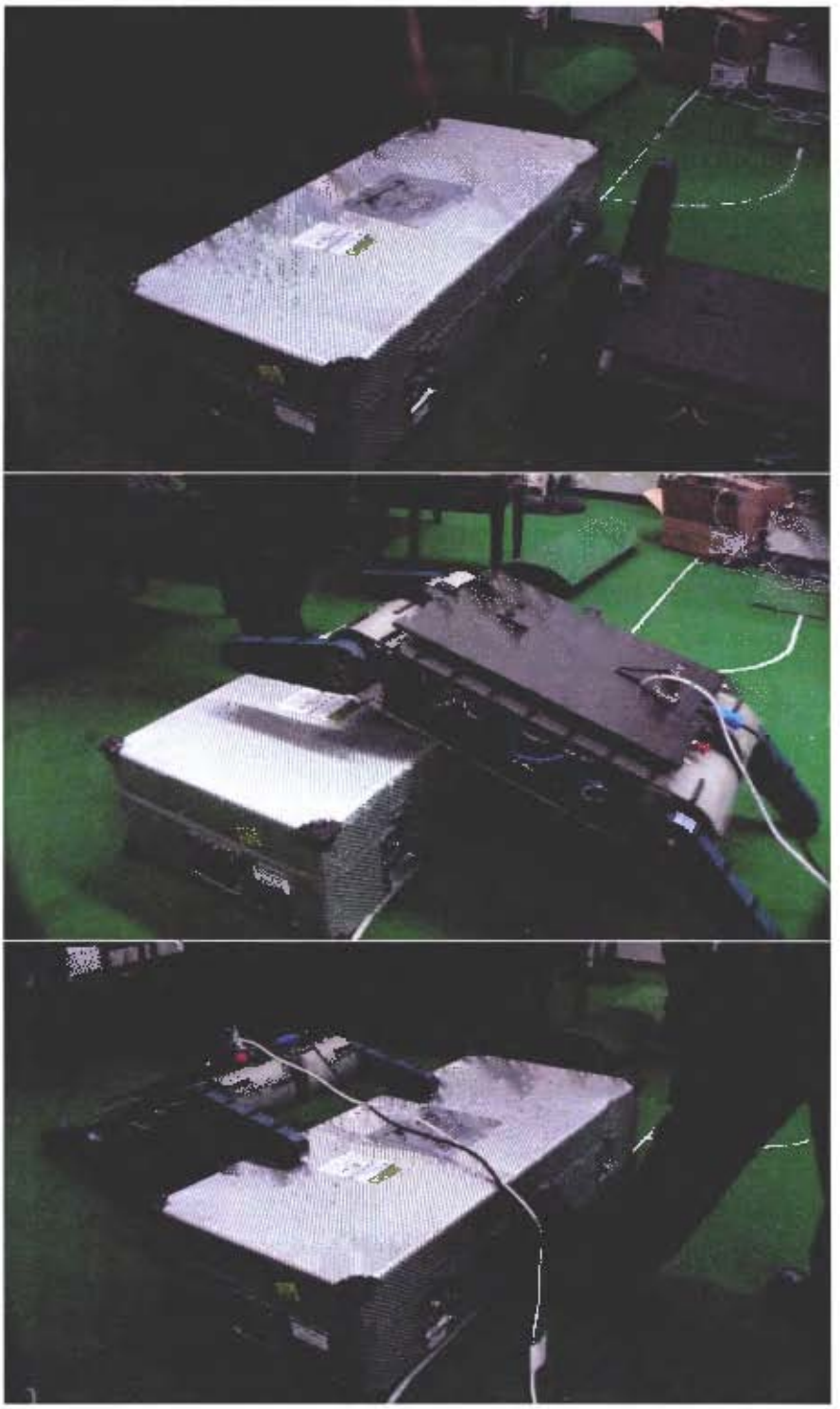

Figure 7.30: The platform climbing over a 250mm high obstacle.

that the platform seems to consistently draw more current when travelling in reverse than when travelling forwards. As the centre of mass is placed deliberately forwards, this could explain the discrepancy between the forwards and reverse motion, although it is unknown through which mechanism this is occurring.

7.3.2 Ramp Tests

The ramp climbing tests highlighted a few points. The speed at which the platform traverses the slope is linearly proportional to the speed given to the controller. The maximum current requirements to climb the slope increase as the speed increases. The current profile as the platform climbs a slope can be seen in Figure 7.23. The current first increases to one level as the platform transitions from being on a horizontal surface to sitting on the slope. As the platform climbs the slope, the current draw increases to a new high and

Figure 7.31: The stairs on which the stair climbing tests were performed.

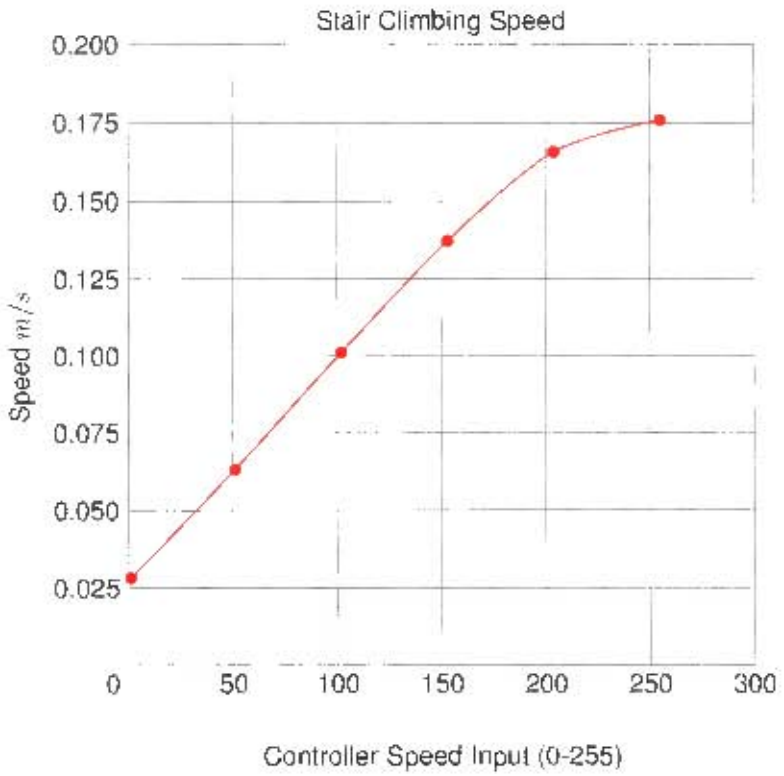

Figure 7.32: A plot of platform speed during the stair climbing tests.

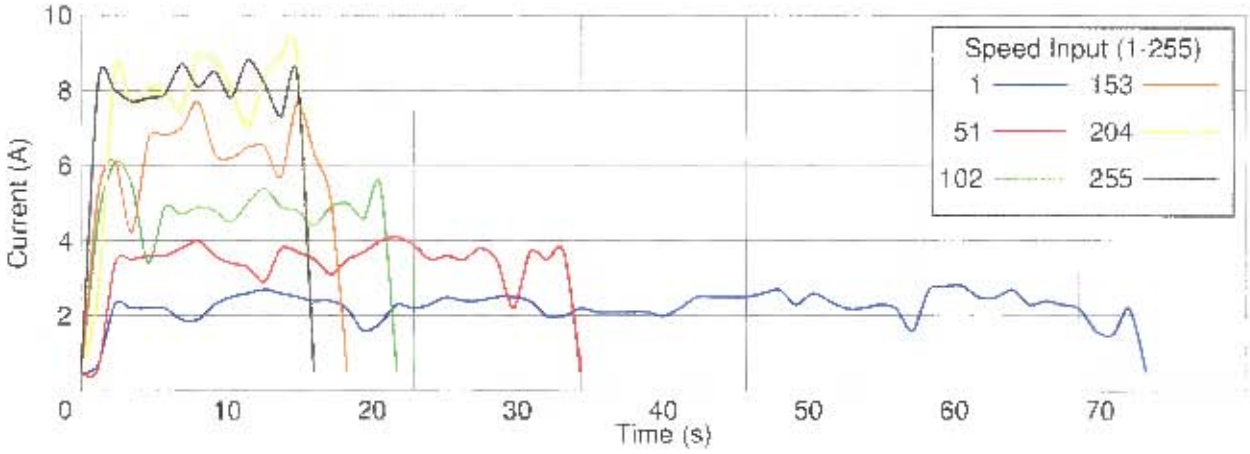

Figure 7.33: The current draw by the platform while climbing stairs at various speeds.

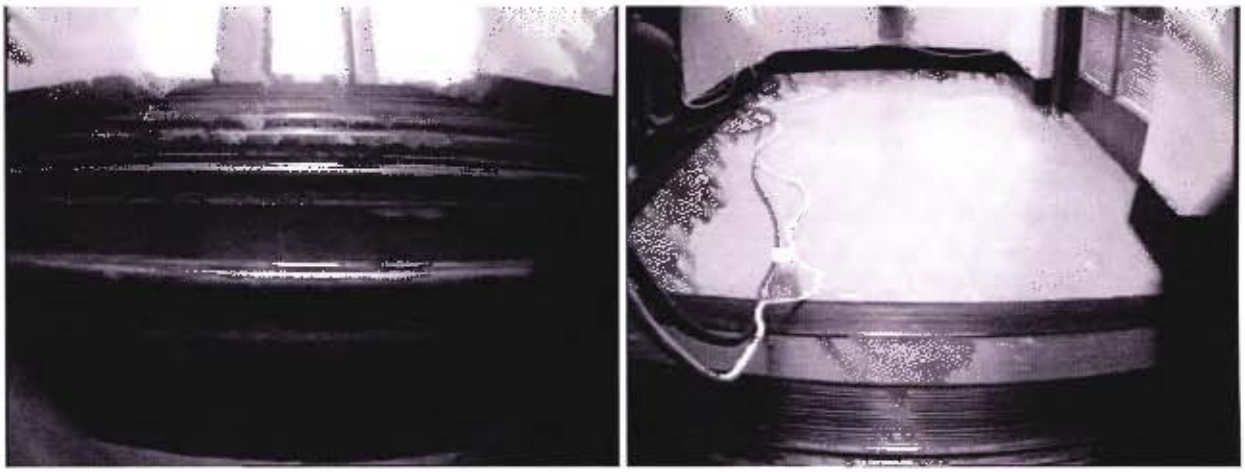

Figure 7.34: The view from the front and rear facing cameras while climbing a set of stairs..

Figure 7.35: The platform climbing a steeper set of stairs.

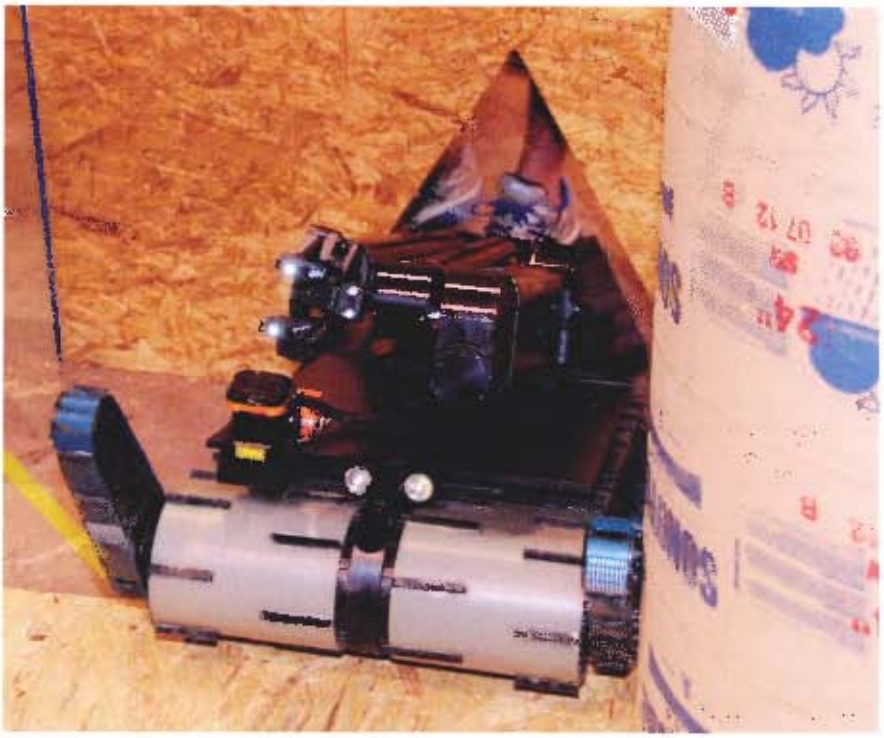

Figure 7.36: The platform driving through a standard size entry triangle (Image courtesy of Richard Whittemore).

then drops from this high as the platform continues climbing. The platform climbs slopes at approximately the same speed at which it travels over flat ground, although the current draw is slightly higher.

7.3.3 Turning Tests

The platform was initially unable to perform an on-the-spot turn at any speed as the motors had insufficient torque to overcome the friction between the drive belts and floor. Using a spring balance to measure the force required to slide the robot across the floor, the friction coefficient between the tracks and the floor was calculated and the calculations in Section 5.6.3 were performed to establish the torque requirements to perform an on-the-spot turn and new motors and gearboxes were fitted.

After the modification, the motors had sufficient torque to spin the platform, but the forces exerted on the tracks were sufficient to cause significant misalignment to the tracks. This ultimately limits the ability of the platform to turn.

7.3.4 Obstacle Climbing Tests

The obstacle climbing tests indicated that the platform can capably climb onto and over obstacles using the flippers. Of note is that the highest current draw during the obstacle climbing test occurred during the use of the flippers to place the platform onto the platform. Also the flippers rotate significantly faster than necessary, and indeed at anything but the slowest speeds rotate too fast to be easily placed. Additionally the keys used to attach the flipper drive shafts to the flippers were not perfectly seated and caused a certain amount of play in the motion of the flippers.

7.3.5 Stair Climbing Tests

The platform climbed stairs at roughly the same speed and current draw as the 30° slope, which could be expected as the slope of the stairs is approximately 30°. During the climbing of the stairs it was noted that the feet bonded to the track were ripped off during climbing. Also, occasionally as one side was supported on a foot while climbing the stairs, the foot would slip off the edge of the stair and cause the platform to momentarily lose footing.

7.4 Concluding Remarks

Testing showed that the platform had sufficient torque to manoeuvre over and around the desired obstacles. The major shortcoming of the platform revolves around issues with track alignment. The next chapter goes on to draw some conclusions on the testing and construction of the platform and to make some recommendations for future work.

Chapter 8

Conclusions and Recommendations

The design, construction and testing of the robot platform has produced valuable insights into the direction future development should take. This chapter first draws conclusions as to the functioning and performance of the current platform, and then goes on to make recommendations for future work.

8.1 Conclusions

8.1.1 Mechanical Design

The greatest difficulty with the development of this platform was in meeting the tight space constraints imposed by the need to fit within the entry triangle. The decision to place the motors within the drive pulleys created challenging design constraints which were ultimately successfully overcome. The drive system design at the front of the platform successfully moves weight distribution forward for added stability while climbing stairs and inclines and opens up considerable space within the platform itself. This is useful for maximising the amount of additional equipment which can be added to the platform, which is important considering the multi-purpose objective of the design. The compact mechanical layout of the motors and gears within the front pulleys successfully drives the platform while still allowing the constraints of the entry triangle to be met.

The platform was initially underpowered. This was resolved by changing the gearbox ratios on the drive and flipper motors, this came at the expense of speed, but the platform is still fast enough to operate effectively. A few assumptions led to the specification of underrated motors for the platform. The first was the assumption of the loading on the drive and flipper motors. The mass of the robot was initially estimated to be 20kg, which was an under-estimation, especially considering the additional mass from sensors and a manipulator arm being attached to the robot.

A second estimate which proved to be incorrect was the torque requirements of a differential drive tracked vehicle. At the time of design, the exact belt material and configuration was unknown, previous experience had shown that the performing an on-the-spot turn was a challenging task for a tracked vehicle, especially with high levels of grip between the tracks and ground. The difficulty of estimating the torque required by a tracked vehicle to perform a turn led to mistaken assumption that, should the motor be able to lift the robot vertically, it should be able to perform a stationary turn. This assumption was found to be incorrect during testing.

The third mistake with regards to motor selection was that the motors could be used beyond their rated specifications for useful periods of time. The motor selection documentation indicated that the limiting factor with regards to motor performance was the temperature of the motor windings exceeding safe limits. Care was then taken to mount each motor so as to allow for additional cooling. Testing revealed this to be a pointless exercise. The motor controllers would not allow the motors to operate above their specified limits, which reduced the estimated output of the motors.

A success of the design was the tight packaging of the motors within the front drive pulleys, this freed up significant amounts of space for other equipment to be mounted internally in the platform. One downside to this design choice is the difficulty of routing wiring into the front drums to drive the motors. This presents perhaps the most significant obstacle to quickly assembling or disassembling the robot.

The polyurethane timing belt used as the drive track was found to be successful in that is was lighter, simpler

and more durable than belts made up of multiple elements. The downside of using this method of drive is that the belts had a tendency to walk off their pulleys. Although this was anticipated and steps were taken to ensure the belts could not shift completely off from the pulleys, the extent to which the belts would walk was not anticipated and as such these steps were insufficient. The tendency of the belts to drift either into the spine or the outside retaining pins resulted in significant amounts of power being lost to friction under certain circumstances.

The flipper arms operate at a much higher speed than necessary and should ideally have more torque to more easily lift the platform. The flipper motors are currently fitted with the largest possible reduction gearbox and adding a further reduction would have to be done by either redesigning the platform to accommodate different motors, or by modifying the flipper drive train to include a larger reduction.

8.1.2 Electrical and Electronic Design

The electrical sub-systems proved themselves to be suitably robust in testing. The power distribution board functioned as required, although tightly packaging the board within the platform proved challenging. Dealing with attachments to the board is most easily done by removing the board from the platform, which is not ideal.

The Ubiquiti RouterStation Pro, 2 of which comprised the communication subsystem, proved itself to be a reliable, low-cost and extensible solution for wireless communication with the platform. One challenge with these boards is their configuration. This issue became apparent during the platforms trip to the RoboCup conference in Mexico, where unknown communications issues could not be quickly rectified. A further point worth considering is that the RouterStation has been discontinued by the manufacturer and as such a different solution might be more appropriate going forward.

The Maxon motor controllers were simple to interface with and proved reliable and problem free during testing. The one caveat is the lack of a built-in ability to lock the motor shaft in place at low speeds. The result of this was that when a torque was applied to the motor under the locked state it would slowly rotate, although not as fast as if the motor was not locked, this was an issue when stopping on a slope or using the flipper arms.

8.1.3 Software Design

The software development for the platform was primarily in the form of an application to read the state of a joystick or other such device attached to a control station and then relay this information over the network connection to the platform. On the platform this data was converted into values for setting the speed of the individual motors. The requirements of the software were that it should be small, fast and quickly portable across whatever computer may be on hand. This was accomplished by using native Windows™ API's (Win32), to write an application using as basic a feature set of the operating system as possible, and embedding these functions within the software through static linking rather than relying on the host system to provide the suitable libraries.

For the wider project, the decision was made that future development would take place with the National Instruments LabVIEW development environment. LabVIEW is a graphical programming environment designed to increase productivity in engineering and scientific applications. Further development of software for the robot platform is likely to make use of National Instruments tools.

8.2 Recommendations for Future Work

The priority for future work on the platform is to correct issues which arose during the construction and testing of the platform. Beyond this recommendations are given to extend the functionality beyond what was designed for the current platform.

8.2.1 Drive Track Alignment

At present the drive tracks are kept in alignment by four pins on each side. This masks the underlying problem that the tracks have a tendency to walk off the pulleys. Tests showed that the drive pulleys are as square as could be realistically achieved with the spine. A modification to the drive pulleys providing a inside and outside lip to prevent the belt from moving on the pulley would be desirable as this would eliminate the

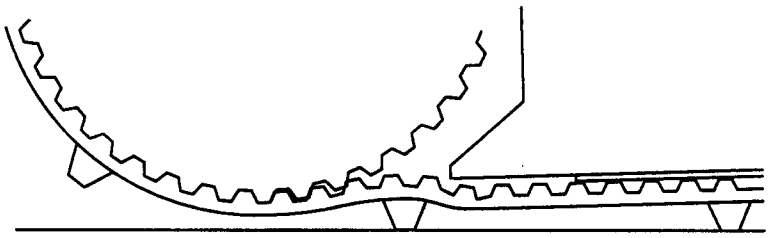

Figure 8.1: Undesired tensioning of drive belts caused by drive belt feet.

friction caused by the belt rubbing against the spine or alignment pins. A solution to this issue is currently under development by David Lwabona, an M.Sc student in the Robotics and Agents Research Laboratory.

8.2.2 Drive Track Tensioning

The centre distance between drive pulleys is currently too large. This has the effect of making the fitting and removal of the drive belts more difficult than it should be. Ideally a test setup consisting of pulleys with an adjustable centre distance should be constructed to determine an ideal center distance for this application. The ideal centre distance would be such that the drive belt can be slipped onto the drive pulleys with minimal force, but does not require a large amount of slack to be taken up by the tensioning system as this would lead to an overly large tensioning system.

8.2.3 Drive Track Support

At present there is a small gap between the drive pulley and the sidepod to which the track skid plate is attached. When lugs were attached to the track, as the lug move into this gap the weight of the platform caused the track to tension as the portion of track to which the lug was attached sunk into the gap, a representation of this can be seen in Figure 8.1. This could be countered by increasing the thickness of the track skid plates fitted to the sidepod. This would have the benefit of effectively shortening the track-base of the robot, decreasing the torque requirements to turn the robot, although this might increase the friction in the drive system as the drive belts will constantly be rubbing on the skid plate. Another potential solution to this issue would be to change the size or arrangement of the drive pulleys. Smaller pulleys, or pulleys moved upwards with respect to the sidepods, would also ensure that lugs on the tracks would only ride on the skids underneath the sidepods. Another solution would be to minimise the gap between the sidepod and the drive pulleys, or to extend the skids into a groove in the drive pulleys so that there is no gap for the drive tracks to run into.

8.2.4 Motor Control

Position control is required for all motors on the platform. For the drive motors, position control is necessary to ensure the motors can be braked, and that the platform will not roll down a ramp or staircase when stopping halfway up. The flipper motors need position control both to accurately place the flippers, and to make sure that the flippers will remain in position when a load is applied to them. Braking could also be achieved through the use of a mechanical brake, although this would add weight and increase complexity. A position control system is currently under development by David Lwabona.

8.2.5 Wiring and Front Drive System Layout

The primary wiring problem with the platform is the routing of cables into the drive pulleys. This results from limited space due to the maximum width of the robot being limited by the necessity of fitting within an entry triangle, and the length of the motors defining the width of each drive pulley. Larger diameter drive pulley bearings would create more space, but even the current bearings are significantly overrated for the application in which they're being used, and were chosen based on the space they provided for wiring and structures to fit through rather than their load rating. Larger bearings of the same type are only commonly available in sizes which are too thick to be realistically used in the front drive system. Solid bushings could be investigated for use instead of rolling bearings. As neither the loads nor the speeds present in the drive system are large, bushings could be manufactured and thus provide more flexibility in the design of the

Figure 8.2: The current spine

Figure 8.3: The spine with modified front and rear for solid bearings and direct motor attachment.

drive system. This could also allow for a more compact and rigid drive assembly. The spine as shown in Figure 8.2, could be modified as per Figure 8.3 to allow the the motors to be fixed directly to the spine and the rolling bearing to be replaced with solid bearings as per Figure 8.4.

8.2.6 Platform Weight

Many problems are exacerbated or even created by the weight of the platform. A lighter platform is ultimately more transportable, has lower power requirements, has lower stresses on components and thus should be more reliable. Weight reduction would be most easily achieved through redesign or machining away sections of the spine, the heaviest single component. Most components could be made significantly thinner, as even with the current weight of the platform, they are thicker than they need to be. The spine for instance could be modified as shown in Figure 8.5 to remove a substantial portion of the spine to reduce mass and allow

Figure 8.4: The fully modified spine with solid bearings shown in blue.

Figure 8.5: The spine with center section cut out to reduce weight.

for the electronics situated within to potentially be removable on a slide out assembly.

8.2.7 Flipper Drive

The flippers should ideally operate at much lower speed with greater torque. Replacing the motors and gearboxes would be both challenging and costly. A more flexible and cost effective solution would be to redesign the flipper drive train to accommodate a larger final reduction.

8.2.8 Power Distribution System

The current power distribution system provides only basic functionality. Ideally a power distribution board should allow for individual power lines or even components to be turned on and off, preferably by some remote command. This would allow for basic troubleshooting without requiring the robot to be removed from its environment. It would also be desirable to measure the current being consumed by different devices on the platform, and provide information as to the level of charge of the battery system. David Lwabona is currently testing a new power distribution board which implements all of these features.

8.2.9 Operator Interface

The current operator interface allows for only basic manipulation of the individual motors. For deployment of the platform in complex situations it would be necessary to have more fine grained control over the motors, especially the flipper motors, and also to have access to the video feeds on the platform.

8.3 Concluding Remarks

Familiarity and insights gained during the construction and testing of the platform are presented in the preceding sections. Perhaps the most critical aspects from the author's point of view would be a redesign of the front drive system, allowing for easier disassembly, a more rigid construction and easier access to components. Following this in importance would be a reduction in weight, probably most easily achieved through a modification of the spine. Improvements to the electronics and software are already underway at the time of writing.

Appendix A

Weight Breakdown

The weight of the platform is critically important and has an effect on almost all aspects of performance. As such a detailed breakdown of the weights of all components, compiled by David Lwabona is given in this Appendix. This should be useful in determining where attention should be focussed for reducing the weight of the platform.

A.1 Component Weights

A graphical representation of the weight breakdown of the platform is shown in Figure A.1. A detailed table of the various component weights is given in Table A.1.

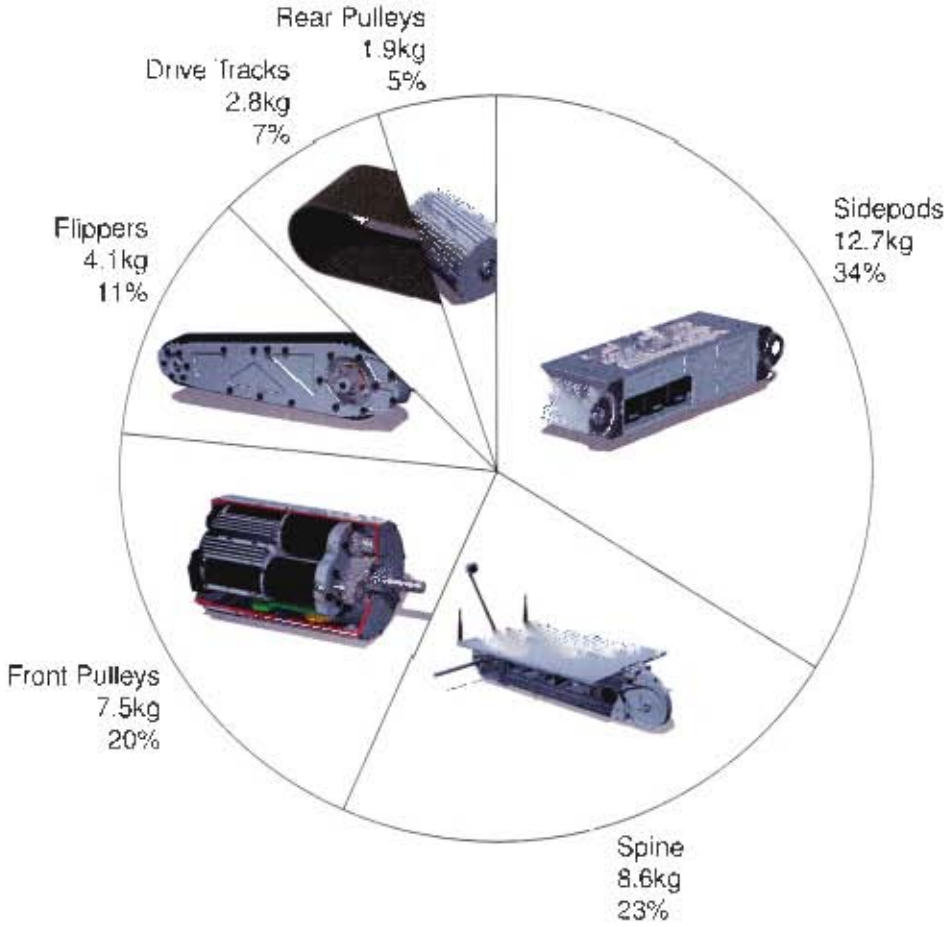

Figure A.1: A visual representation of the weight breakdown of the platform.

Table A.1: Table of component weights in grams. Quantity refers to the number of components on the entire platform rather than in each sub-assembly.

Component	Quantity	Unit Weight (g)	Total Weight (g)
Spine			**8591**
Centre Spine	1	4960	4960
Sidepod Support Rails	4	40	160
Mount Plate	1	1870	1870
Mount Plate Rear Support	1	170	170
Light Housing Inner	4	20	80
Light Housing Outer	4	20	80
LED Mount	4	10	40
Camera Cover	2	6	12
Fan	1	90	90
Arm to Base Interface	1	240	240
Front Cable Cover	1	9	9
Rear Gear Cover	1	130	130
Rear Shaft Cover	1	60	60
Rear Flipper Drive Gear	1	50	50
Rear Flipper Idler Gear	2	60	120
Rear Flipper Gear	1	70	70
Rear Flipper Drive Shaft	1	40	40
Rear Flipper Drive Idler Shaft	2	15	30
Rear Flipper Shaft	2	60	120
Rear Flipper Coupling	2	100	200
SKF608	6	10	60
Sidepods			**12749**
Sidepod Bottom	2	1090	2180
Sidepod Top	2	940	1880
Sidepod Upright	3	467	1401
Rear Motor Mount	1	430	430
Rear Motor Clamp	1	90	90
Track Tensioning Bar	6	120	720
Track Tensioning Bar Holders	6	3	18
Outside Hub Support	4	200	800
Sidepod Side Cover	2	355	710
Slider Clamp	12	5	60
Battery Ejector Plate	4	20	80
Batteries	6	610	3660
Battery Guide Plate and Contact Holder	2	360	720
Drive Pulleys	**2**	**3740**	**7480**
Pulley	2	610	1220
Front Pulley Inside Cover	2	140	280
Front Pulley Outside Cover	2	100	200
Outside Center	2	20	40
Motor Mount 1	2	210	420
Motor Mount 2	2	60	120
Motor Mount 3	2	90	180
Motor Mount Connect	2	140	280
Rear Pulleys	**2**	**950**	**1900**
Rear Pulley Inside Cover	2	110	220
Rear Pulley Outside Cover	2	140	280
Pulley	2	610	1220
Flipper	4	1030	4120
Flipper Inside Plate	4	190	760
Flipper Arm Plate	4	120	480
Flipper Pulley	4	90	360
Flipper Small Pulley	4	90	360

Component	Quantity	Unit Weight (g)	Total Weight (g)
Flipper Track Support	8	40	320
Flipper Arm Hub	4	70	280
Small Pulley Hub	4	10	40
Small Pulley Nut	10	4	40
Small Pulley Shaft	4	5	20
Flipper Tensioner	8	7.5	60
Flipper Rear Brace	4	15	60
Flipper Track	4	210	840
Flipper Pulley Bearing	4	80	320
Flipper Shaft Bearing	4	60	240
Other			
Drive Tracks	2	1400	2800
Maxon Motor	5	860	4300
Maxon Motor Controller (In Box)	5	180	900
Maxon Motor Controller (Board)	5	30	150
Sum/Total	**188**		**37640**
Rescue robot with all components, electronics, fasteners, wiring and sundries			**42700**

A.2 Concluding Remarks

The sidepods are the heaviest sub-assemblies, their mass being primarily determined by the batteries and the 4 structural members in each sidepod (sidepod top, sidepod bottom, and sidepod uprights). The spine sub-assembly, the next biggest sub-assembly has its mass primarily made up of the weight of the spine itself. These assemblies present the greatest oppurtunity for reducing the mass of the platform, particularly in modifying the spine and sidepod structural members to reduce their mass.

Appendix X

Drawings

Drawing Register		
Drawing	Drawing Number	Page
Explorer Robot Platform	ERP-A-01	117
Center Spine	ERP-SA-01	118
Left Sidepod	ERP-SA-02	119
Front Pulley	ERP-SA-03	121
Flipper	ERP-SA-04	122

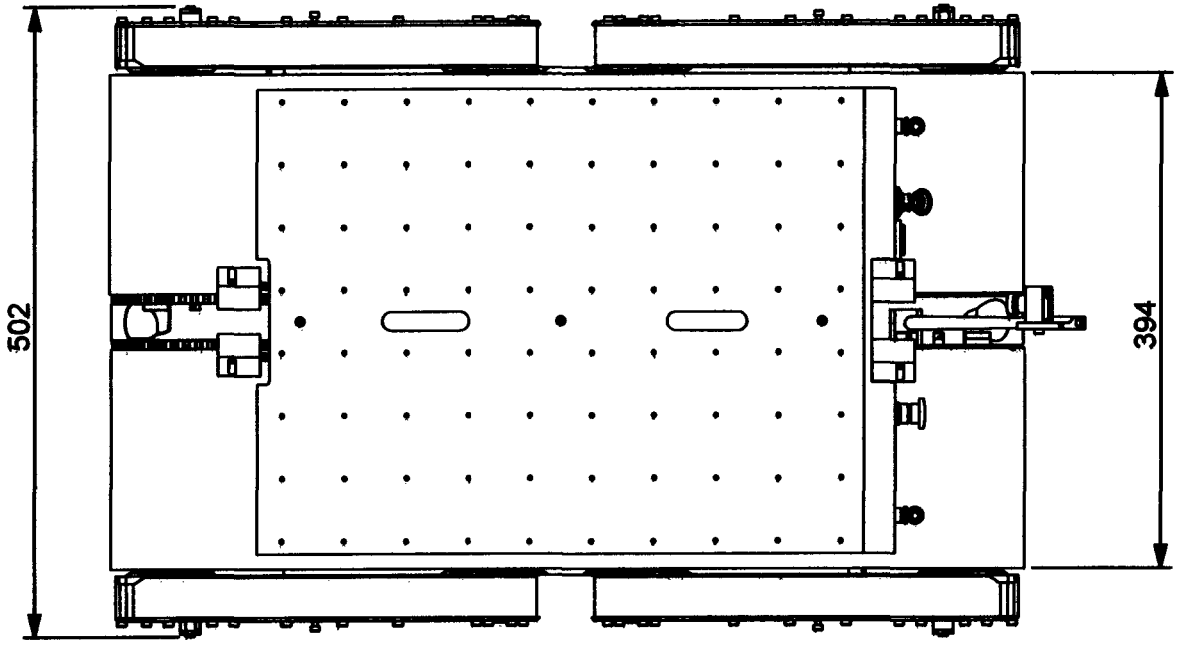

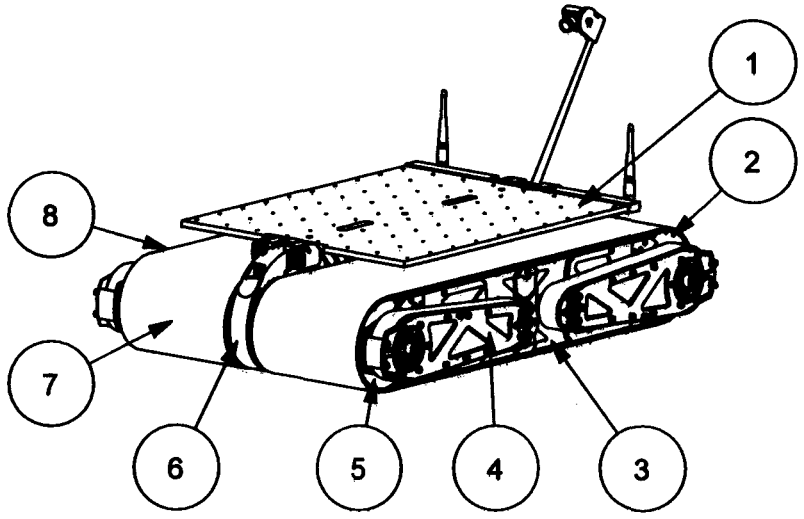

SCALE 0,100

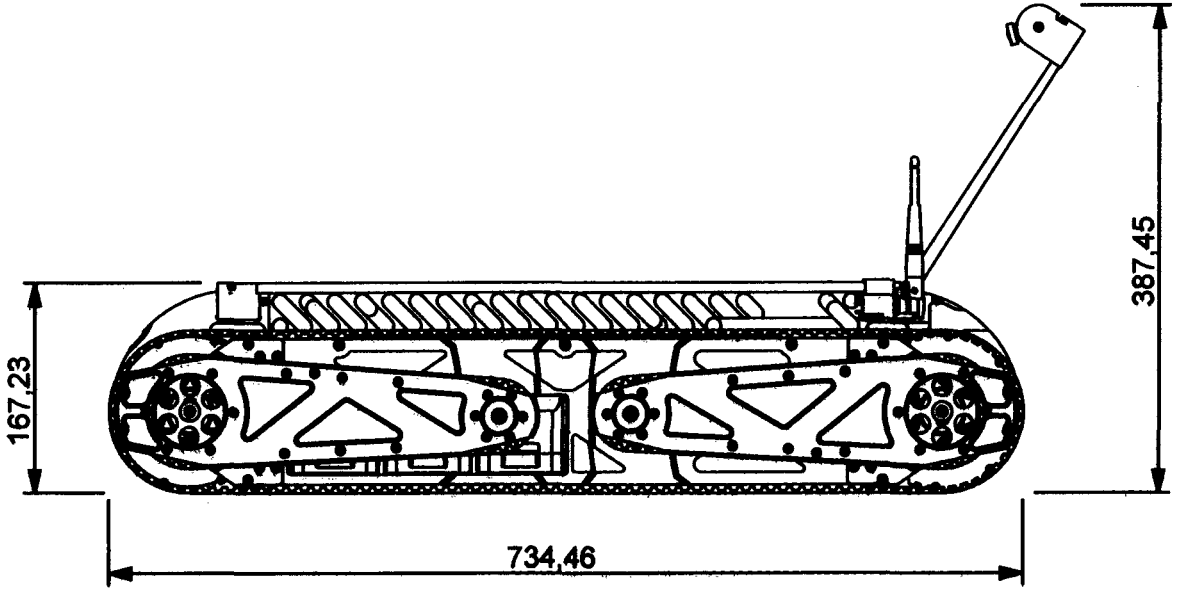

Item	Name	Qty	Material
8	RIGHT_SIDEPOD	1	
7	DRIVE_BELT	2	
6	CENTER_SPINE	1	
5	FRONT_PULLEY	2	
4	FLIPPER	4	
3	LEFT_SIDEPOD	1	
2	BACK_PULLEY	2	
1	ACCESSORY_PLATE	1	

University of Cape Town
Department of Mechanical Engineering

Title
EXPLORER ROBOT PLATFORM

Dimensions in mm Tolerance U.O.S.	Scale	Date	Sheet	of
0.1	0,166	01-Aug-12	1	1
	Drawn By: E.L. DREYER		Drawing Number: ERP-A-01	

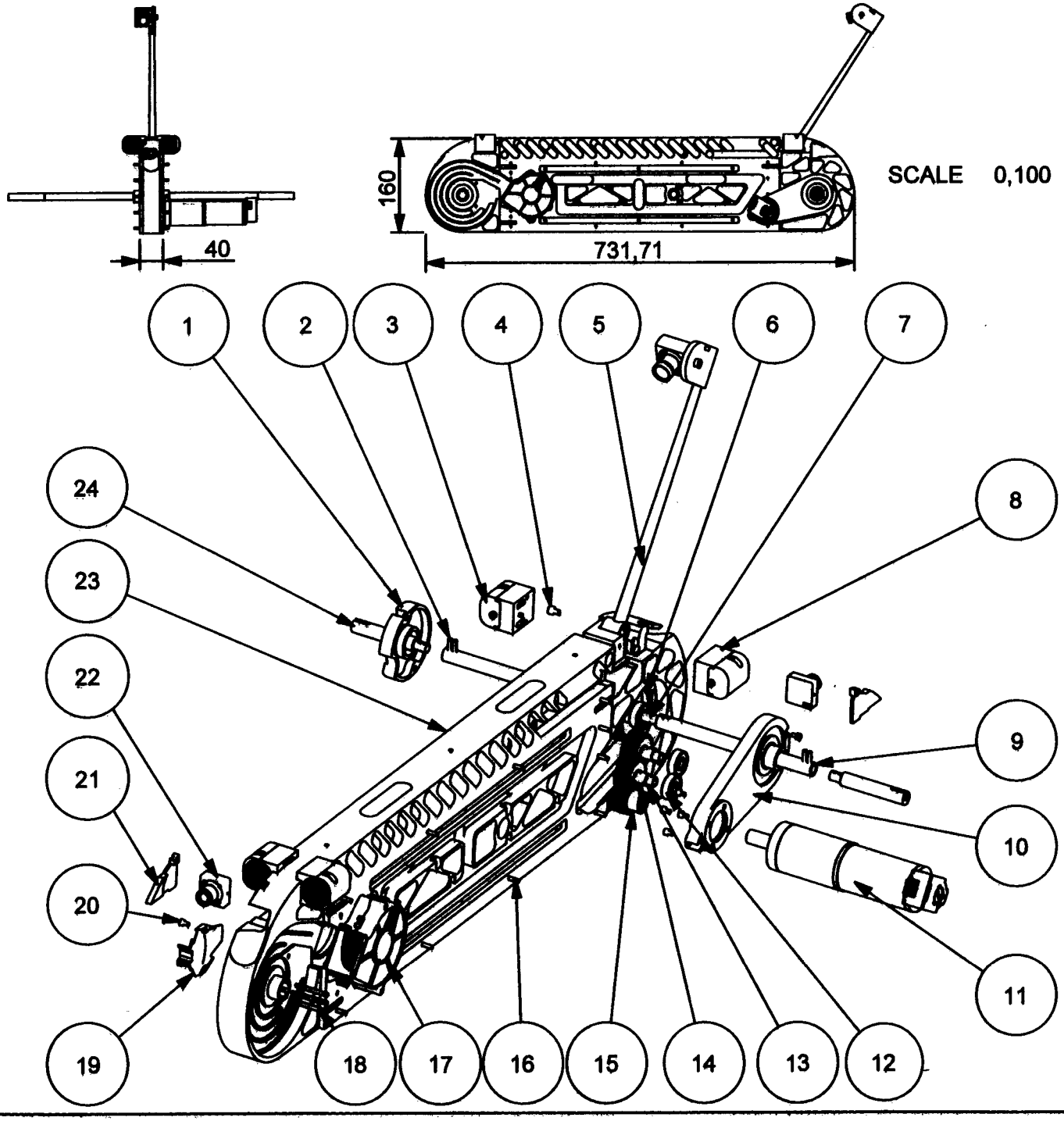

Item	Name	Qty	Material
24	REAR_FLIPPER_DRIVE_SHAFT	2	
23	CENTER_SPINE	1	
22	BASECAM	2	
21	CAMERA_COVER	2	
20	M3X6 ALLEN CAP	10	
19	FRONT_CABLE_COVER	1	
18	3X32 DOWEL PIN	6	
17	BLOWER	1	
16	3X60 DOWEL PIN	12	
15	M1T24REAR	1	
14	M1T28	2	
13	REAR_DRIVE_IDLER_SHAFT	2	
12	BEARING_SKF_608	6	
11	MOTOR	1	
10	REAR_GEAR_COVER	1	
9	REAR_FLIPPER_COUPLING	2	
8	LIGHT_ASM_RIGHT	2	
7	REAR_PULLEY_DRIVE_SHAFT	1	
6	M1T48	1	
5	STALK_CAM	1	
4	M4X6 ALLEN CAP	1	
3	LIGHT_ASM_LEFT	2	
2	3X12 ROLL PIN	8	
1	REAR_SHAFT_COVER	1	

University of Cape Town
Department of Mechanical Engineering

Title: CENTER SPINE

Dimensions in mm Tolerance U.O.S.	Scale	Date	Sheet	of
0.1	0,200	01-Aug-12	1	1

Drawn By: E.L. DREYER

Drawing Number: ERP-SA-01

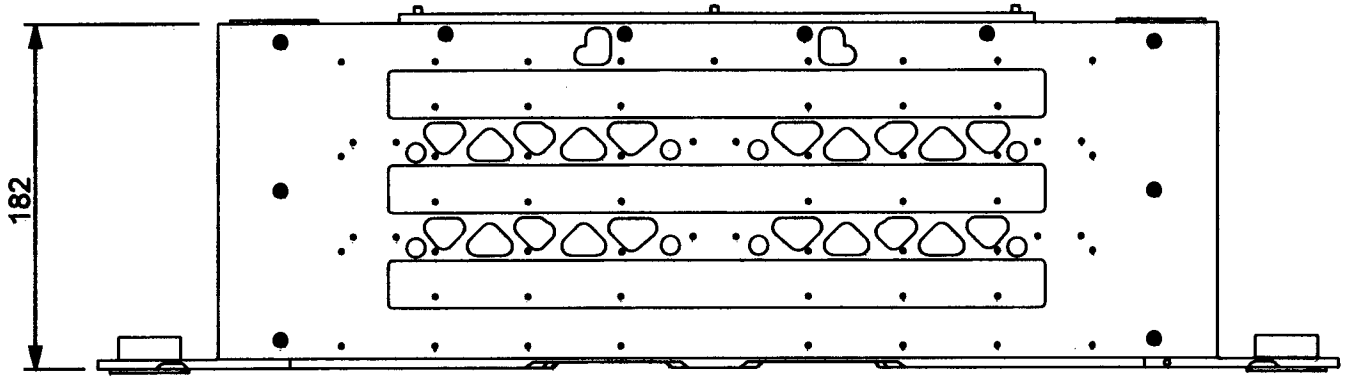

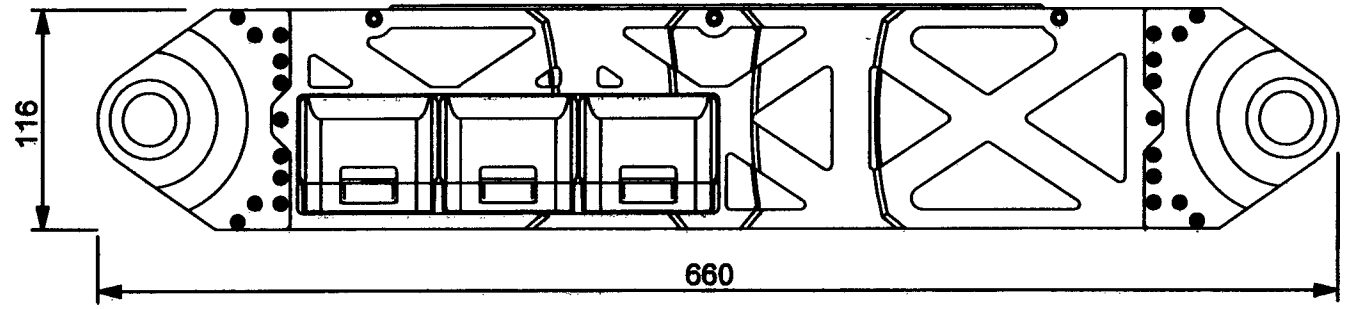

Item	Name	Qty	Material
23	TENSIONER_RISER_ASSEMBLY	3	
22	M3X6 ALLEN CAP	12	
21	ROUTERBOARD	1	
20	M3X8 ALLEN CAP	4	
19	SIDEPOD_UPRIGHT	1	
18	BATTERY_CLIP	1	
17	FRONT_OUTSIDE_DRIVE_BEARING	2	
16	M4X10 ALLEN CAP	20	
15	SIDE_COVER	1	
14	OUTSIDE_HUB_SUPPORTS	2	
13	OUTSIDE_HUB_SUPPORT_MOD	1	
12	FUSES	1	
11	M3X14 ALLEN CAP	2	
10	SIDEPOD_BOTTOM	1	
9	MAXON_CONTROLLER _MOUNT	1	
8	REAR_MOTOR_MOUNT	1	
7	REAR_MOTOR_CLAMP	1	
6	SIDEPOD_SUPPORTS	2	
5	POWERBOARDMOUNT	1	
4	SLIDER_CLAMP	6	
3	TENSIONER_SLIDER	1	
2	M4X6 ALLEN CAP	40	
1	SIDEPOD_TOP	1	

University of Cape Town
Department of Mechanical Engineering

Title
SIDEPOD

Dimensions in mm Tolerance U.O.S.	Scale	Date	Sheet	of
	0,250	15-Aug-05	1	2
	Drawn By		Drawing Number	
0.1	E.L. DREYER		ERP-SA-02	

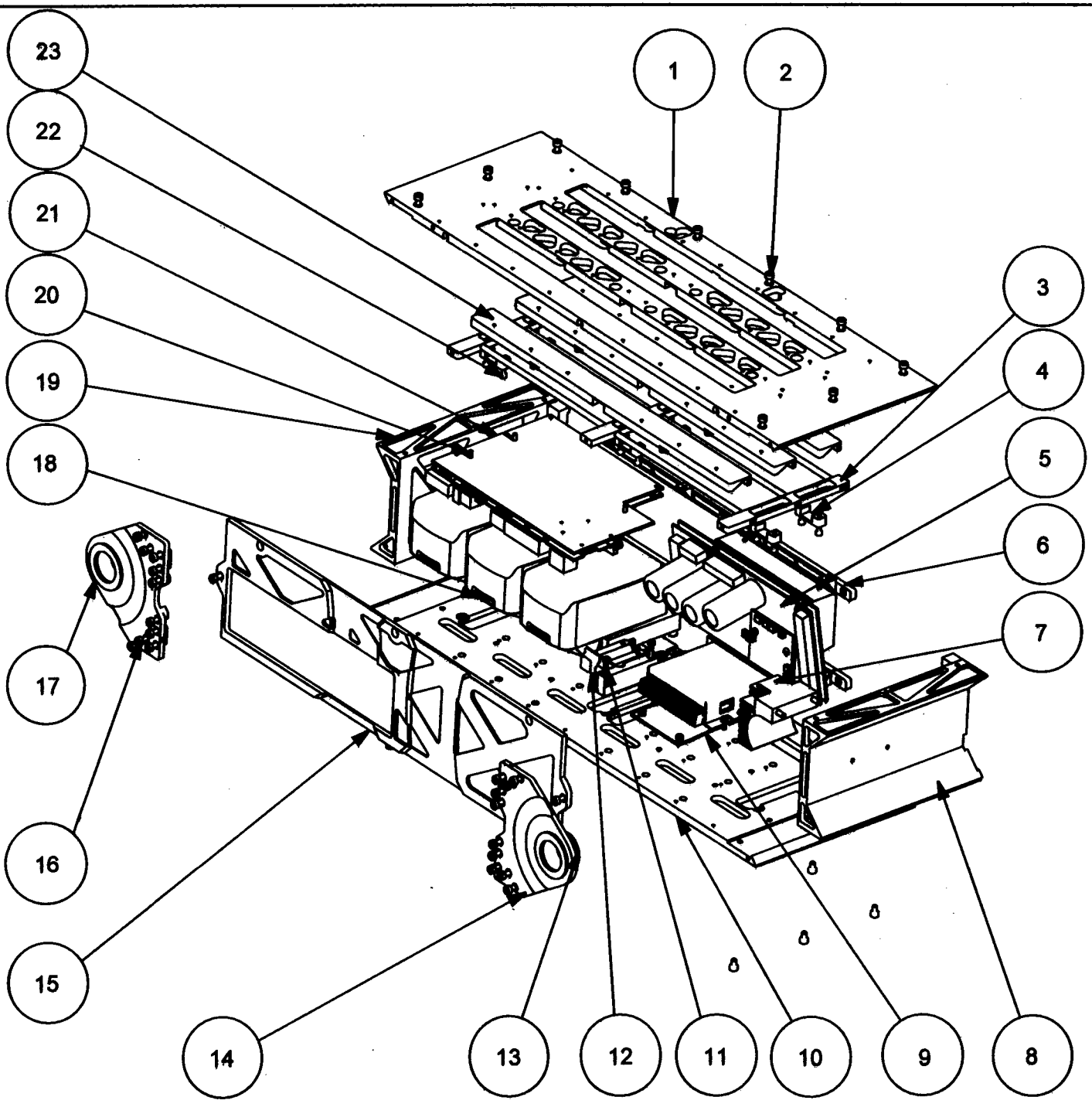

Item	Name	Qty	Material
23	TENSIONER_RISER_ASSEMBLY	3	
22	M3X8 ALLEN CAP	12	
21	ROUTERBOARD	1	
20	M3X8 ALLEN CAP	4	
19	SIDEPOD_UPRIGHT	1	
18	BATTERY_CLIP	1	
17	FRONT_OUTSIDE_DRIVE_BEARING	2	
16	M4X10 ALLEN CAP	20	
15	SIDE_COVER	1	
14	OUTSIDE_HUB_SUPPORTS	2	
13	OUTSIDE_HUB_SUPPORT_MOD	1	
12	FUSES	1	
11	M3X14 ALLEN CAP	2	
10	SIDEPOD_BOTTOM	1	
9	MAXON_CONTROLLER _MOUNT	1	
8	REAR_MOTOR_MOUNT	1	
7	REAR_MOTOR_CLAMP	1	
6	SIDEPOD_SUPPORTS	2	
5	POWERBOARDMOUNT	1	
4	SLIDER_CLAMP	6	
3	TENSIONER_SLIDER	1	
2	M4X6 ALLEN CAP	40	
1	SIDEPOD_TOP	1	

University of Cape Town
Department of Mechanical Engineering

Title: SIDEPOD

Dimensions in mm Tolerance U.O.S.	Scale	Date	Sheet	of
0.1	0,200	15-Aug-12	2	2

Drawn By: E.L. DREYER

Drawing Number: ERP-SA-02

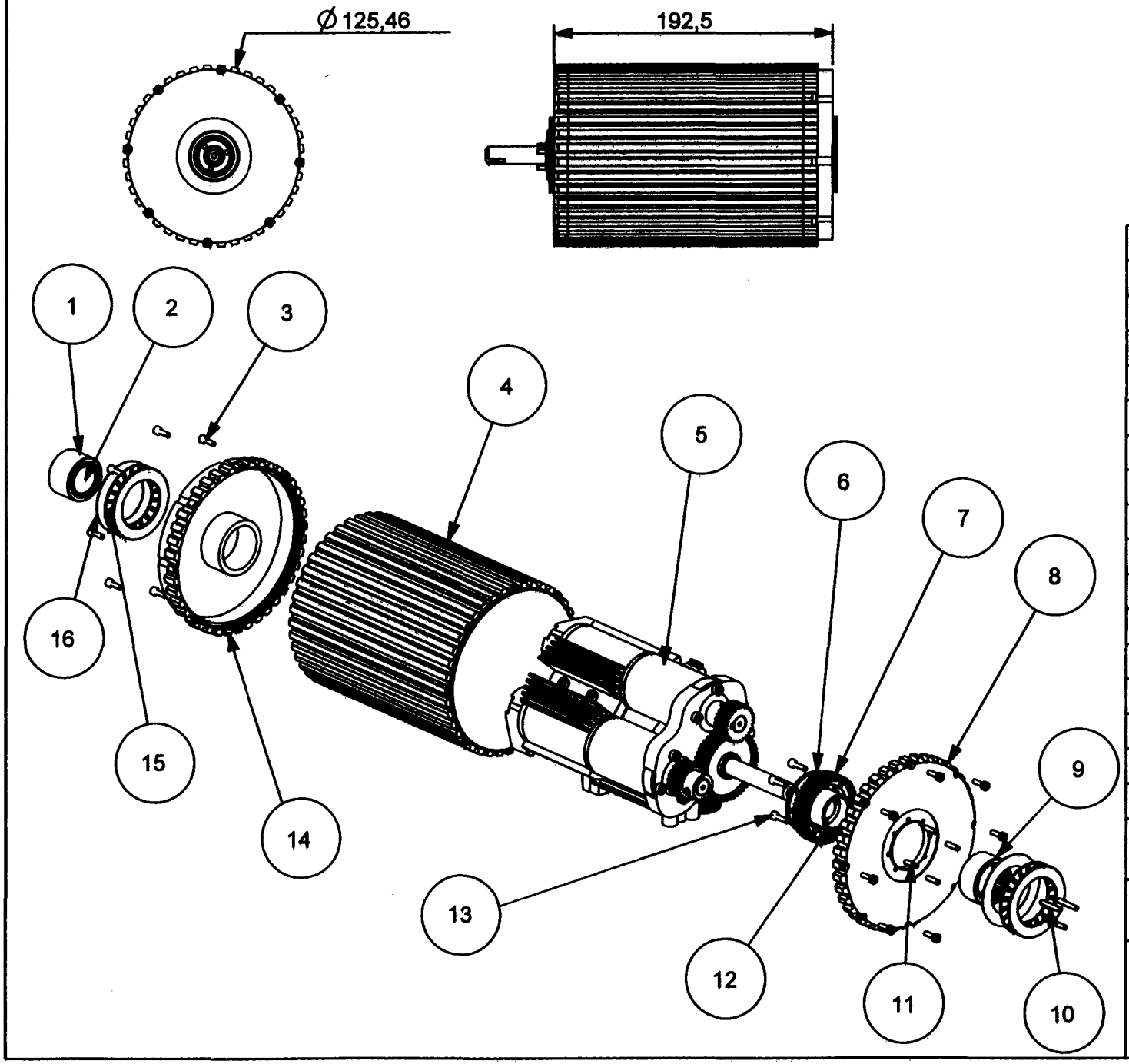

Item	Name	Qty	Material
16	THRUST_BEARING_RACE	4	
15	THRUST_BEARING_CAGE	2	
14	DRIVE_PULLEY_INNER	1	
13	M3X12 ALLEN CAP	4	
12	OUTER_BEARING_INNER_RACE	1	
11	3X12 DOWEL PIN	4	
10	3X20 DOWEL PIN	3	
9	OUTSIDE_BEARING_OUTER_RACE	1	
8	OUTSIDE_COVER	1	
7	M1T47	1	
6	OUTSIDE_CENTER	1	
5	DRIVE_ASSEMBLY	1	
4	PULLEY	1	
3	M3X10 ALLEN CAP	16	
2	INSIDE_BEARING_INNER_RACE	1	
1	INSIDE_BEARING_OUTER_RACE	1	

University of Cape Town
Department of Mechanical Engineering

Title
FRONT PULLEY

Dimensions in mm Tolerance U.O.S.	Scale	Date	Sheet	of
	0,250	01-Aug-12	1	1
0.1	Drawn By: E.L. DREYER		Drawing Number: ERP-SA-03	

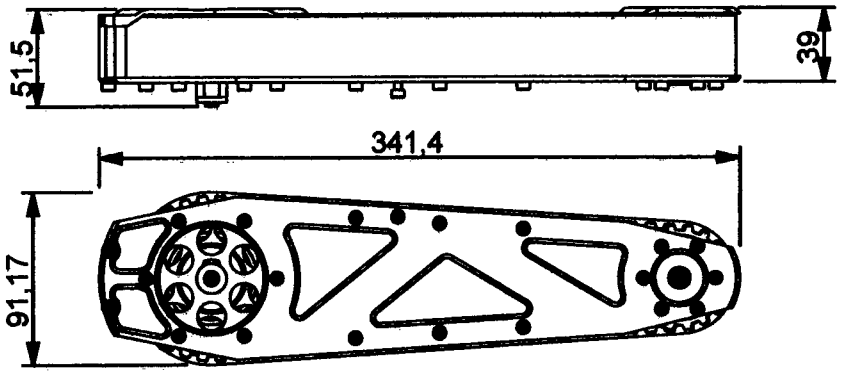

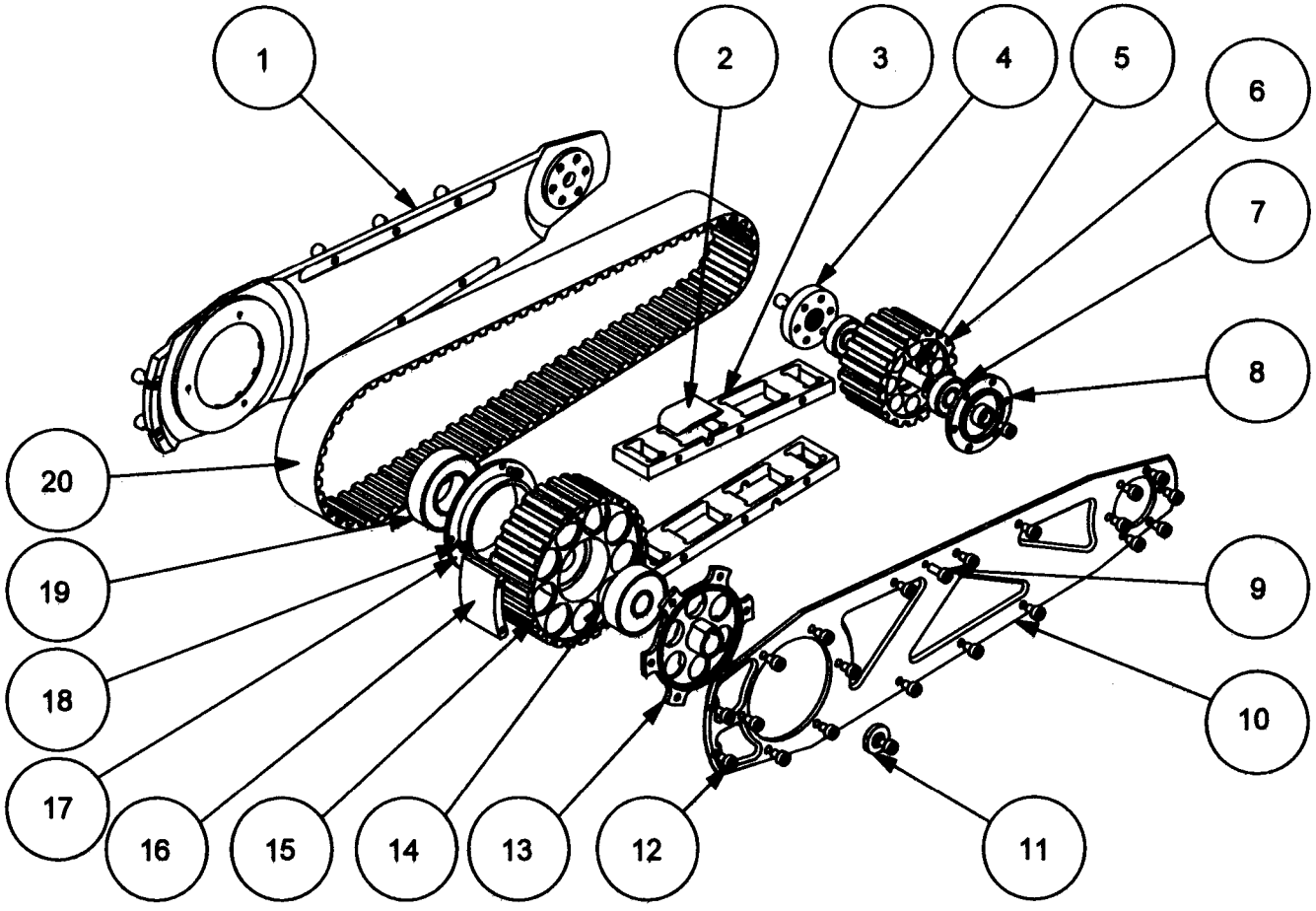

Item	Name	Qty	Material
20	FLIPPERBELT	1	
19	BEARING_SKF_6022	1	
18	M3X6 ALLEN CAP	3	
17	BEARING_SLEEVE	1	
16	FLIPPER_REAR_BRACE	1	
15	FLIPPER_PULLEY	1	
14	FLIPPER_BEARING	1	
13	FLIPPER_ARM_HUB	1	
12	M4X6 ALLEN CAP	37	
11	FLIPPER_WASHER	1	
10	FLIPPER_ARM_PLATE	1	
9	M4X10 ALLEN CAP	1	
8	SMALL_PULLEY_HUB	1	
7	BEARING_SKF_608	2	
6	FLIPPER_SMALL_PULLEY	1	
5	SMALL_PULLEY_SHAFT	1	
4	SMALL_PULLEY_NUT	1	
3	FLIPPER_TRACK_SUPPORT	2	
2	FLIPPER_TENSIONER	1	
1	FLIPPER_INSIDE_PLATE	1	

University of Cape Town
Department of Mechanical Engineering

Title
FLIPPER ARM

Dimensions in mm Tolerance U.O.S.	Scale	Date	Sheet	of
0.1	0,250	01-Aug-12	1	1

Drawn By	Drawing Number
E.L. DREYER	ERP-SA-04

References

[1] B. Siciliano and O. Khatib, *Springer Handbook of Robotics*. Springer, 2008.

[2] National Science Foundation Press Release, "At WTC Search, Graduate Students Deploy Shoebox-Sized Robots." http://www.nsf.gov/od/lpa/news/press/01/pr0178.htm, 2001.

[3] iRobot Corporation, "iRobot 510 PackBot Configurations." http://www.irobot.com/gi/ground/510_PackBot/.

[4] E. Messina, A. Jacoff, J. Scholtz, C. Schlenoff, H.-M. Huang, A. Lytle, and J. Blitch, "Statement of Requirements for Urban Search and Rescue Robot Performance Standards," tech. rep., Department of Homeland Security Science and Technology Directorate and National Institute of Standards and Technology, 2005. Available at http://www.isd.mel.nist.gov/US&R_Robot_Standards/Requirements%20Report%20(prelim).pdf.

[5] Future Robotics Technology Center, "Quince." http://furo.org/en/works/quince.html, 2007.

[6] N. Tesla, "Method of and apparatus for controlling mechanism of moving vessels or vehicles," Patent 613809, United States Patent Office, November 1898.

[7] A. Lychagin, "What is teletank (in russian)." http://www.odintsovo.info/news/?id=1683.

[8] O. Drozd-Koroleva and A. Korolev, "Means of communication on the battlefield (in russian)." http://mobimag.ru/Articles/283/Sredstva_svyazi_na_pole_boya.htm.

[9] A. Finn and S. Scheding, *Developments and Challenges for Autonomous Unmanned Vehicles: A Compendium*. Intelligent Systems Reference Library, Springer Verlag, 2010. Available at http://books.google.com/books?id=TbHo4n4YrZ4C.

[10] J. Lepage, *German military vehicles of World War II: an illustrated guide to cars, trucks, half-tracks, motorcycles, amphibious vehicles and others*. McFarland & Co., 2007. Available at http://books.google.com/books?id=JbeYqc5DBFAC.

[11] "The german weekly newsreel." http://www.youtube.com/watch?v=cpwV0OYg1J4, 1944.

[12] R. Arndt, "Nagayama - Remote controlled armored tractor." http://japan.greyfalcon.us/NAGAYAMA.htm.

[13] Staff Writer, "No Men in Radio Operated Tank," *Popular Science Monthly*, August 1930. Available at http://books.google.com/books?id=aigDAAAAMBAJ.

[14] A. Takizawa, "Taki's Imperial Japanese Army Page." http://www3.plala.or.jp/takihome/.

[15] Royal Army Ordinance Corps Online, "321 Explosive Ordinance Disposal." http://raoc.websitetoolbox.com/post?id=2546076, 2008.

[16] Remotec UK Ltd, "Remotec Wheelbarrow Revolution Remote EOD Vehicles." http://www.armedforces-int.com/article/remotec-wheelbarrow-revolution-remote-eod-vehicles.html.

[17] J. Casper and D. R. Murphy, "Human-Robot Interactions during the Robot-Assisted Urban Search and Rescue Response at the World Trade Center," *IEEE Transactions on Systems, Man, and Cybernetics, Part B: Cybernetics*, vol. 33, pp. 367–385, 2003.

[18] N. Hodge, "Where Humans Fear to Tread," *Wall Street Journal*, 2011. Available at http://online.wsj.com/article/SB10001424052748703702004576269173404660688.html.

[19] The Robocup Foundation, "A brief history of robocup." http://www.robocup.org/about-robocup/a-brief-history-of-robocup/.

[20] The Robocup Foundation, "Robocup rescue main page." http://www.robocuprescue.org/.

[21] A. Jacoff, "RoboCupRescue Robot League Progress Update and Future Directions." http://www.isd.mel.nist.gov/projects/USAR/2009/RoboCupRescue_Robot_League_Overview_(2007-2008).pdf.

[22] Australian Research Council Center of Excellence for Autonomous Systems (CAS), "The homepage of team casualty." http://rescue.web.cse.unsw.edu.au/.

[23] Maxonmotor ag, "Maxon receives NASA award for Mars Exploration Rover." http://www.maxonmotor.com.au/media_releases_maxon-receives-NASA-award-for-Mars-Exploration-Rover%20.html.

[24] iRobot Corporation, "irobot packbot explorer." http://www.irobot.com/filelibrary/pdfs/gi/robots/iRobot_PackBot_Explorer.pdf.

[25] E. Poulton, *Tracking skill and manual control*. Academic Press, 1974. Available at http://books.google.co.za/books?id=k4gQAQAAIAAJ.

[26] M. Rank, Z. Shi, H. J. Muller, and S. Hirche, "Perception of Delay in Haptic Telepresence Systems," *Presence: Teleoperators and Virtual Environments*, 2010. Available at http://www.lsr.ei.tum.de/fileadmin/publications/rank/Rank_PerceptionOfDelay.pdf.

[27] A. Jacoff, "RoboCup Rescue 2008 Photographs."

[28] A. Jacoff, A. Virts, and T. Downs, "RoboCupRescue Robot League Arenas: Major Component Description," tech. rep., National Institute of Standards and Technology, 2008. Available at http://robotarenas.nist.gov/2008/RoboCupRescue_Robot_League_Arenas_Components(2008.1).pdf.

[29] I. Buchman, "What's the Best Battery? - Advabntages and limitations of the different types of batteries." http://batteryuniversity.com/learn/article/whats_the_best_battery, 2010.

[30] Makita Corporation, "Makita Product Information." http://www.makita.biz/product/li-ion/index.html.

[31] The World Bank, "Global Economic Monitor." http://data.worldbank.org/data-catalog/global-economic-monitor.

[32] B. Maclaurin, "A skid steering model with track pad flexibility," *Journal of Terramechanics*, vol. 44, no. 1, pp. 95 – 110, 2007. Available at http://www.sciencedirect.com/science/article/pii/S0022489806000425.

[33] J. Stewart, *Calculus: Concepts and Contexts*. Stewart's Calculus Series, Cengage Learning, 2009.

[34] Bosch Security Systems, "Vip x2 dual-channel video encoder." http://products.boschsecurity.us/en/TAMS/products/bxp/SKU15467074672961417099-P1.

[35] Maxonmotor GmBH, "Maxon Motor Catalogue," 2008.